FG

FALLOUT HAZARD PREDICTION INCONSISTENCIES

General Electric Company—TEMPO
DASIAC
816 State Street
Santa Barbara, California 93102

1 October 1979

Final Report for Period 1 October 1978 - 1 October 1979

DTIC
S ELECTE **D**
JUL 3 1980

B

Destroy this report when it is no longer
needed. Do not return to sender.

REPORT DOCUMENTATION PAGE	READ INSTRUCTIONS BEFORE COMPLETING FORM

1. REPORT NUMBER	2. GOVT ACCESSION NO.	3. RECIPIENT'S CATALOG NUMBER
DASIAC-SR-174	AD-A086 216	

4. TITLE (and Subtitle)	5. TYPE OF REPORT & PERIOD COVERED
FALLOUT HAZARD PREDICTION INCONSISTENCIES.	Final Report, for Period 1 Oct 78—1 Oct 79.
	6. PERFORMING ORG. REPORT NUMBER
	DASIAC SR 174

7. AUTHOR(s)	8. CONTRACT OR GRANT NUMBER(s)
Howard A. Hawthorne	DNA 001-79-C-0081

9. PERFORMING ORGANIZATION NAME AND ADDRESS	10. PROGRAM ELEMENT, PROJECT, TASK AREA & WORK UNIT NUMBERS
General Electric Company—TEMPO DASIAC, 816 State Street Santa Barbara, California 93102	Subtask P99QAXDC008-09

11. CONTROLLING OFFICE NAME AND ADDRESS	12. REPORT DATE
Director Defense Nuclear Agency Washington, D.C. 20305	1 October 79
	13. NUMBER OF PAGES
	112

14. MONITORING AGENCY NAME & ADDRESS(if different from Controlling Office)	15. SECURITY CLASS (of this report)
	UNCLASSIFIED
	15a. DECLASSIFICATION/DOWNGRADING SCHEDULE

16. DISTRIBUTION STATEMENT (of this Report)

Approved for public release; distribution unlimited.

17. DISTRIBUTION STATEMENT (of the abstract entered in Block 20, if different from Report)

19. KEY WORDS (Continue on reverse side if necessary and identify by block number)

Fallout Models	Prediction Errors
Fallout Patterns	Radiation Fields
Fallout Predictions	

20. ABSTRACT (Continue on reverse side if necessary and identify by block number)

An elementary review of modelling of fallout processes is presented, with lists of some of the important variables that modules within models are called on to parameterize. A brief historical synopsis of the development of modelling includes a description of efforts with a standardized input data to produce output directly comparable among models, including illustrations of the output over the nuclear yield range of less than 1 KT to 15 MT. Model output is compared to observed data from field weapons tests, and estimates are made

DD 1 JAN 73 1473 EDITION OF 1 NOV 65 IS OBSOLETE

20. ABSTRACT (Continued)

of the degree of fit between observed nuclear data and predicted parameters from models.

TABLE OF CONTENTS

LIST OF ILLUSTRATIONS

2

3

4

LIST OF TABLES

SECTION 1

INTRODUCTION

In applications where computer output is relied upon for daily problem solving, it is easy to overlook that the parameters in the codes may be incomplete and the subsequent output less than reliable. This is especially so when submodel outputs become the direct and electronic internal input to a large code and the transfer is made without any review or human evaluation of the data. An elementary review was indicated by code user experiences to show how different fallout models handled common input data that might be passed along to a damage assessment code or a code used to estimate collateral damage from radiation. The code outputs are being more frequently directly incorporated into forecasts of strategic and tactical maneuvers and response. The comparability of the several fallout predictor models has a strong influence upon the validity of comparisons made in deciding whether or not some tactical objective might be achieved.

In this review, the questions of how the outputs compare is presented visually to the reader. From that inspection the effects of inconsistencies on his work can be made. A brief introduction to the tools needed for working in the field is presented in Sections 2 and 3. The processes simulations are expected to bridge across are discussed here with graphic illustrations, including the application of ellipsoidal figures to simple questions about gamma fallout radiation fields. The DELFIC code is introduced and its basic structure is described. The various models that were used during atmospheric testing are divided into groups and the source of a data standardization effort to obtain input to the models is specified.

7

SECTION 2
SIMULATION OF FALLOUT RADIATION PROCESSES

This tutorial is initially directed towards demonstrating the variations that can be observed in the output after identical input data to different fallout predictor systems. The output variations originate in the way that fallout processes are simulated in the radiation predictor systems. Simulations utilize parameters that only partially can reproduce fallout processes in a conceptual sense, and do not at all reproduce the complexities of the actual nuclear device fallout processes.

The passage that follows describes the phenomenology of fallout. Devices then under study were generally tower-supported at less than 150 meters elevation over the Nevada Test Site Ground Zeros and were less than 100-KT yield. This is direct quote from a 1954 report done by offsite, fallout particle collector teams (Reference 2-1).

CONCEPTS OF THE FALLOUT PHENOMENON

"The subject of this report is but one of the many physical phenomena associated with an atomic detonation. As such, it is related to, and is a function of, many factors. Therefore the inclusion of a brief discussion of those factors which are presently considered by this group to play a major role in the determination of the mechanics and the characteristics of fallout is necessary. For other interpretations and a more detailed account, the reader is referred to any one of the numerous reports on the subject.

Mechanics of Formation of Fallout Material

At the time of detonation, enormous amounts of energy are released in the form of heat and ionizing radiation. Within a few microseconds, an intensely hot, luminous sphere of compressed gases, called the "fireball," is formed. The fireball contains, in vapor form, the fission products as well as any of the remaining unfissioned primary materials. Also present are the vaporized bomb casing and any auxiliary equipment necessary for a

particular test detonation. The fireball is extremely radioactive, due to both fission products and radioactivity induced in the bomb casing, tower, and auxiliary equipment.

The fireball rapidly expands, reaching a maximum diameter in less than 1 sec and at the same time begins to rise in the air and cool. As it rises, a toroidal system develops with strong internal revolving or circulating air currents. Coincidental to this development, the thermal energy emitted by the fireball strikes the surface of the ground, causing a disc-shaped cloud of dust and smoke to rise for considerable distances from Ground Zero. On striking the ground the blast wave, reinforced by its reflected wave, travels outward from Ground Zero. This is preceded by a wave of increased pressure. As the pressure fronts pass over the soil surface, dense clouds of dust arise showing strong turbulent motions with the forward dislocation of both dust and large objects (drag effects or secondary missiles). Shortly thereafter, violent and high-velocity updrafts are created in the wake of the rising fireball. Large volumes of dust from the region of Ground Zero and at considerable distances from it are drawn in and up toward the fireball. This forms a rapidly rising stem, containing tons of soil and debris, directly beneath the rising fireball. Much of the material in the stem may be circulated through and around the toroidal-shaped fireball or perhaps even sucked into the fireball itself. Depending upon the height of the burst from the ground surface, a portion of this lifted material will contain some neutron-induced radioactivity. This surface material may become either molten or vaporized, or, in the cooler regions of the cloud, i. may remain unchanged. This phase reaction would be dependent upon the chemical properties of the soil, e.g., the melting point of silica is lowered by the presence of certain carbonates. The foreign material provides surfaces for the adsorption of vaporized fission products or nuclei for condensation. As the fireball cools, one may expect particle growth and solidification. The physical and chemical properties will be dependent upon the chemical content of the soil and the interrelation of the many reactions which take place during the process of radioactive particle formation, i.e., the transition from a vaporized and/or molten state to the final solidification of the fall-out material. The height of detonation

influences the amount of material which, in addition to the fission fragments, is available for particle formation.

Ultimately the cloud rises to an elevation where the density of the gases is the same as that of the surrounding air, and the familiar mushroom-capped cloud with a long stem of debris is observed. Wind shearing may distort the symmetry of the cloud and stem at any level.

Thus, we may group together all the phenomena of the detonation and the subsequent growth and rise of the fireball, cap, and stem, as being some of the more important factors which give rise to the initial distribution of radioactive particles in the air over Ground Zero.

Distribution of Fallout Material

The subsequent dispersal and the ultimate pattern of fall-out from the initial particle distribution over and adjacent to Ground Zero is a very complex phenomenon depending, among other factors, upon the particle size, the particle density and shape, the distribution of particles as a function of height, and the various meteorological conditions following the detonation. Owing to the heights to which particles may rise and to the size spectrum, some particles may remain in the air for very long periods of time, their ultimate location being dependent upon various climatic influences. With even moderate winds opportunity is provided for large-scale movements with or without appreciable dilution due to turbulence. Thus large areas may be severely contaminated with probable local variations of large magnitude resulting from localized weather conditions and topography.

Definitions of Primary Fallout and Airborne Material

Although all the radioactive material which settles out of the cloud may be described as fall-out, a practical distinction should be made between material which remains suspended for long periods of time and material which settles out within the "reasonable" time of the survey period and remains associated with the surfaces of soil, vegetation, etc. The distinction is primarily one of particle size. Throughout this report, settled fall-out material will be designated as "primary fall-out," or

11

"fallout" and material sampled while still airborne will be described as "airborne material." Some movement of fallout material picked up from the ground and temporarily airborne by the local winds can be expected at any time, but, since this occurrence cannot be identified except on rare occasions, it will be mentioned only when directly observed."

This verbal description specified in graphic terms that there is an enormous number of processes, physical and chemical, occurring simultaneously throughout the detonating fireball development, and transport and deposition of fission product radiation fields.

Effective modeling of the processes described in the prior paragraphs concerning generation of the cloud, stabilization at altitude, transport of the radioactive residue, and deposition of radioactivity upon the earth's surface requires a variety of parameter inputs. The magnitude of the several parameters requires a system of controls from algorithms or by other controls directly upon the magnitude of the input parameter. For example, cloud diameter may be controlled by yield of the device that the model can accept as input data. The numbers of parameters required as model input can be substantial. The stored data array reported by Seery (Reference 2-2) for the TINCAN model had 59 parameters that required reading new values from data cards. These parameters dealt with cloud heights, particle settling rates, refractory mass fraction and radioactivity, particle-size radioactivity frequency distribution, particle size mass frequency distributions, and a host of related input parameters. Seery demonstrated the sensitivity of TINCAN output to variation in selected input parameters and his report should be consulted for specific response by the TINCAN model as well as the example of how a fallout model is created.

A controlled listing of variables needed for modeling fallout pattern contours and surface radiation dose rates is as follows. (They were chosen because if their parameter analogs are neglected in deterministic computing models, the output may noticeably deviate from the standard pattern.)

12

1. INITIAL CONDITIONS

   a. Yield range
   b. Height-of-burst ,
   c. Surface particle matrix at GZ

2. CLOUD RISE

   a. Top altitude f(yield)
   b. Bottom altitude f(top)
   c. Stem height
   d. Puff radii
   e. Radioactivity distribution
        (1) Puff/stem
        (2) Within puff
   f. Fission fraction
   g. Radioactive decay to deposition of size fraction
   h. K-factors used (or not used)
   i. mCi/KT at H+1 hr estimated for fissile source
   j. Transported induced radioactivity
   k. Wind shear during cloud rise
   l. Local GZ winds used (or not used)

3. TRANSPORT OF CLOUD

   a. Fractionation
   b. Specific activity
   c. Mass, distribution function from site GZ
   d. Particle size: fractions vs distribution function/fraction down
   e. Density of particles, downed
   f. Partical size: radioactivity distribution function per size fraction
   g. Mean particle size distribution for each H + hr in cloud/on gnd pattern
   h. Induced activity produced
   i. Induced activity at GZ and base surge
   j. Rainout effects in transit
   k. Wind shear during particle fall
   l. Stochastic winds during particle fall

4. DEPOSITION SURFACE

   a. Orographic features
   b. Shielding effects at surface
   c. Meter response to energy spectra present
   d. Parameter, normalization factors

The variables listed are those having parameters that are important to Section 6
for their influence upon differences in the radiation levels predicted by models.
They are given here to illustrate the relationships among one another and their
general relation to the principal subroutines that have been modeled. Variables

pertinent to fallout prediction are grouped in functional units for representation by parameters that are collected into subroutines. The main variable groups in the listing are, respectively, INITIAL CONDITIONS, CLOUD RISE, TRANSPORT, and DEPOSITION. In the DELFIC fallout prediction model the corresponding parameter subroutines, or modules, are INITIAL CONDITIONS, CLOUD RISE, TRANSPORT, PARTICLE ACTIVITY, and OUTPUT. Verbal descriptions of the functions modeled are shown in block diagram format in Figure 2-1 and as a formal flow chart for data in Figure 2-2. The DELFIC model has been computerized and is maintained with frequent updating and documentation as the main DoD fallout prediction system. The various documentations and the basic logic were published in a series of reports (References 2-3 through 2-9) with a number of updates following (Reference 2-10). DELFIC was designed as a reference code for research use and works from first principles, without shortcuts, and without being "bent" to match observed patterns.

The DELFIC model produces a smoothed fallout pattern at the ground plane with a small number of discs, each representing one altitudinal section within the stabilized cloud, by transporting and grounding the top of the disc and its base at separate impact points. The end result of utilizing separate impact points for the base and top sections is calculated in DELFIC as a bivariate Gaussian function to obtain distribution of fallout particles over the ground plane. Vertical wind shear during transport of the disc is converted into an ellipsoidal deposition function at the ground plane. Fallout pattern parameters are computed by summing the contributions from overlapping disc elements at each map point.

Isodose contours for radiation fields generated by fallout have been idealized elsewhere by starting with a succession of elliptical figures that have ground zero as their common origin. An example of this application in predicting radiation dose exposure has been taken from Schiff (Reference 2-11). His results are shown for detonation yields of 10 and 100 KT and are based on crossing the pattern at a distance "ℓ" downwind from ground zero. Wind velocity in all illustrations was included at 10 knots. The starting model is in Figure 2-3, and the line of march is calculated as crossing the pattern at right angles, i.e., the shortest route. While in transit, the dose rate is diminishing, with

14

the diminishing accumulation of radiation with time indicated in Figure 2-4, resulting in a non-symmetric exposure rate which is complex to model. Gamma dose rates for H+1 hr were taken from graphs in EM-1 (Reference 2-12), and the times to delay before transit were calculated on an office calculator (Figures 2-5 and 2-6, respectively). Using the ellipse format radiation field, Schiff estimated the radioactive decay time interval to reach a preset radiation accumulation in the transit period, at the several distances downwind from ground zero (Figures 2-7 and 2-8). The absorbed rads, consequences of misjudging weapon yields, are readily seen in this simple, illustrated approximation. However, better field decisions about proceeding or delay can be constructed from limited equipment for help with decisions, until hard data can be acquired directly from the deposited fallout pattern.

The basic variable in all the prediction methods is the device yield; both total *yield* and fission proportion are needed for a competent prediction of fallout radiation levels and their probable locations. With an accurately known yield, relatively simple prediction methods can assist in deciding how to respond until hard data become available from field-monitoring measurements.

REFERENCES

2-1. Rainey, C.T., J.W. Neel, H.M. Mork and K.H. Larson. Distribution and Characteristics of Fallout at Distances Greater than 10 Miles from Ground Zero, March and April 1953. WT-811. University of California, Atomic Energy Project, Los Angeles, CA 90024. February 1954.

2-2. Seery, C.J. Fallout Model Analysis. TRC-68-46. Ford Instrument Division, Sperry Rand, Long Island City, New York. November 1968. Department of Defense Land Fallout Prediction System DASA-1800 Series.

2-3. Norment, H.G. Vol. I - System Description. DASA-1800-I. Technical Operations Research, Burlington, MA. June 1966.

2-4. Norment, H.G., W.T.G. Ing, and J. Zuckerman. Vol. II - Initial Conditions. DASA-1800-II. Technical Operations Research, Burlington, MA. September 1966.

2-5. I.O. Huebsch and S.H. Cassidy, U.S. Naval Radiological Defense Laboratory, San Francisco, CA, and H.G. Norment, J. Zuckerman and T.W. Schwenke, Technical Operations, Inc., Burlington, MA, Volume III, Cloud Rise, DASA-1800-III, May 1967.

2-6. T.W. Schwenke, I. Kohlberg, H.G. Norment, and W.P.G. Ing, Vol. IV - Atmospheric Transport, DASA-1800-IV, Technical Operations Research, Burlington, MA, February 1967.

2-7. Tompkins, R.C., Vol. V - Particle Activity. DASA-1800-V. U.S. Army Nuclear Defense Laboratory, Edgewood Arsenal, MD, February 1968.

2-8. Schwenke, T.W. and P. Flusser, Vol. VI - Output Processor. DASA-1800-VI. Technical Operations Research, Burlington, MA, February 1967.

2-9. Winegardner, D.K., Vol. VII - Operators Manual. DASA-1800-VII, U.S. Army Nuclear Defense Laboratory, Edgewood Arsenal, MD, April 1968.

2-10. Dillingham, J.H., I. Kohlberg and A. Cohen (Editor E.F. Wilsey) Department of Defense Land Fallout Prediction System-DELFIC EDTES: Extension of the Transit Exposure Capability of DELFIC-TES, BRL-CR-296, Analytical Systems Corp., Burlington, MA 01803, April 1976.

2-11. Schiff, A.,"Problems with Predicting Fallout Radiation Hazard in Tactical Battlefield Situations," UCRL-51440. Lawrence Livermore Laboratory, Livermore, CA, August 1973.

2-12. Dolan, P.J. (Editor)"Capabilities of Nuclear Weapons, Part I Phenomenology," Stanford Research Institute, International, Palo Alto, CA, Unpublished.

```
                    ┌─────────┐
                    │  START  │
                    └─────────┘
                         │
                         ▼
┌────────────────────────────────────────────────────────┐
│              INITIAL CONDITIONS  MODULE                 │
│                                                         │
│  Begins with basic weapon and environmental parameters  │
│  and provides a set of cloud properties defined at the  │
│  beginning of entrainment—controlled cloud rise         │
└────────────────────────────────────────────────────────┘
                         │
                         ▼
┌────────────────────────────────────────────────────────┐
│                 CLOUD  RISE  MODULE                     │
│  Develops from these results a description of the cloud rise │
│  that yields the time—temperature history of the cloud rise,│
│  as well as cloud altitude and dimensions               │
└────────────────────────────────────────────────────────┘
                         │
                         ▼
┌────────────────────────────────────────────────────────┐
│                 TRANSPORT  MODULE                       │
│  Accounts for transport of the fallout particles by ambient winds │
│  and ultimately records their points of impact on the ground │
└────────────────────────────────────────────────────────┘
                         │
                         ▼
┌────────────────────────────────────────────────────────┐
│             PARTICLE  ACTIVITY  MODULE                  │
│  Works in liason with the Output Processors Module to compute │
│  particle activities at any time or times specified by the user │
└────────────────────────────────────────────────────────┘
                         │
                         ▼
┌────────────────────────────────────────────────────────┐
│             OUTPUT  PROCESSOR  MODULE                   │
│  Interprets the results of the Transport and Particle Activity modules │
│  in the light of user requests for particular tabulations │
└────────────────────────────────────────────────────────┘
                         │
                         ▼
                    ┌─────────┐
                    │  STOP   │
                    └─────────┘
```

Figure 2-1. Basic flow diagram of the DELFIC system (Reference 2-10).

START

DETONATIONS AND
GZ PARAMETERS

INITIAL CONDITIONS
MODULE

FIREBALL PROPERTIES
AT START OF RISE

ATMOSPHERIC
PROPERTIES
ABOVE GZ

CLOUD RISE
MODULE

DESCRIPTION OF
TOPOGRAPHY AND A
TIME AND SPACE
VARIANT ATMOSPHERE

TRANSPORT
MODULE

SPATIAL DISTRIBUTION
OF PARTICLES ABOVE GZ;
TIME−TEMPERATURE
HISTORY OF THE CLOUD
RISE

DESCRIPTIONS OF
IMPACTED PARTICLES

PARTICLE ACTIVITY
MODULE

REQUESTS FOR
OUTPUTS

OUTPUT PROCESSOR
MODULE

OUTPUTS AND
ANALYSIS

STOP

Figure 2-2. Data flow in the DELFIC system (Reference 2-10).
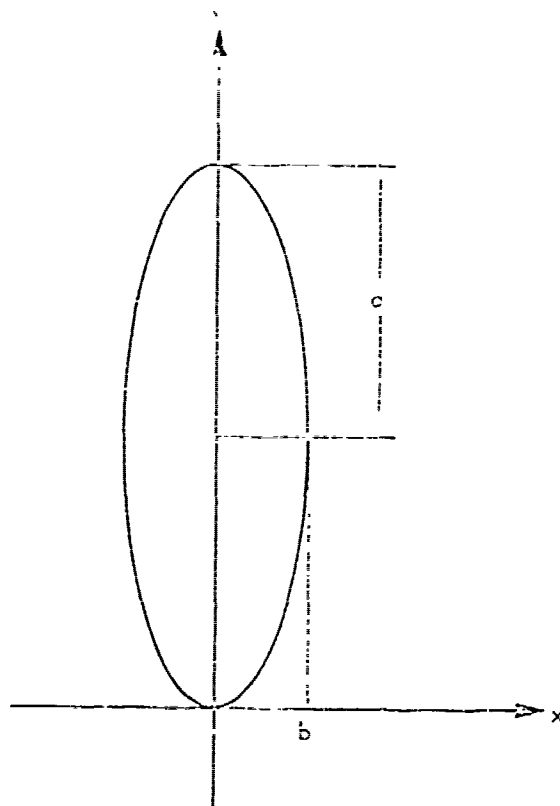
Figure 2-3. Isodose ellipse with focus at
origin (ground zero) (from Reference
2-10).
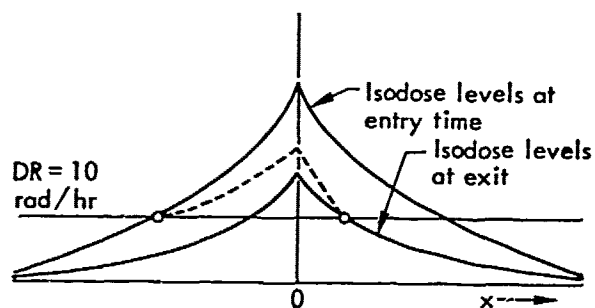
Figure 2-4. Dose-rate levels experienced because
of time delay (dashed line) (from
Reference 2-10).

19
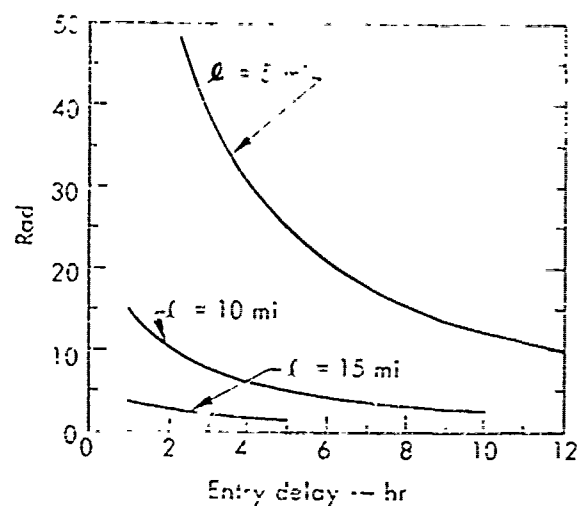
Figure 2-5. Total radiation exposure, after area-entry
delay, for various distances from ground zero,
of a 10-KT detonation. [The expected march
rate is 1 mph (from Reference 2-10).]
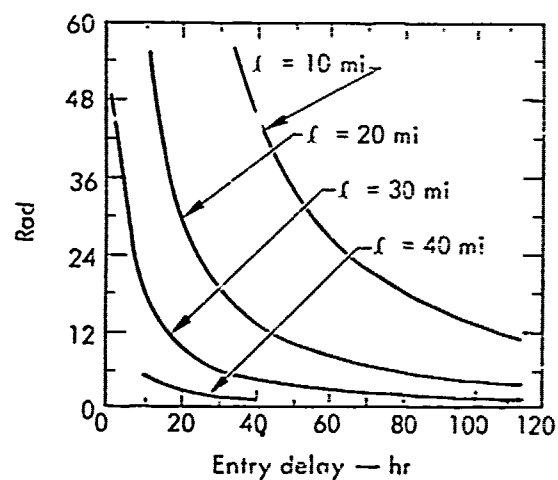
Figure 2-6. Total radiation exposure, after area-entry
delay, for various distances from ground zero,
of a 100-KT detonation. [The expected march
rate is 1 mph. (from Reference 2-10).]

Figure 2-7. Entry delay to gamma radioactive areas, following a 10-KT detonation (from Reference 2-10).

Figure 2-8. Entry delay to gamma radioactive areas, following a
100-KT detonation (from Reference 2-10).

SECTION 3
DEVELOPMENT OF FALLOUT PREDICTION MODELS

An intensive effort took place in September 1962 within the radiation fore-
casting community to describe the operational fallout models and to define the
sources of their differences in pattern forecasts (Reference 3-1). Reports of
the results from that symposium and its associated "homework" problems were
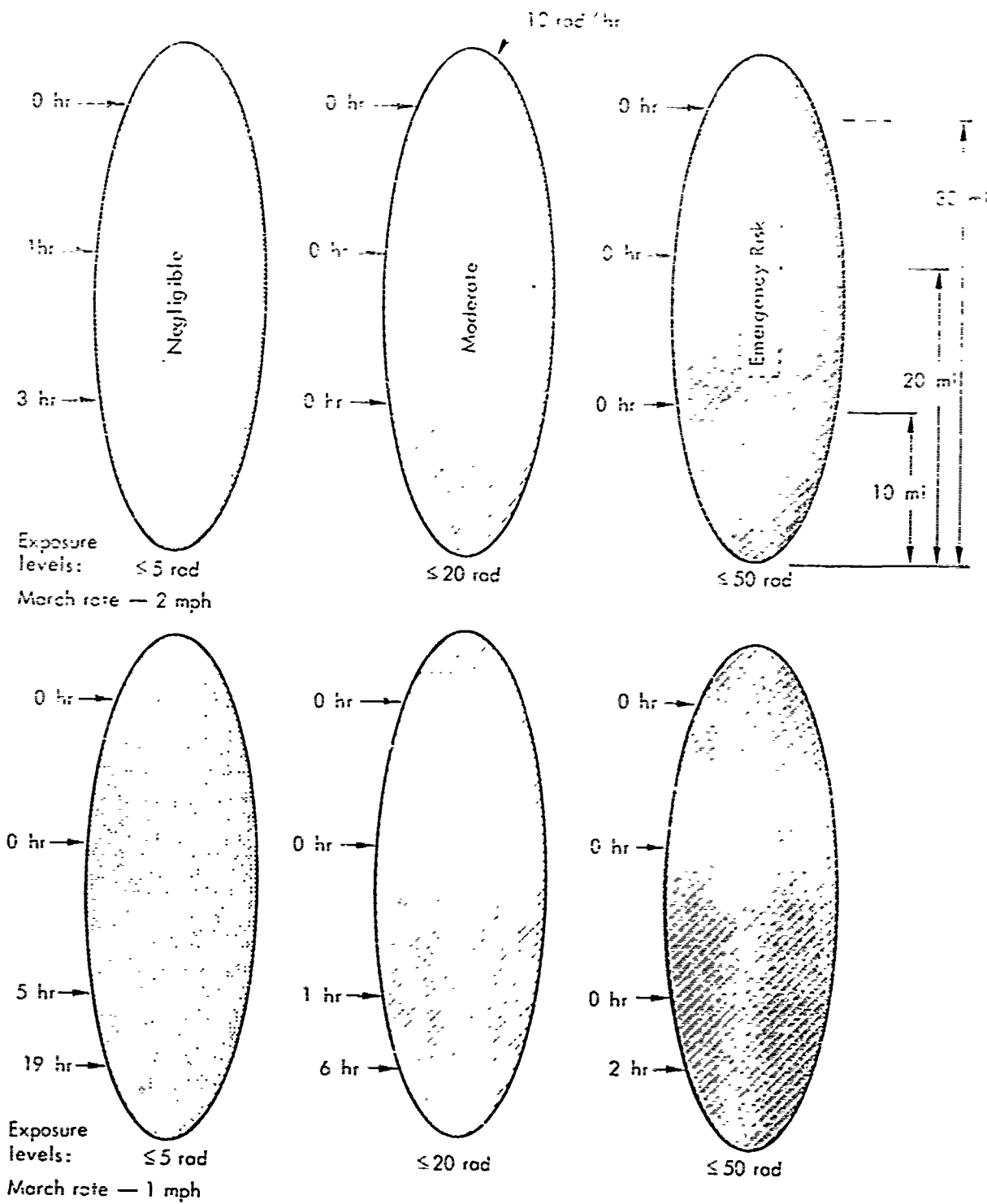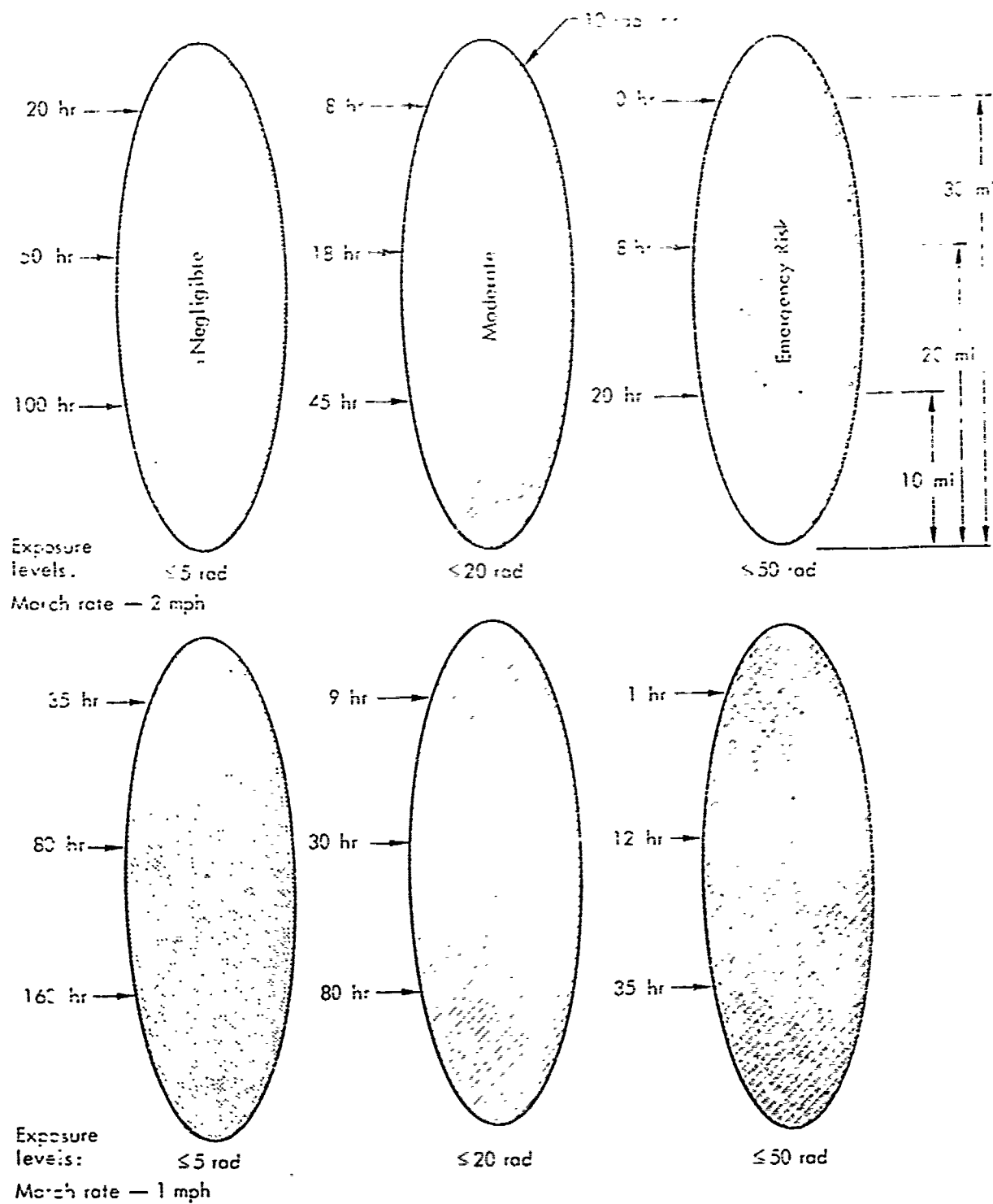issued during the next six years (References 3-2, 3-3). Collecting the active
fallout modelers into one place for discussion and presentation of their work
was helpful in stabilizing the technology and the semantics, as well as in
modeling. Terminology from the symposium of 1962 is utilized in this digest
of sources of differences in fallout forecasts.

Symposia terms are grouped into two categories: those which relate processes
occurring in formation of fallout, and those terms representing model output.
Terms that characterize the cloud submodel are quoted directly from Volume I of
Reference 3-2.

> "Early dynamics - Treatment of the processes that occur from the time of
> burst to the time of cloud stabilization.

> Cloud geometry - Description of the shape, height, vertical thickness,
> and diameter of the cloud. Equations, tables, and figures are used.

> Cloud radioactivity distribution - Distribution of radioactivity between
> the main parts of the cloud (cap and stem) and with height and
> radius. Representative curves show the vertical distribution of
> radioactivity within the cloud for typical 20-KT and 30-MT land
> surface bursts at mean sea level (msl).

> Radioactivity-Particle-size distribution - Distribution of radioactivity
> with particle size (or other parameter). Representative curves are
> given for models that include this characteristic.

23

Normalization - Conversion of cloud radioactivity from fission yield per unit area on an ideal plane to exposure rate, and the reduction of the latter by a shielding factor for 'average' ground terrain, are usually performed in the cloud submodel.

The transport submodel describes the movement of the fallout through the atmosphere from the initial spatial distribution defined by the cloud submodel to the point where it lands on the earth's surface. The characteristics involved are as follows:

Wafers - Division of the cloud into the smallest element (wafer or disc) transported, frequently determined by slicing the cloud into its smallest geometric sections, and dividing the radioactivity in a section among representative particle sizes. Not all models so divide the cloud.

Particle settling rates - Method of calculation of the particle settling rates and the particle diameters (diameter, density, shape) and atmospheric parameters (temperature, pressure) used.

Winds - Discussion of the wind inputs (single wind vector, winds varying with height, shear factors, etc.) and their determination and application.

Transport - Movement of a wafer from its initial position in the cloud to its landing point, as determined by the winds and the particle settling rates.

The output submodel produces exposure-rate and/or exposure contours, or other related information, from the wafer-landed positions. These outputs vary among the models from simple danger zones to the time history of particle sizes and radionuclides landing at various points. The submodel characteristics are the following:

Summing - Addition and decay of the radioactivity from each landing wafer such that the exposure rate or exposure can be computed for any time or time interval.

Contours - Procedures for construction of exposure-rate or exposure
contours or other outputs from the results of summing."

Little additional terminology is needed beyond the observations given here:

"W" is used for total-energy yield derived from nuclear processes, smaller yields are given in kilotons (KT) and large yields in megatons (MT). The elevation of the device is designated as the height-of-burst (HOB) and the HOB scaled for yield to 1 KT is a scaled-height-of-burst (SHOB). Detonations fired below a surface are specified in terms of the depth-of-burst (DOB). The intersection of a perpendicular through the center of the device and the earth is designated ground zero (GZ), or surface zero (SZ) for water.

Models are designated by their common acronym in this digest and these are translated as:

RAND	The RAND Corporation
WSEG	Weapon Systems Evaluation Group, DoD
NREC	National Resource Evaluation Center, Office of Emergency Planning
DIA	Defense Intelligence Agency
CDRP	Civil Defense Research Project, University of California
TOR	Technical Operations Research
Ford	Ford Instrument Company, Sperry Rand Corporation
NRDL	U.S. Naval Radiological Defense Laboratory
LRL	Lawrence Radiation Laboratory, University of California
USWB	U.S. Weather Bureau
RADFO	Radiological Forecast, U.S. Navy
DROPSY	Developed at Sandia Corporation from a LASL model
LASL	Los Alamos Scientific Laboratory, University of California
SIDAC	Single Integrated Damage Analysis Capability
PROFET	Prediction of Fallout at Early Times
DELFIC	Department of Defense Land Fallout Interpretive Code
CIVIC	Civilian Vulnerability Indicator Code

Classifications to describe the various ways used to predict where fallout from a given device will settle into a fallout pattern are arbitrary. In this

digest of fallout predictors the analytical apparatus utilized by different agencies was initially divided into four groups of models. These are also the same as the initial groupings made for models used in the DASA symposium in 1962 (Reference 3-2). These were:

1. Manual solutions intended to be used in on-going field problems,

2. Field mobile, hard-wired electronic plotters based on submodels,

3. Single-wind, operations models used in analytic exercises and gaming,

4. Models based on physics and meteorology that combine a multilayer
   wind field with cloud layers or "discs" in an electronic solution.

An analysis of the models was carried out after the symposium "homework" was returned, and they were grouped as shown in Table 3-1.

Table 3-1. 1962 Fallout pattern predictors by functional groups.

Manual (Field) Models	Portable Electronic Plotters	Operations Analysis Models	Physical Processes Forecasts
Signal Corps (Army)[a]	Dropsy (Sandia)[a]	WSEG (DoD)[a]	NRDL-D (NRDL)[a]
RADFO (Navy/NATO)[a]	AN/GMQ-18 (NBS/AEC)[a]	RAND (surface)[c]	Miller-Anderson (NRDL-D)[a]
USWB (NTS-unit)[a]	AN/GMQ-21[a,d] (Ford-T)	DIA (EM-1)[b]	Ford-T
US Army		NREC (Emergency Planning)[a]	LRL-b (barographic, surface)[c]
		TOR (DNA)[a]	
		CDRP (Civil Defense)[a]	LRL-h (hydrographic, cratering)[c]

[a]Support agency/predecessor model.

[b]Subsequent application of methods.

[c]Featured parameter.

[d]Model discontinued before completion.

Classifying models by functional characteristics indicates how they operate
and tells something about their relative size but leaves unexplored any compari-
son of their adequacy in prediction of fallout deposition. A more useful grouping
is based upon the way that models handle wind effects, upon the location of the
site at which particles are deposited. Two basic approaches were recognized early
as distinguishing among models in their predictions of fallout deposition. There
were models that used a single effective fallout wind (EFW) vector and models
that partitioned the cloud vertically into segments or "discs" which are acted
upon by winds prevailing at the disc altitude. Some of the "disc throwers"
allowed program compensation for wind changes during the transport process.
Models compared via the "homework" problems at the 1962 symposium are listed in
Table 3-2 according to whether EFW or multilayer winds are used in predicting
the site of fallout deposition.

Table 3-2. Fallout model classes compared by USNRDL-DASA
symposium (Reference 3-3).

Single Effective Fallout Wind (EFW)	Disc Transport, Multiwind Models
RAND	FORD-T
DIA	NRDL-D
NREC*	USWB
ARMY	DROPSY
WSEG	TOR
RADFO	AN/GMQ-18
OCD-Miller[a]	SIG-C[b]
TINCAN[a]	LRL-b
	LRL-h
	DELFIC[a]

*Changes hourly during transport.

[a]From Reference 3-4 and 1962 homework problems III, V, VIII, and XI.

[b]Signal Corps model.

27

Determination of the genesis of individual models is tenuous because few were documented during assembly and many changes were made before the models were documented. Serry and Polan (Reference 3-3) gave their views, which are shown in Table 3-3.

Once a fallout model was developed to output a particular parameter other investigators claimed copies of it so that they could develop output parameters for their interests. A succession of "generations" of versions of fallout models evolved, and in some cases the entire fallout model was incorporated into a code. Examples of successions of model diversion and their stated objectives are given in schematic format in Figure 3-1. The transition from one version of a model to a point at which it is recognized as a different model is tenuous unless a model is bodily incorporated into a code. An example of this latter transition is the movement of the DELFIC derivative, SEER III, into the damage assessment code DACOMP, and further into CIVIC, for collateral damage assessment. The number of modifications and of direct incorporation into codes is large. The faults of fallout models then become the faulty input to a larger code.

REFERENCES

3-1. Anon. "Working Papers Compiled for the USNRDL-DASA Fallout Symposium Project Week of 17 September 1962." Compilation of Radioactive Fallout Prediction Systems. Volumes 1, 2, and 3.

3-2. Polan, M. An Analysis of the Fallout Prediction Models Presented at the USNRDL-DASA Fallout Symposium of September 1962. Volume I: Analysis, Comparison, and Classification of Models. USNRDL-TRC-68. Ford Instrument Company, Long Island City, New York, 8 September 1966.

3-3. Seery, C.J. and M. Polan. An Analysis of the Fallout Prediction Models Presented at the USNRDL-DASA Fallout Symposium of September 1962. Volume II: Analysis, Comparison, and Evaluation of Model Predictions. NRDL-TRC-68-59. Ford Instrument Division, Sperry Rand Corp., Long Island City, New York, 28 August 1968.

3-4. Seery, C.J. Fallout Model Analysis. TRC-68-46. Ford Instrument Division, Sperry Rand, Long Island City, New York, November 1968.

Table 3-3. Output formats for homework problems from 1962 USNRDL-DASA symposium

MODEL (NF)[a]	20T Fission — Sandy Loam Soils — Wind 10 Knots	20T Fission — Sandy Loam Soils — Wind 43 Knots	1.2KT Fission — Winds Vary by Altitude — Sands	1.2KT Fission — Winds Vary by Altitude — Clay Soils	1.2KT Fission — Wind 20 Knots Sandy Loam	100KT Fission — Sandy Loam — Wind 10 knots	100KT Fission — Sandy Loam — Wind 40 Knots	IMT Fission — Sandy Loam — Varied Winds	10MT Fission — Sandy Loam Soil — Wind 10 Knots	10MT Fission — Sandy Loam Soil — Wind 40 Knots	1SMT Half Fission — Winds Vary by Altitude — Coral	1SMT Half Fission — Winds Vary by Altitude — Sandy Loam
FORD-T (Computer Maps) 25%[b] (900)	$\underline{DR}$ Contours Infinite Exposure Contours	$\underline{DR}$ Contours Infinite Exposure Contours	$\underline{DR}$ Contours					$\underline{DR}$ Contours Infinite Exposure Contours	$\underline{DR}$ Contours	$\underline{DR}$ Contours Infinite Exposure Contours	$\underline{DR}$ Contours	
NRDL-D (Computer Maps) (1,093)	$\underline{DR}$ Contours	$\underline{DR}$ Contours	$\underline{DR}$ Contours		$\underline{DR}$ vs DWD	$\underline{DR}$ Contours	$\underline{DR}$ Contours	$\underline{DR}$ Contours	$\underline{DR}$ Contours	$\underline{DR}$ Contours	$\underline{NP}$ Contours	$\underline{DR}$ Contours
RAND (Manually Drawn Contours) (1,200)								$\underline{DR}$ vs DWD $\underline{R}$ vs DWD	$\underline{DR}$ vs DWD	$\underline{DR}$ vs DWD	$\underline{DR}$	
USWB SSI (1,025)	$\underline{DR}$ Contours (Manual) Tab Data $\underline{DR}$ vs DWD	$\underline{DR}$ Contours (Manual) Tab Data $\underline{DR}$ vs DWD	$\underline{DR}$ Contours (Manual) Tab Data $\underline{DR}$ vs DWD			$\underline{DR}$ Contours (Manual) Tab Data $\underline{DR}$ vs DWD	$\underline{DR}$ Contours (Manual) Tab Data $\underline{DR}$ vs DWD	$\underline{DR}$ Contours (Manual) Tab Data $\underline{DR}$ vs DWD	$\underline{DR}$ Contours (Manual) Tab Data $\underline{DR}$ vs DWD	$\underline{DR}$ Contours (Manual) Tab Data $\underline{DR}$ vs DWD	Tab Data $\underline{DR}$ vs DWD	
DROPSY (2,585)	Infinite Exposure Contours	Infinite Exposure Contours	Infinite Exposure Contours			Infinite Exposure Contours	Infinite Exposure Contour		Infinite Exposure Contours	Infinite Exposure Contours	Infinite Exposure Contours	
DIA[c] (1,100)	$\underline{DR}$ vs DWD data GZ radius	$\underline{DR}$ vs DWD data GZ radius	$\underline{DR}$ vs DWD data GZ radius			$\underline{DR}$ vs DWD data GZ radius	$\underline{DR}$ vs DWD data GZ radius	$\underline{DR}$ vs DWD data GZ radius	$\underline{DR}$ vs DWD data GZ radius	$\underline{DR}$ vs DWD data GZ radius	$\underline{DR}$ vs DWD data GZ radius	
TOR (870)								2-day Exposure Contours Tab Data	2-day Exposure Contours Tab Data	2-day Exposure Contours Tab Data	2-day Exposure Contours Tab Data	
NREC (Computer Maps'd) (2,500)							Tab Data $\underline{DR}$ vs DWD	Tab data $\underline{DR}$ vs DWD	Tab Data $\underline{DR}$ vs DWD	Tab Data $\underline{DR}$ vs DWD	Tab Data $\underline{DR}$ vs DWD	
Problem No.	VI	VII	III	IV	IIIa	VIIIa	VIII	IX	V	V	I	II

[a] Normalization factor for grounding fallout particles from atmosphere.

[b] Fission radioactivity in cloud stem as percent.

[c] Area calculated at Ford Instrument by the equation

$$A = 1.05 \ast ab/4$$

Where a = CWD (cross-wind distance)
       b = DWD · R (downwind distance + radius @ GZ)
       R = Radius at GZ

[d] Computer maps received much later than Tab Data; hence, they were not displayed as contour plots. The maps were used to check the $\underline{DR}$ vs DWD and area curves at H+1 hr.

Table 3-3. Output formats for homework problems from 1962 USNRDL-DASA symposium (continued)

| MODEL (NF)[a] | 20T Fission, Sandy Loam Soils | | 1.2KT Fission, Winds Vary by Altitude | | Wind 20 Knots | 100KT Fission, Sandy Loam | | | | 1MT Fission, Sandy Loam | | 100MT Fission, Sandy Loam Soil | | | 15MT Half Fission, Winds Vary by Altitude | |
	Wind 10 Knots	Wind 40 Knots	Sands	Clay Soils	Sandy loam	Wind 10 Knots		Wind 40 Knots	Varied Winds	Sandy Loam	Wind 10 Knots	Wind 10 Knots		Coral	Sandy Loam
AN/GMQ-18 (-)			DR Contours Tab Data DR vs DMD			DR Linear Plots Tab Data DR vs DMD		DR Linear Plots Tab Data DR vs DMD		DR Contours Tab Data DR vs DMD	DR Linear Plots Tab Data DR vs DMD	DR Linear Plots Tab Data DR vs DMD		DR Contours Tab Data DR vs DMD	
Signal Corps 90% (689)			DR & 14=50 Exposure Contours Tab Data DR vs DMD			DR Contours Tab Data DR vs DMD		DR Contours Tab Data DR vs DMD		DR & 14=50 Exposure Contours Tab Data DR vs DMD	DR Contours Tab Data DR vs DMD	DR Contours Tab Data DR vs DMD		DR & 14=50 Exposure Contours Tab Data DR vs DMD	
Army (-)	Infinite Exposure Contours 150 R	Infinite Exposure Contours 150 R	Infinite Exposure Contours 150 R			Infinite Exposure Contours 150 R		Infinite Exposure Contours 150 R		Infinite Exposure Contours 150 R	Infinite Exposure Contours 150 R	Infinite Exposure Contours 150 R		Infinite Exposure Contours 150 R	
WSEG (2,400)	Results For 20KT Not 0.02KT		Tab Data DR vs DMD		DR vs DMD	Tab Data DR vs DMD		Tab Data DR vs DMD	DR vs DMD	Tab Data DR vs DMD	Tab Data DR vs DMD	DR vs DMD	DR vs DMD	Tab Data DR vs DMD	
LRL-II (2,700)										Infinite Exposure Contours	Infinite Exposure Contours				
ADFO [e] (-)	2-day Exposure Contours		2-day Exposure Contours			2-day Exposure Contours		2-day Exposure Contours		2-day Exposure Contours	2-day Exposure Contours				
DELFIC					DR vs DMD		DR vs DMD DR Contours		DR vs DMD DR Contours			DR vs DMD			
OCD-MILLFR							DR vs DMD [f] R vs DMD [f]		DR vs DMD R vs DMD			DR vs DMD R vs DMD			
TINCAN					DR vs DMD		DR vs DMD DR Contours R vs DMD		DR vs DMD DR Contours R vs DMD			DR vs DMD R vs DMD			
Problem No.	VI	VII	III	IV	IIIa	VIII	VIIIa	IX	Va	V	Y	XI	XIa	I	II

[e] Exposure contour generated at Ford Instrument according to procedures of Ref. 4-2

[a] GZ surface

[f] DR contours = 14-day radiation exposure dose in external roentgens.

30
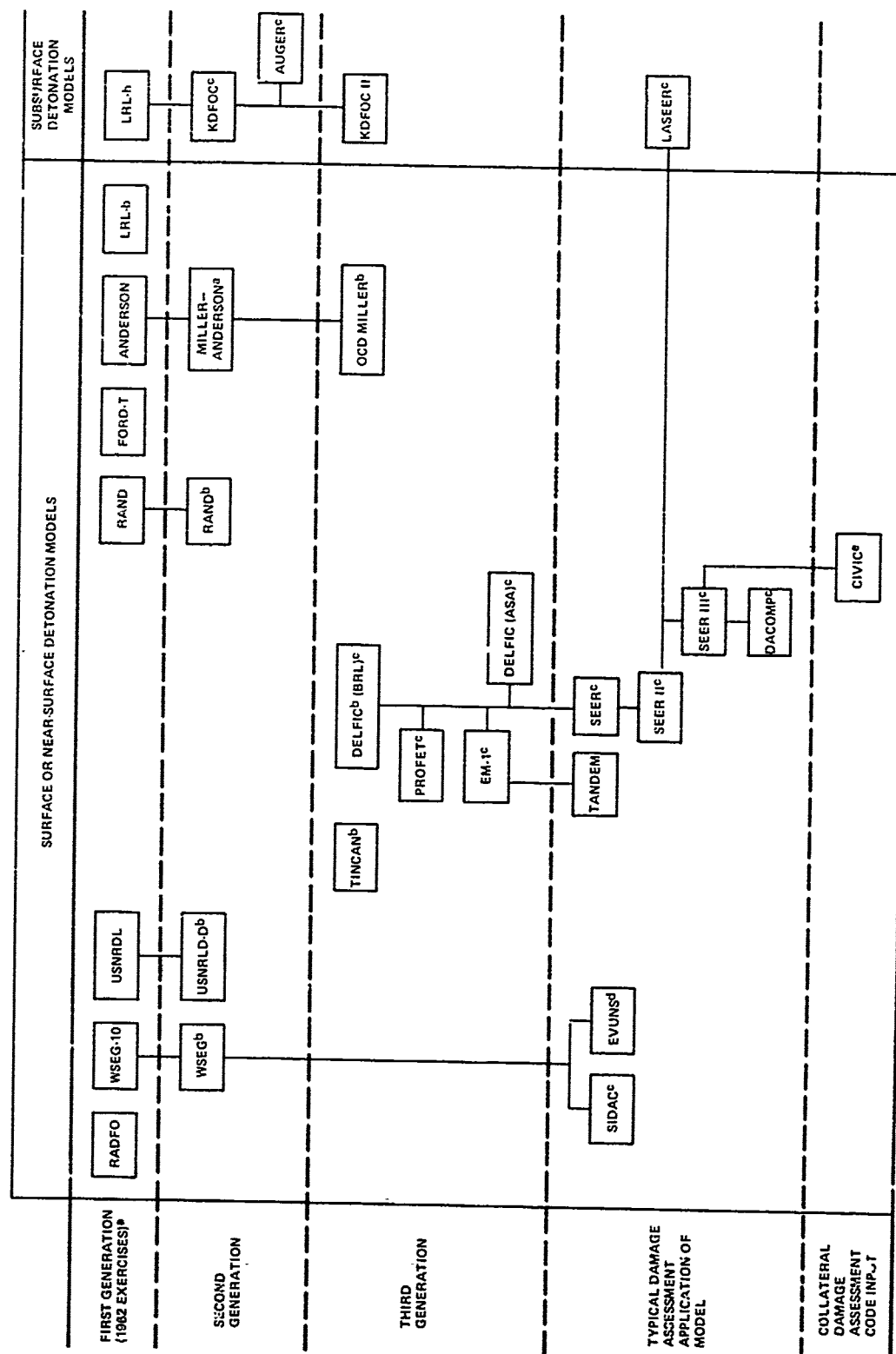
Figure 3-1. Evolution of selected fallout forecasting models, 1962-1978.

3-5. Norment, Hillyer G., "Analysis and Comparison of Fallout Prediction Models," Atmospheric Science Associates, P.O. Box 307, Bedford, Massachusetts 01730, Unpublished.

3-6. Wong, P.W. and H. Lee, "Utilization of the SEER Fallout Model in a Damage Assessment Computer Program (DACOMP)," DNA 3608F, Stanford Research Institute, Menlo Park, CA 94025, February 1975.

3-7. Wong, P., H. Lee and K. Klemba, "Civilian Vulnerability Indicator Code (CIVIC)," DNA 4224F, SRI International, Menlo Park, CA 94025, December 1976.

SECTION 4

COMPARATIVE FALLOUT PATTERN PREDICTIONS FROM COMMON INPUT DATA

The diversity of models, and their varied output, in dose rate (DR) contours, originates in their having specific and limited objectives. Since they were first documented, some of the models were embodied into other larger models and later into codes, such as the various damage assessment codes (e.g., SEER, LASEER, SIDAC, DACOMP, TANDEM) and recently further extended their predictions into collateral damage estimating (CIVIC, TANDEM, MARS). Projections of the differences in predicted radiation field intensity and in fallout pattern locations can be translated into entirely different levels of damage/collateral damage and casualty projections. By starting with the basic fallout predictor modules, an understanding can be developed of how their applications produce divergent predictions. The basic differences in data handling among WSEG, DELFIC, and KDFOC, for example, will remain incorporated in their extrapolated outputs. Utilization of their different outputs as input to subsequent code modules will cause the code outputs to also differ. Assembling DELFIC, incorporated materials from several of the NRDL and TECH/OPS models plus data from 56 shots of 6 different test series into just the modules for CLOUD RISE and INITIAL CONDITIONS alone (References 4-1, 4-2). Output curves from DELFIC were used in EM-1 as basic fallout parameters in graphs for hand calculations (Reference 4-3). The EM-1 graphs were incorporated into the damage assessment code TANDEM.

A standardized input is needed by which the determination of differences can be defined in predicted fallout pattern radiation intensity areas, and azimuth. A selection of predicted output parameters are collected here from fixed parameter inputs, those given in the 1962 USNRDL-DASA Fallout Symposium "homework problems" (Reference 4-4). These selected outputs range over yields from 20 T to 15 MT, at ground zero, from coral to sands, to clay soils, and within a variety of wind conditions (Table 3-3).

OUTPUT IN DOSE RATES

For direct comparisons on the reproduced data, an arbitrary H+1 hr dose rate of 10-30 R/hr was selected as the reference external gamma dose range,

33

producing a nominal infinite dose "emergency level" exposure of $\leq$ 150 R in the event that fallout pattern crossing is halted during transit. A limited number of reproductions are shown in this document; however, enough examples are included that illustrations of many hypothetical cases can be worked out among yields, winds, and fallout predictor modules.

H+1 hr DR contour plots are reproduced that cover weapon yields from 1.2 KT to 10 MT with intermediate steps of 100 KT and 1,000 KT. The predicted shapes of DR contours generally retain a "family resemblance" across yield range and winds aloft. The range of dose rates at 1.2 KT is relatively uniform among the contours a few miles downwind. The 10 R/hr lines for three of five patterns end close together on Figure 4-1, but the areas included in 10 R/hr are substantially different among 1.2-KT patterns. The difference in input between Figures 4-2 and 4-3, at 100-KT yield, is a single speed wind vector of 10 knots in the former and 40 knots in the latter. At higher wind speeds, the Signal Corps predicts a 10 R/hr hot spot the others do not show. At 10 MT, a suggestion of a 50 R/hr hot spot is indicated in the FORD-T pattern (Figure 4-7) and not in the others. Other effects of wind velocity upon pattern shape are readily seen in the paired Figures 4-2, 4-3, and 4-7, 4-8.

Comparison of Figures 4-2, 4-3, and 4-4 show the ancestoral inheritance DELFIC got from the NRDL models. In Figures 4-5 and 4-6, the differences in scale between DELFIC and NRDL-D outputs can be seen through WSEG which is common to both figures. SEER, which was created to reproduce DELFIC output, is shown to scale with DELFIC and WSEG (Figure 4-6). Versions of SEER have been prominent in codes for damage assessment.

OUTPUT IN ACCUMULATED ROENTGENS

Radioactivity infinite dose contours for the military operations fallout models (RADFO, ARMY, and DROPSY), Figures 4-9 through 4-12, are not immediately comparable to the R/hr contours of the earlier discussed model outputs. The effects of 10- and 40-knot winds are shown between Figures 4-10 and 4-11.

The military operations model DR contours are comparable to the DR contours of the other models at identical times, and that comparison is shown in Figure 4-12 for eight predictors.

Differences in relative size of areas included in a given infinite R or R/hr contour are not readily seen from contoured patterns. They are shown in Figures 4-22 through 4-25 as square miles, for easier interpretation.

DR Distance Comparisons

Downwind projections of the 30 R/hr contour, for weapons yielding 1.2 KT to 10 MT, were led by the WSEG output in seven of the eight cases reproduced (Figures 4-13 through 4-20). The ratios between the shortest and the WSEG distance, to the 30 R/hr contour, varied from $1\frac{1}{2}$ to 9. At 100-KT yield the spread between the closest and most distant 30 R/hr contour was more than at 1 KT or at 1,000 KT. The nearest 30 R/hr contour varied with wind velocity and yield among the twelve models. In five of the eight illustrations the shortest distance to the 30 R/hr contour was predicted by a different model, with two models being closest to GZ twice each. The quantitative characteristics of the models in downwind forecasts of the distance to a particular dose rate contour are emphasized by DR-DWD plots. The original reports carry a variety of figures for model outputs that were not reproduced and they should be consulted for additional predictions with fewer than 5 models included per figure.

Comparisons of Areas Enclosed by Contours

Comparison of the areas predicted to be enclosed by specific DR contours is possible from Figures 4-21 through 4-30. Areas predicted to be enclosed by the 30 R/hr contour, Figures 4-21 through 4-24, differed among the output from eight models by factors from 5 to 15 times. The variation in predicted area was greatest at 1 KT and smallest at 1 MT for the 30 R/hr contour, with an intermediate variance at 100 KT. The seven models compared in Figures 4-25 through 4-27 are derivatives of the eight models represented by output in plots of DR versus squared miles. The newer model's output is dimensioned in squared kilometers. Log_{10} outputs are shown in Figures 4-25, 4-26, and 4-27.

The linear variations in area included by the 30 R/hr contour are similar in variance from figure to figure, respectively, having ratios of 9-1/2 to 12-1/2. In the range among output areas from an underground 1 KT at a scaled DOB of 5.0, the predicted areas differ in size within the 30 R/hr contour by a factor of 13, which is little difference from the range among surface shots. Not all of the newer fallout prediction models are competent under the conditions imposed in the runs of Figures 4-21 through 4-28, as indicated by their omission from the figures. Additional comparisons are possible from Figures 4-29 and 4-30 which show the relative infinite dose versus enclosed area or downwind distance to contours. In all of the parameters, the original unclassified material should be consulted for detail of the output generated by a particular model, even though the cited report may be classified for other reasons than the fallout model.

REFERENCES

4-1   Norment, H.G., W.Y.G. Ing and J. Zuckerman. Department of Defense Land Fallout Prediction System. Volume II - Initial Conditions. DASA-1800-II. Technical Operations Research, Burlington, MA September 1966.

4-2   Huebsch, I.O., S.H. Cassidy, H.G. Norment, J. Zuckerman and T.W. Schwenke. Department of Defense Land Fallout Prediction System, Volume III - Cloud Rise. U.S. Naval Radiological Defense Laboratory, San Francisco, CA 94135 and Technical Operations, Inc., Burlington, MA, May 1967.

4-3   Norment, H.G., Analysis and Comparison of Fallout Prediction Models. DNA 4569F. Atmospheric Science Associates, Bedford, MA 01730, March 1977.

4-4   Seery, J.C. and M. Polan. An Analysis of the Fallout Prediction Models presented at the USNRDL-DASA Fallout Symposium of September 1962. Volume II: Analysis, Comparison, and Evaluation of Model Predictions. NRDL-TRC-68-59. Ford Instrument Division, Sperry Rand Corp., Long Island City, NY, August 1968.

4-5   Seery, J.C. Fallout Model Analysis TRC-68-46. Ford Instrument
       Division, Sperry Rand, Long Island City, NY, November 1968.

4-6   Lee, H., P.W. Wong and S.L. Brown. Seer II: A New Damage Assessment
       Fallout Model. DNA 3008F, Stanford Research Institute, Menlo Park,
       CA 94025. May 1972.

Figure 4-1.   DR contour plots, cases III and IV - 1.2 KT
              (Reference 4-4).

37

Figure 4-2. DR contour plots, case VIII – 100 KT (Reference 4-4).

NRDL-D

3,000R/HR 1,000R/HR 500R/HR 300R/HR 100R/HR 50R/HR 30R/HR

USWB

300R/HR 100R/HR 30R/HR 10R/HR

SIGNAL CORPS

850R/HR 400R/HR 200R/HR 100R/HR 50R/HR 25R/HR 10R/HR 6R/HR 3R/HR

DIA

1,000R/HR 100R/HR 10R/HR 1R/HR

0   24   ST. MILES

Figure 4-3. DR Contour plots, case IX – 100 KT (Reference 4-4).

39

DELFIC

TINCAN
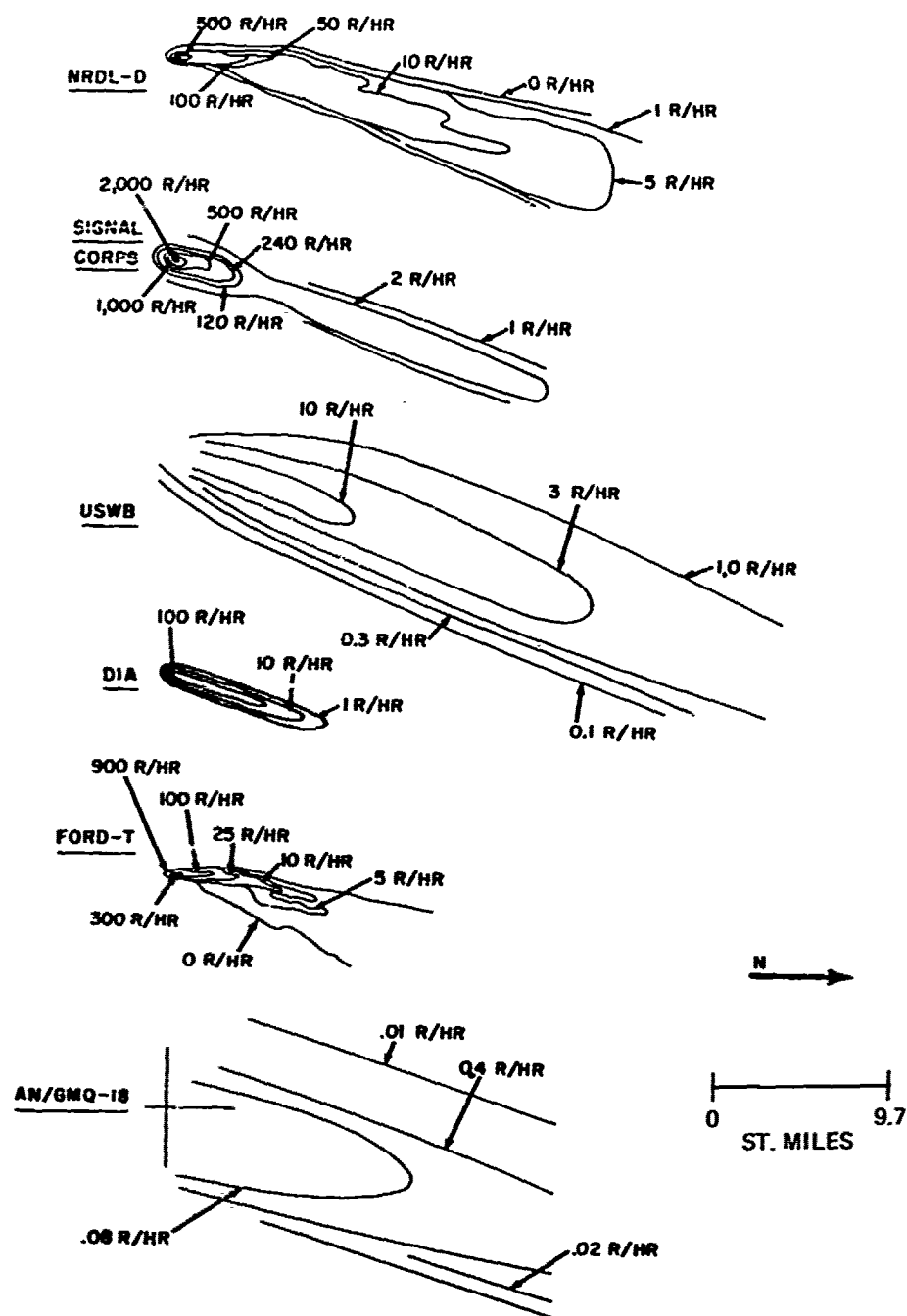
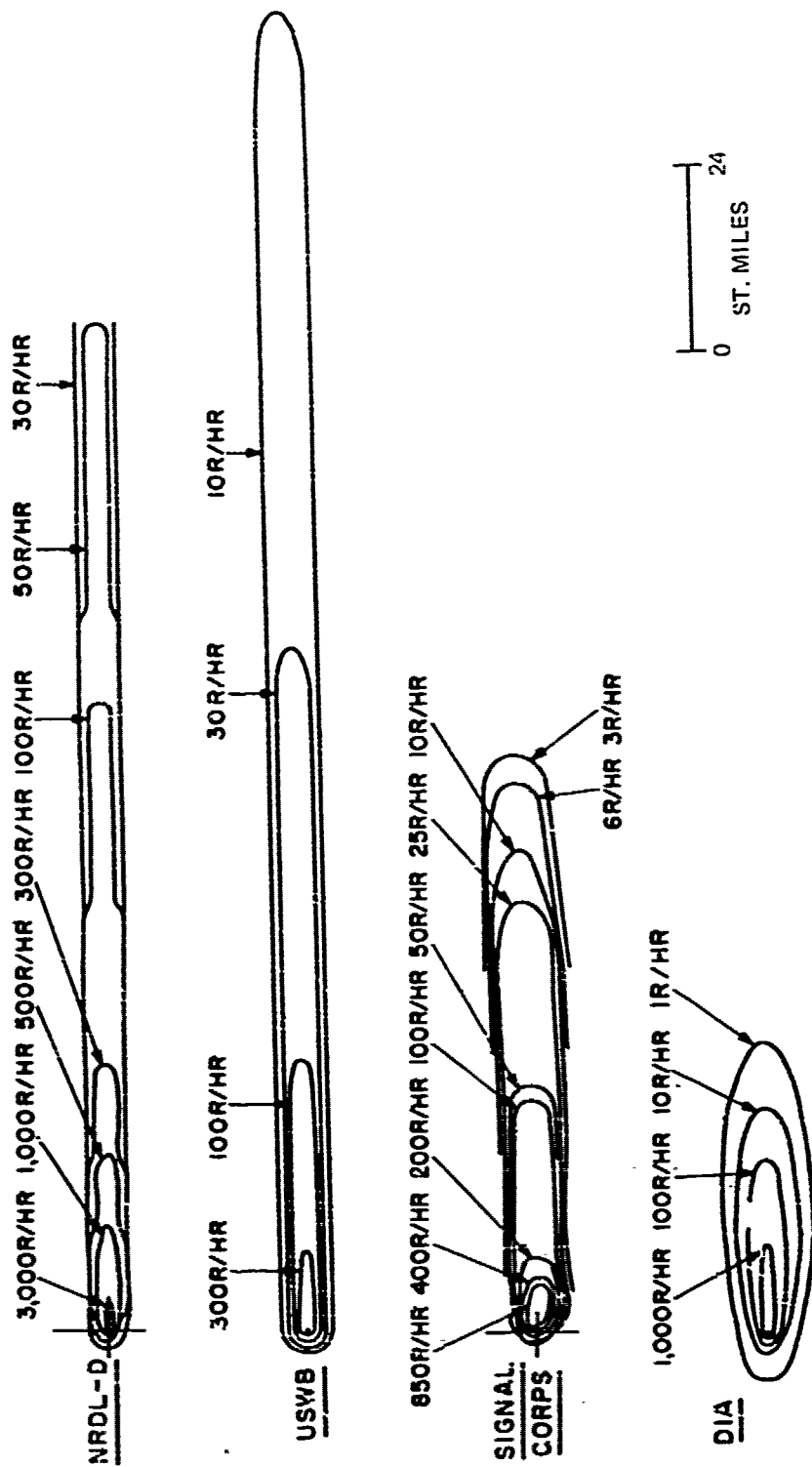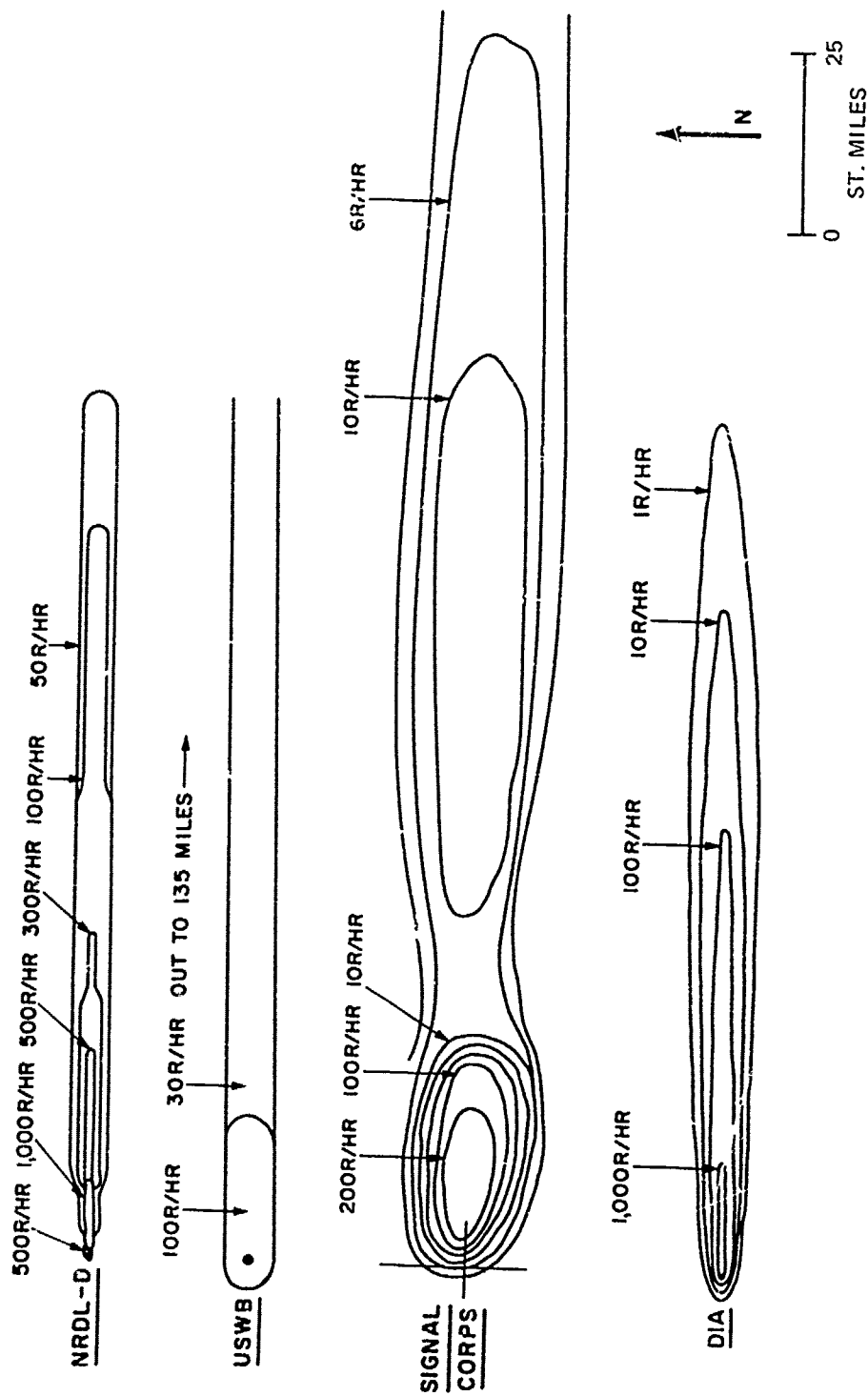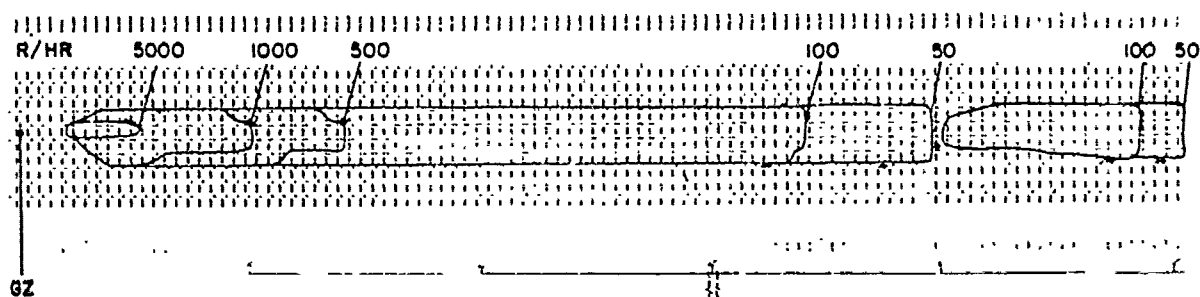Figure 4-4. DR contour plots, case VIII - 100 KT (Reference 4-5).

Figure 4-5. DR contour plots, case V - 1 MT (Reference 4-4).

The figure shows DR contour plots for multiple models:

FORD-T: 300 R/HR, 100 R/HR, 50 R/HR, 25 R/HR, 5 R/HR

WSEG: 1,000 R/HR, 300 R/HR, 100 R/HR, 30 R/HR, 10 R/HR, 3 R/HR

NRDL-D: 5,000 R/HR, 3,000 R/HR, 1,000 R/HR, 100 R/HR, 5 R/HR, 50 R/HR, 500 R/HR, 300 R/HR, 30 R/HR, 5 R/HR

RAND: 500 R/HR, 300 R/HR, 100 R/HR

USWB: 1,000 R/HR, 300 R/HR, 100 R/HR, 30 R/HR, 10 R/HR, 3 R/HR

AN/GMQ-18: 50 R/HR, 10 R/HR, 2 R/HR

SIGNAL CORPS: 6,000 R/HR, 200 R/HR, 400 R/HR, 200 R/HR, 100 R/HR, 50 R/HR, 35 R/HR

DIA: 1,000 R/HR, 100 R/HR, 10 R/HR, IR/HR

Scale: 0 to 170 ST. MILES

N (north arrow)

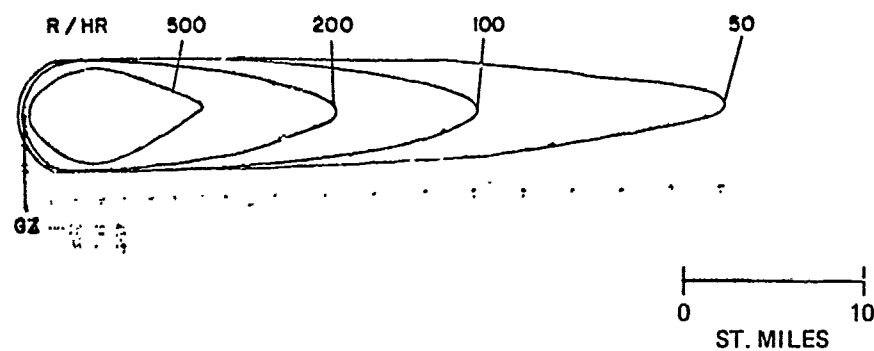Figure 4-6. Fallout pattern comparisons for 1-MT case V winds - DR contour plot (Reference 4-6).
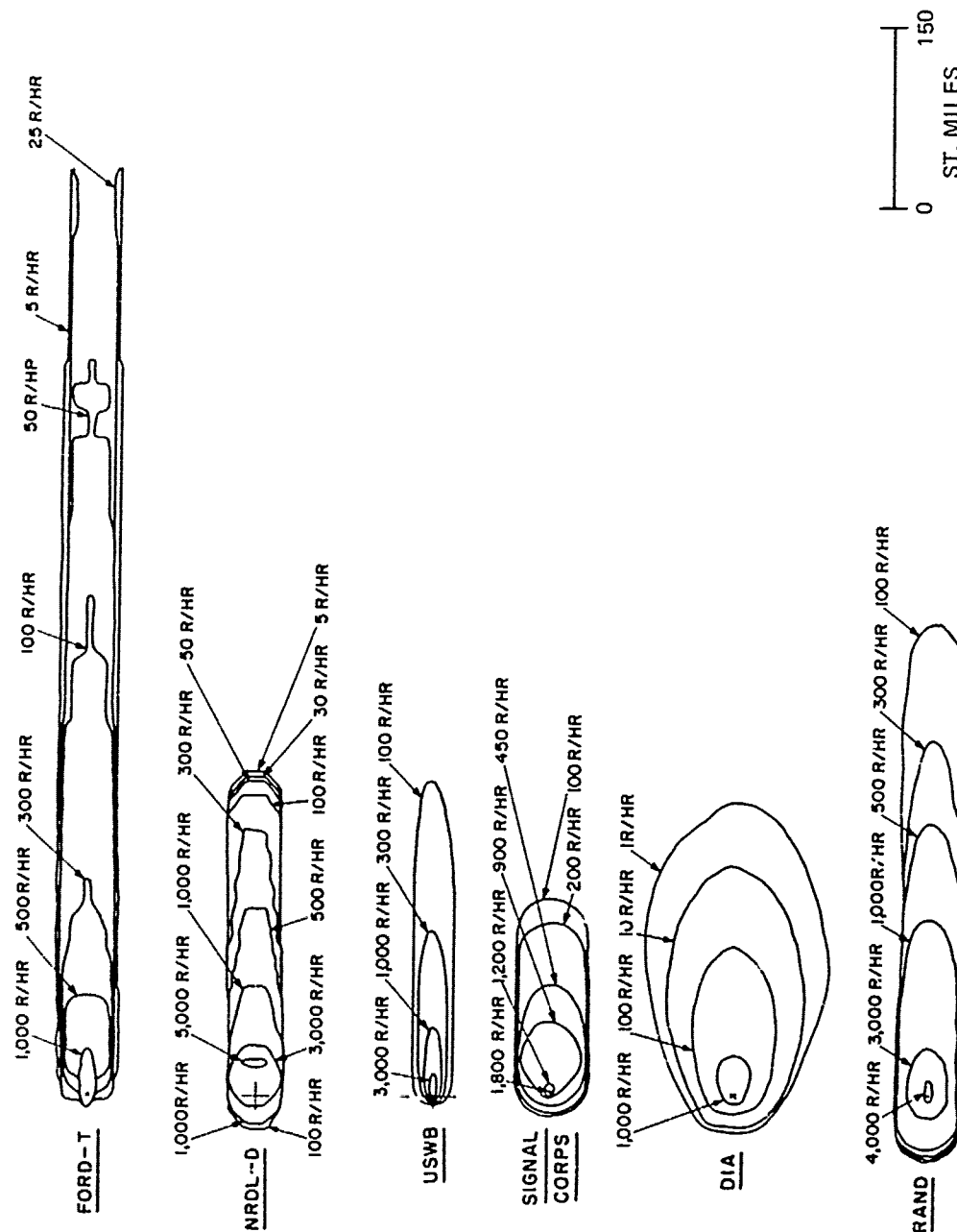
Figure 4-7. DR contour plots, case X - 10 MT (Reference 4-4).

43

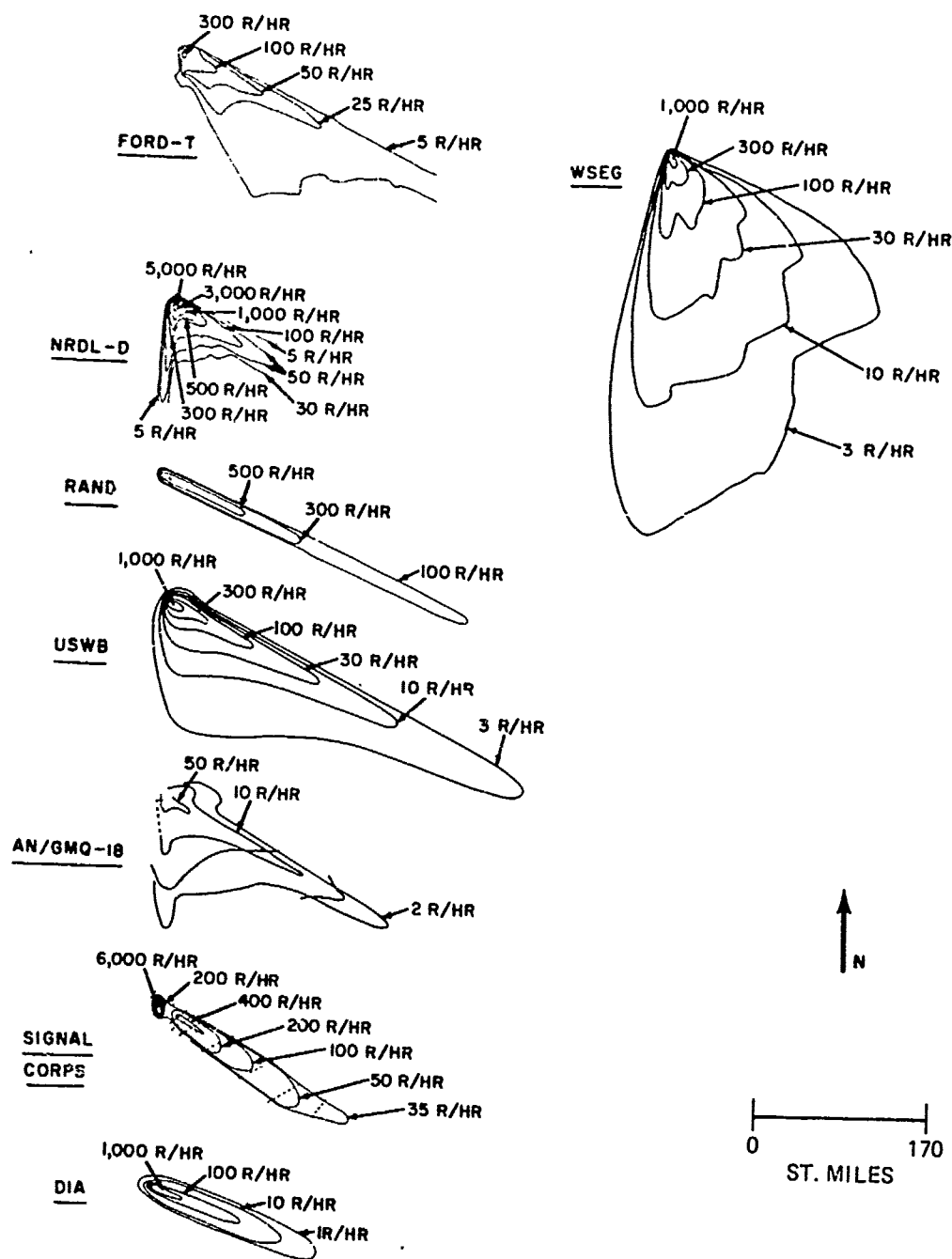Figure 4-8. DR Contour plots, case XI - 10 MT (Reference 4-4).

44
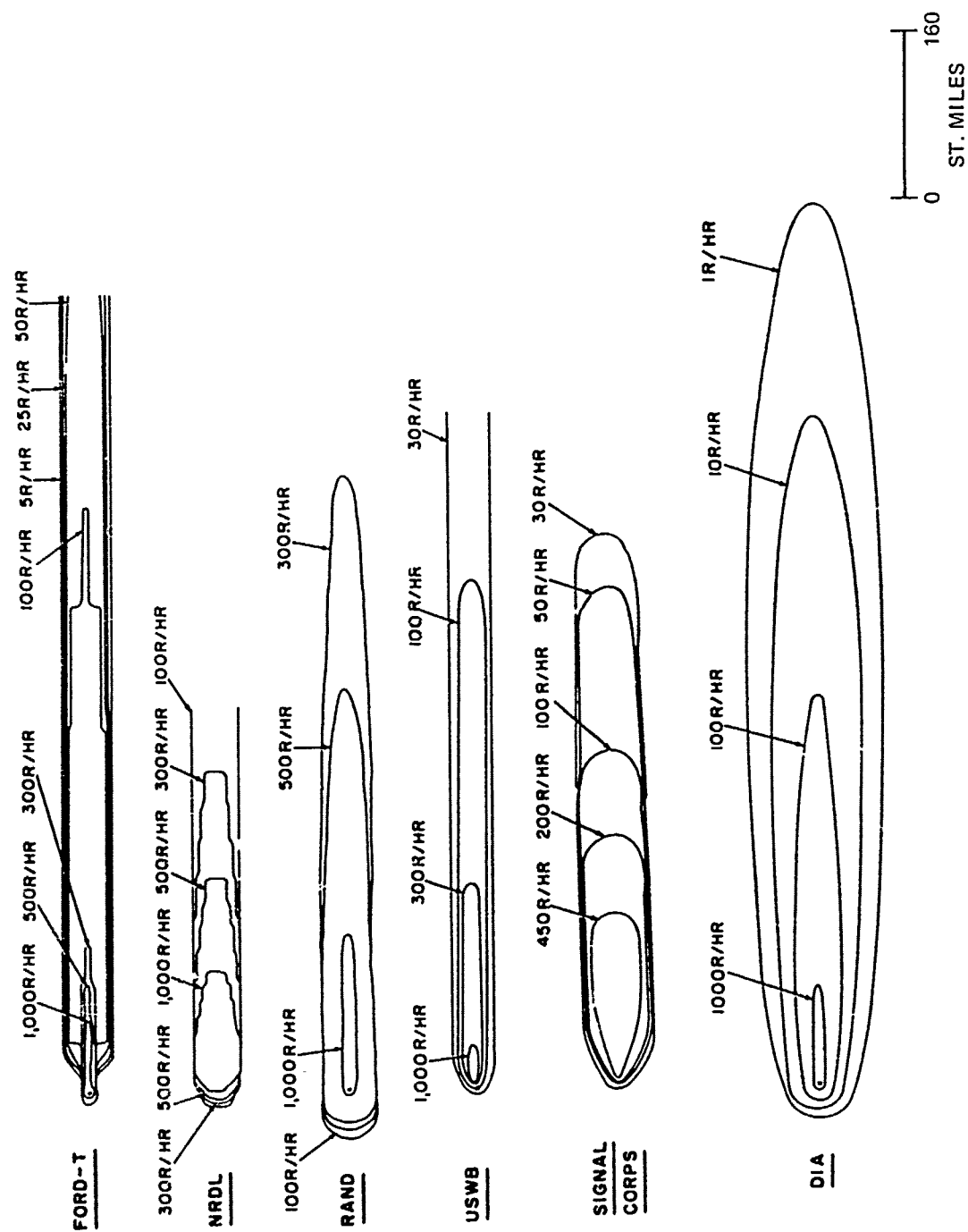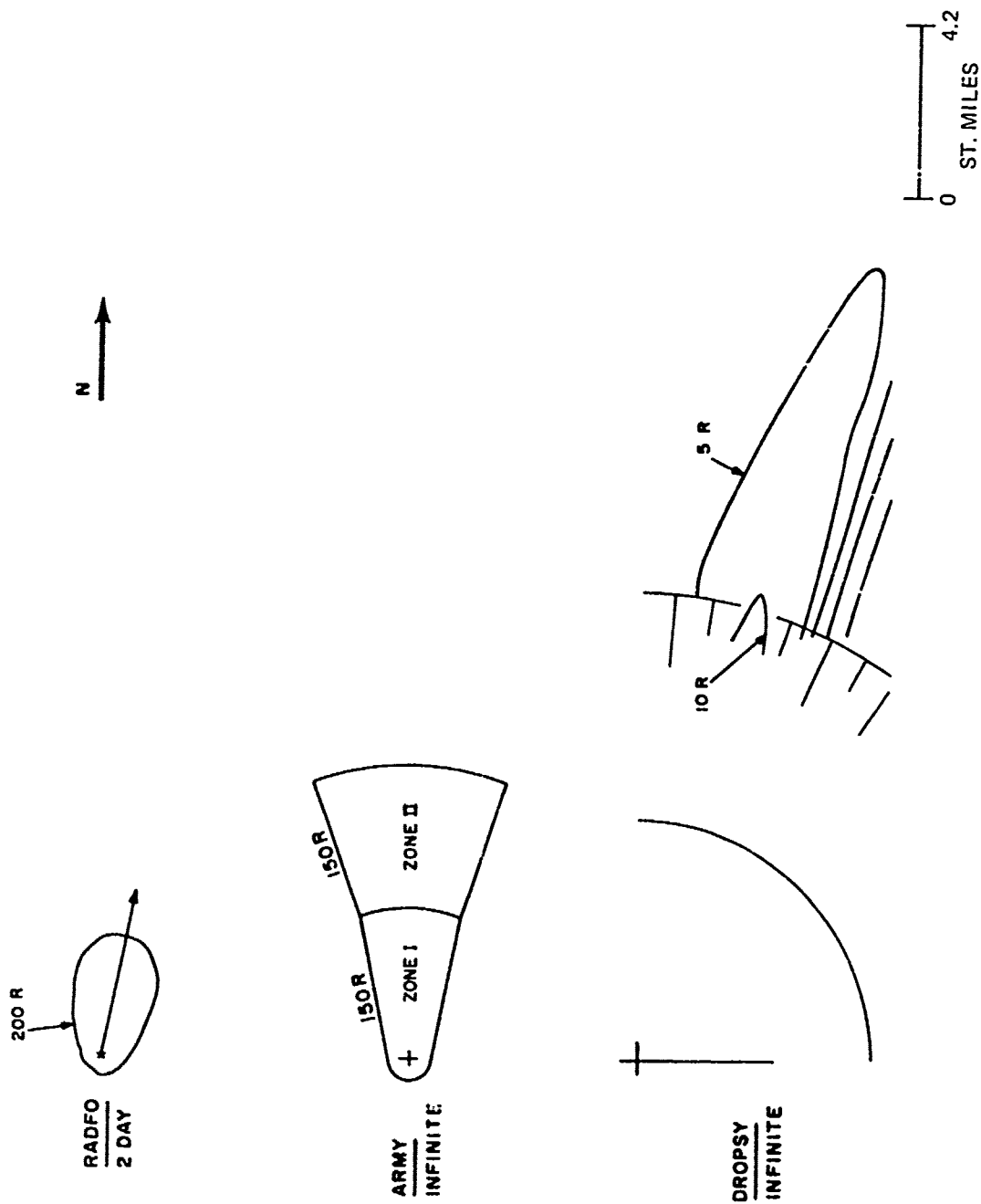
Figure 4-9. Two-day and infinite time exposure plots, cases III and IV - 1.2 KT (Reference 4-4).
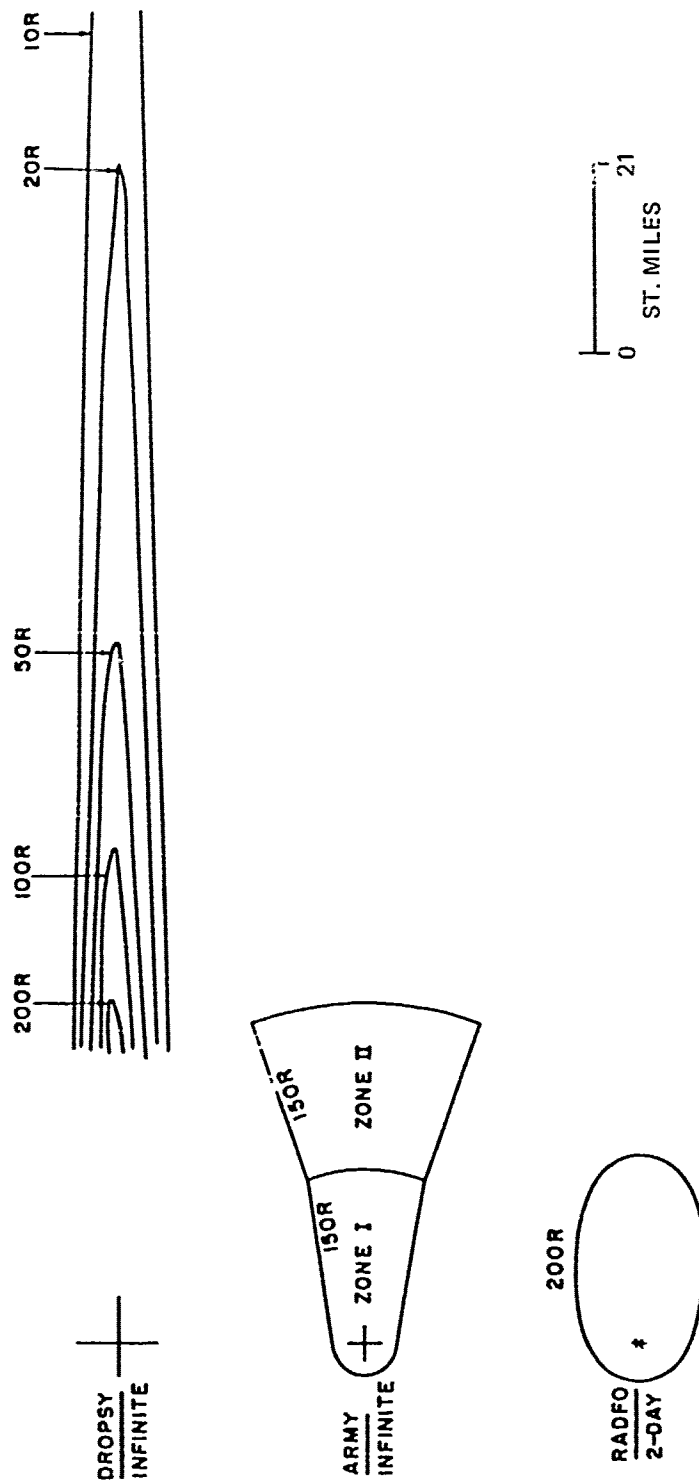
Figure 4-10. Two-day and infinite time exposure plots, case VIII – 100 KT (Reference 4-4).
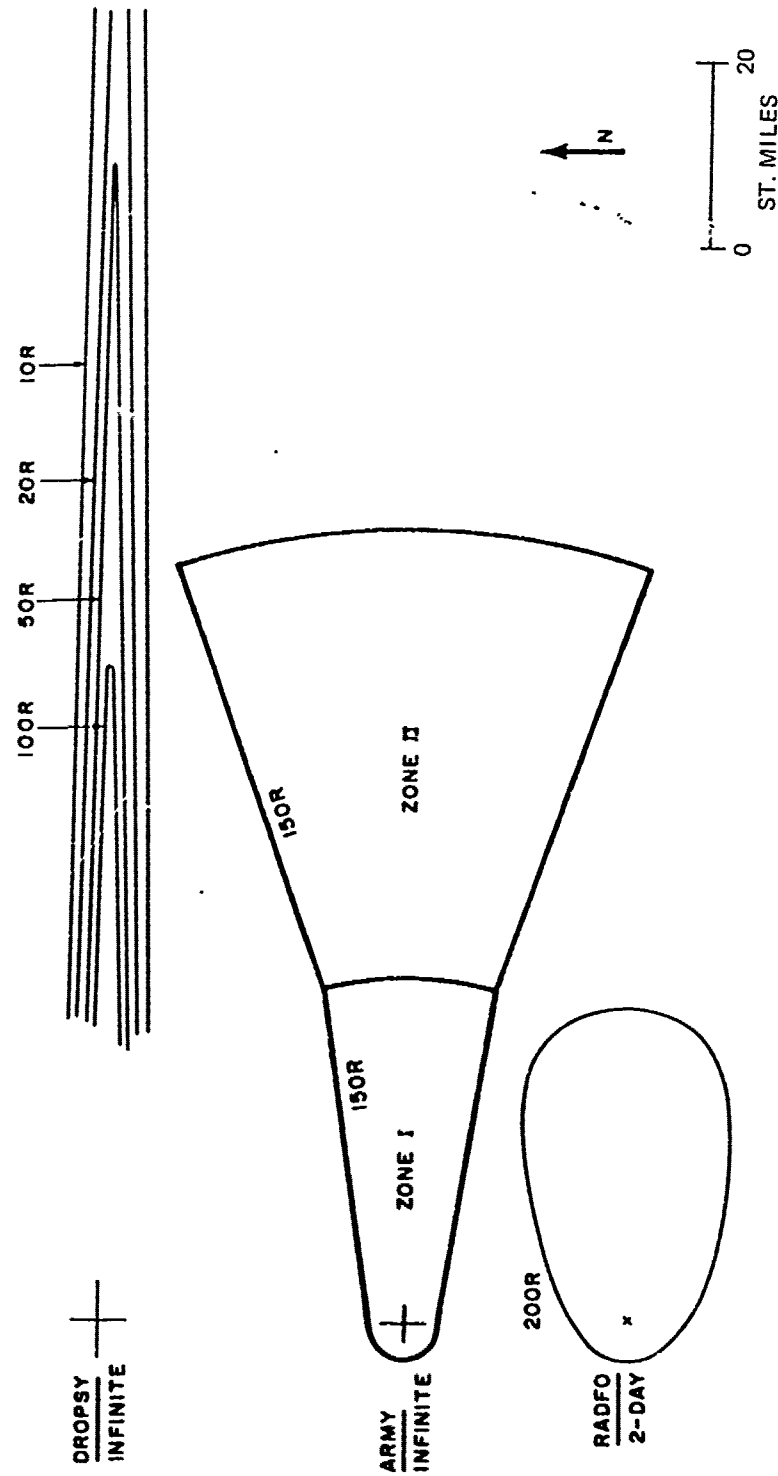
Figure 4-11. Two-day and infinite time exposure plots, case IX - 100 KT (Reference 4-4).

47
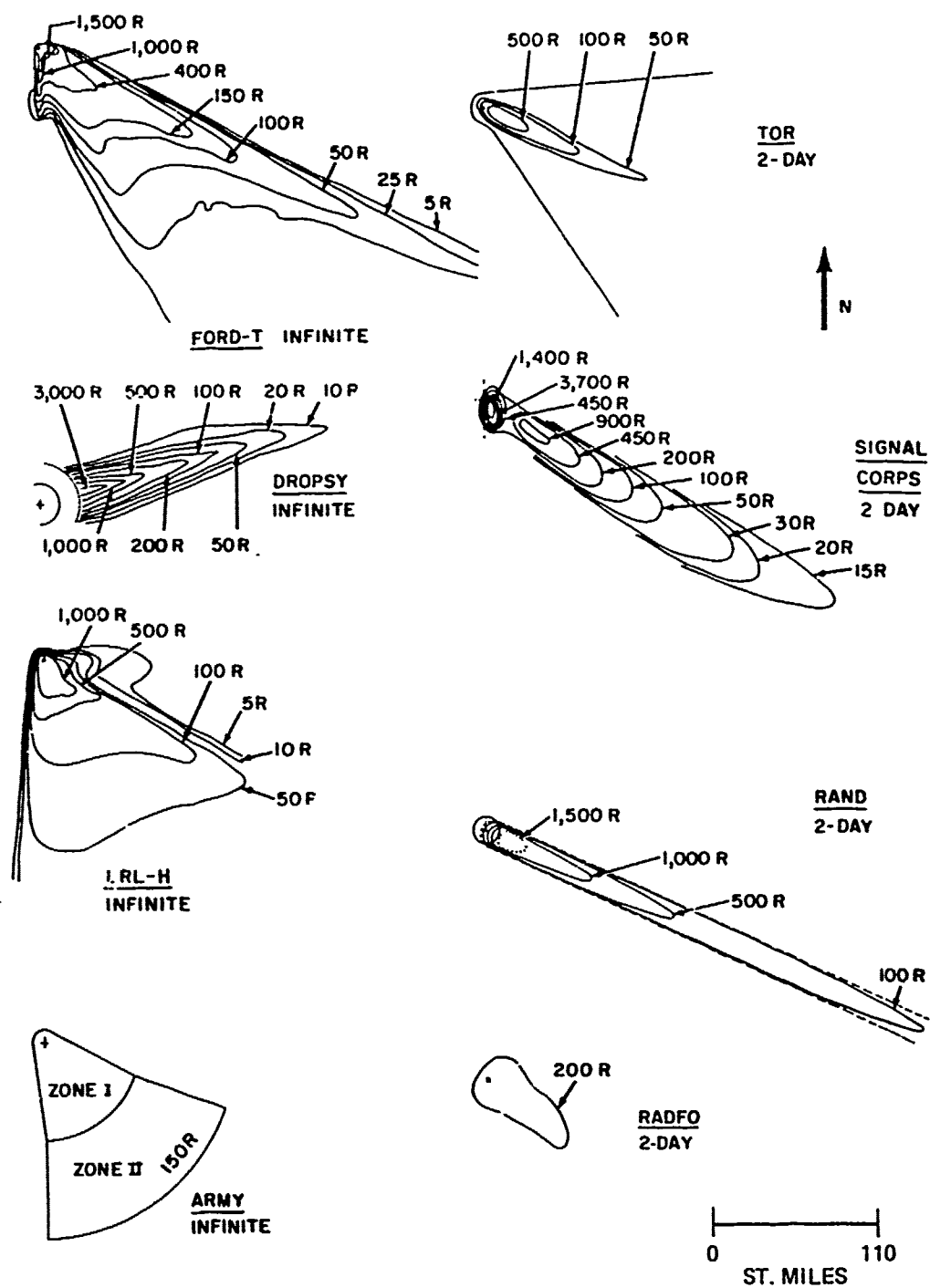
Figure 4-12. Two-day and infinite time exposure plots, case V -
1 MT   (Reference 4-4).
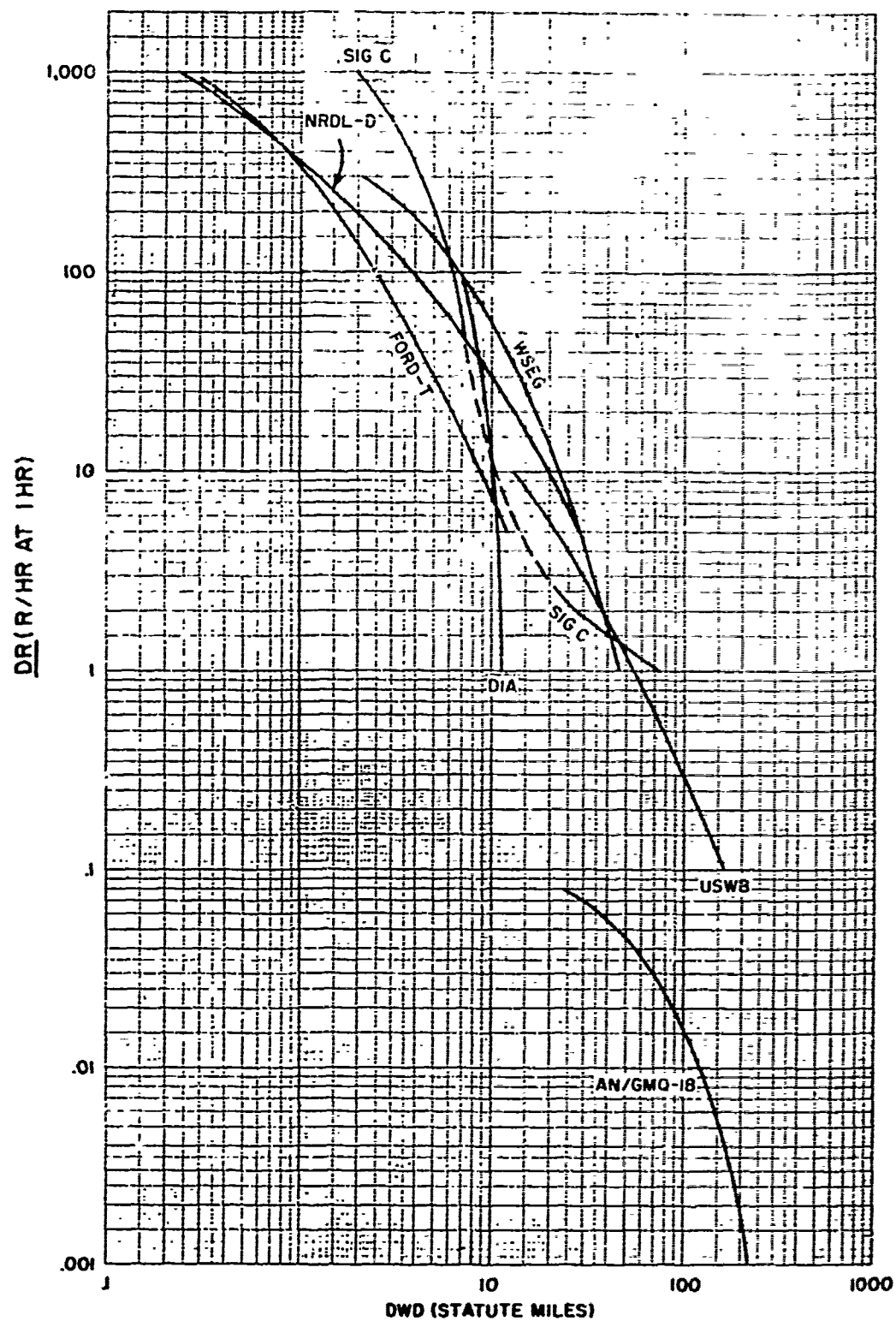
Figure 4-13.   DR as a function of DWD, cases III and IV - 1.2 KT
(Reference 4-4).
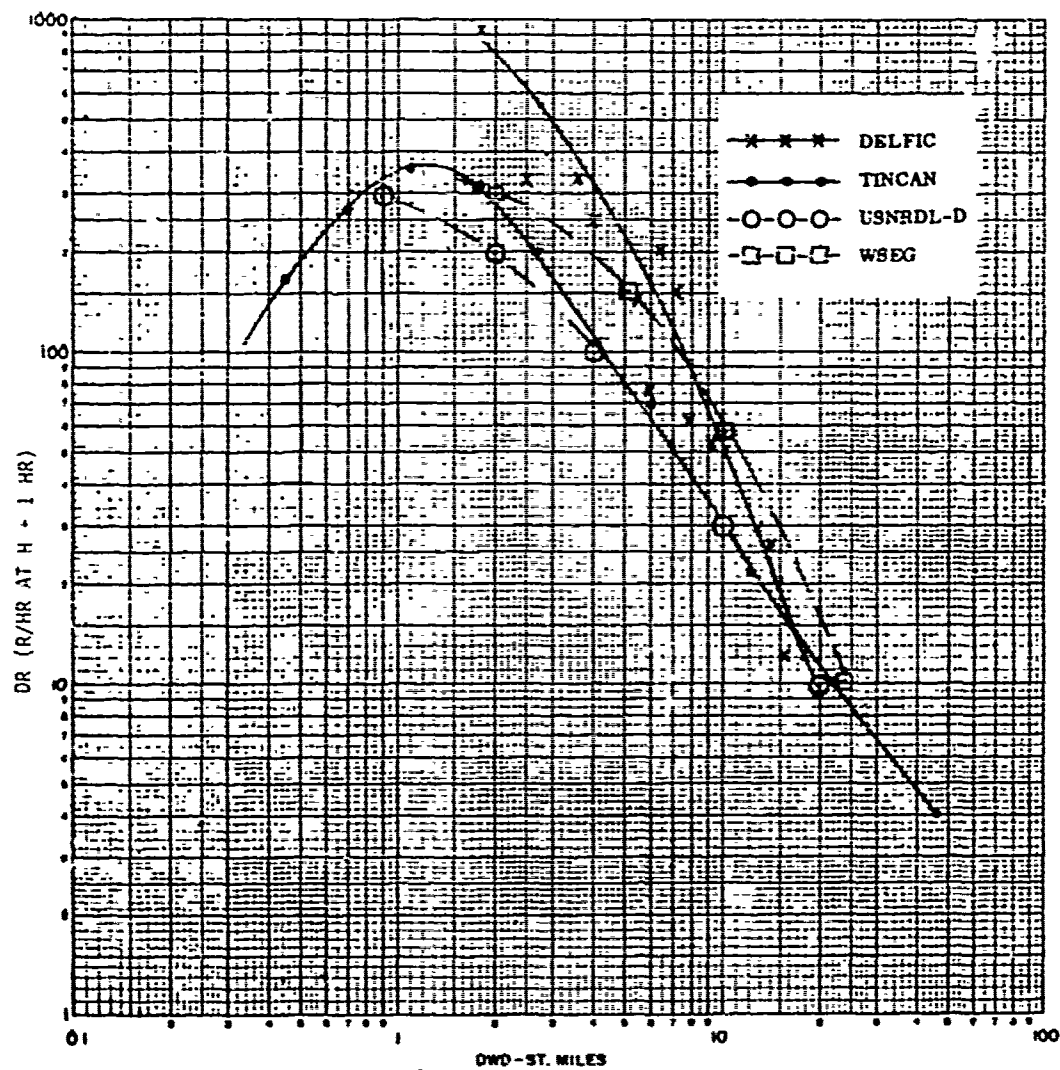
Figure 4-14. DR as a function of DWD, case III - 1.2 KT
(Reference 4-5).
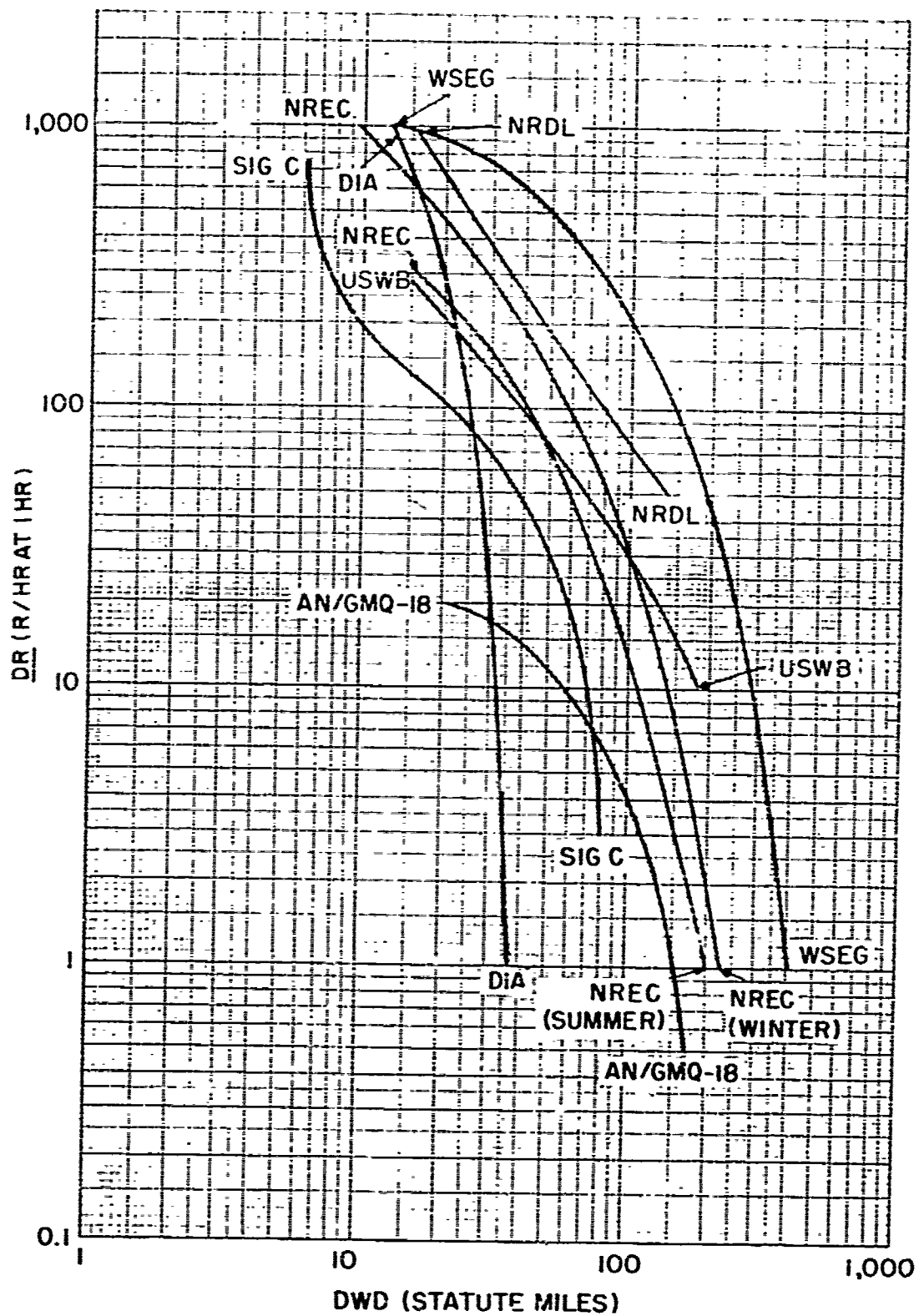
Figure 4-15. DR as a function of DWD, case VIII-100 KT
(Reference 4-4).
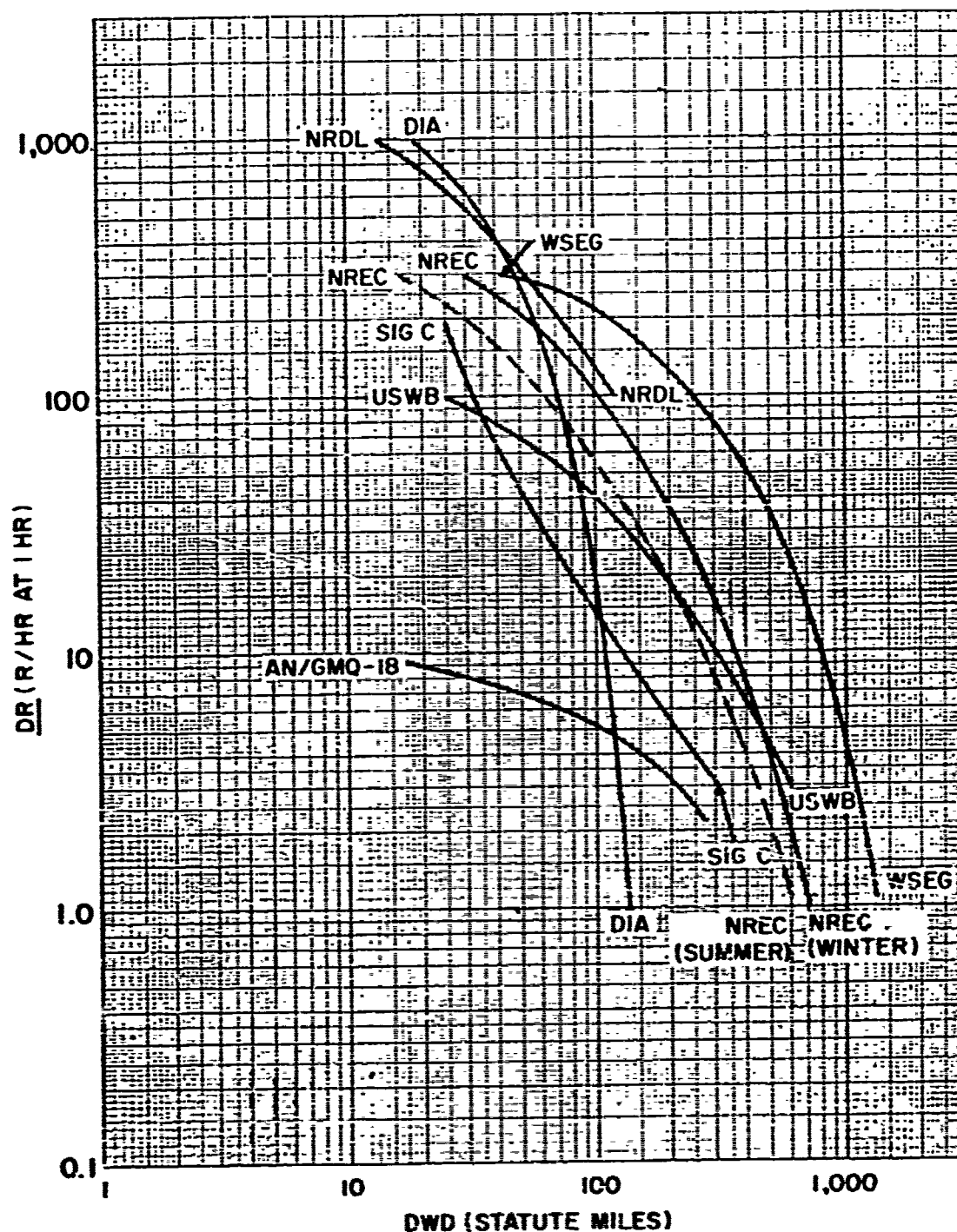
Figure 4-16.   DR as a function of DWD, case IX - 100 KT
(Reference 4-4).
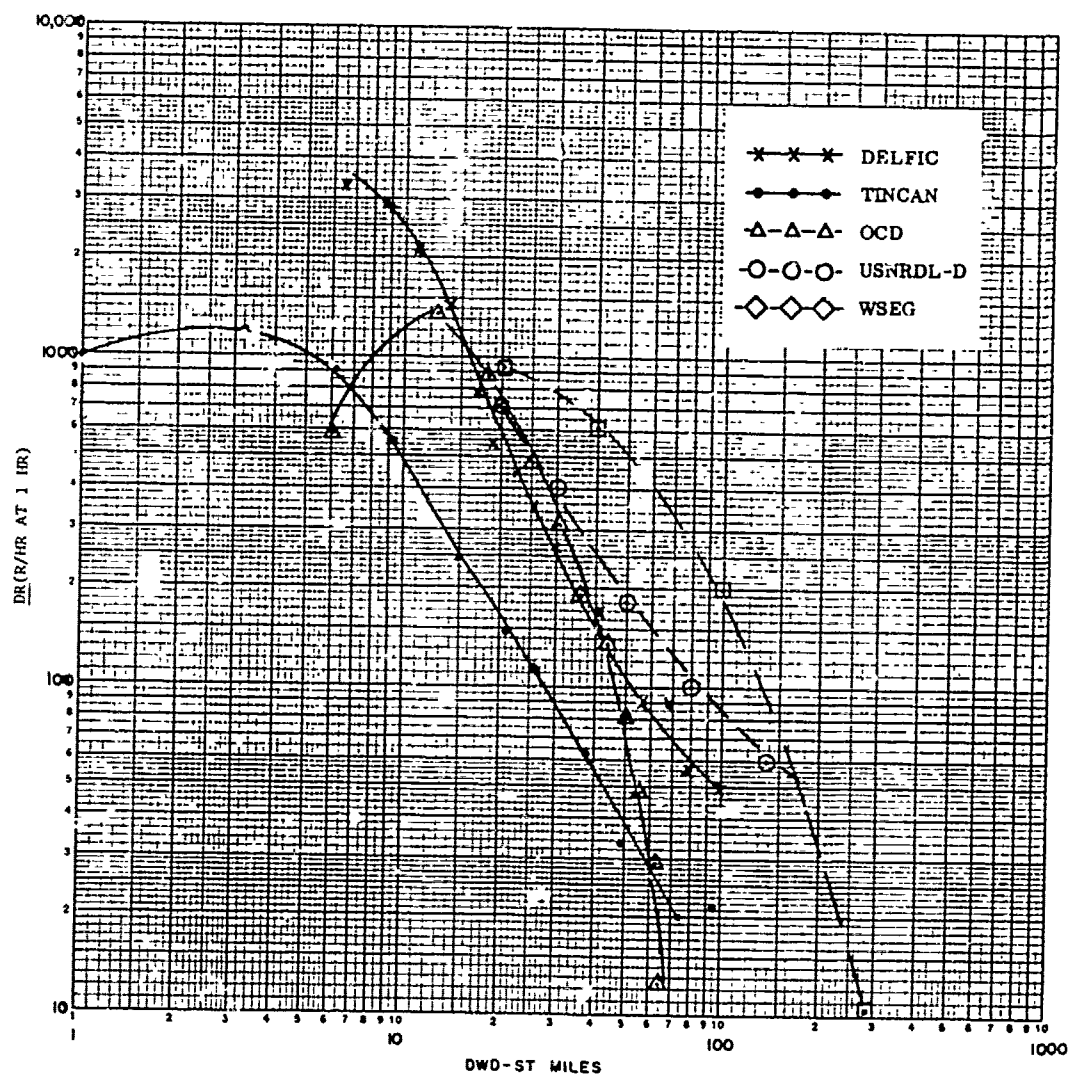
Figure 4-17.　DR as a function of DWD, case VIII - 100 KT
(Reference 4-6).

Figure 4-18.   DR as a function of DWD, case VI - 1 MT
(Reference 4-4).

54
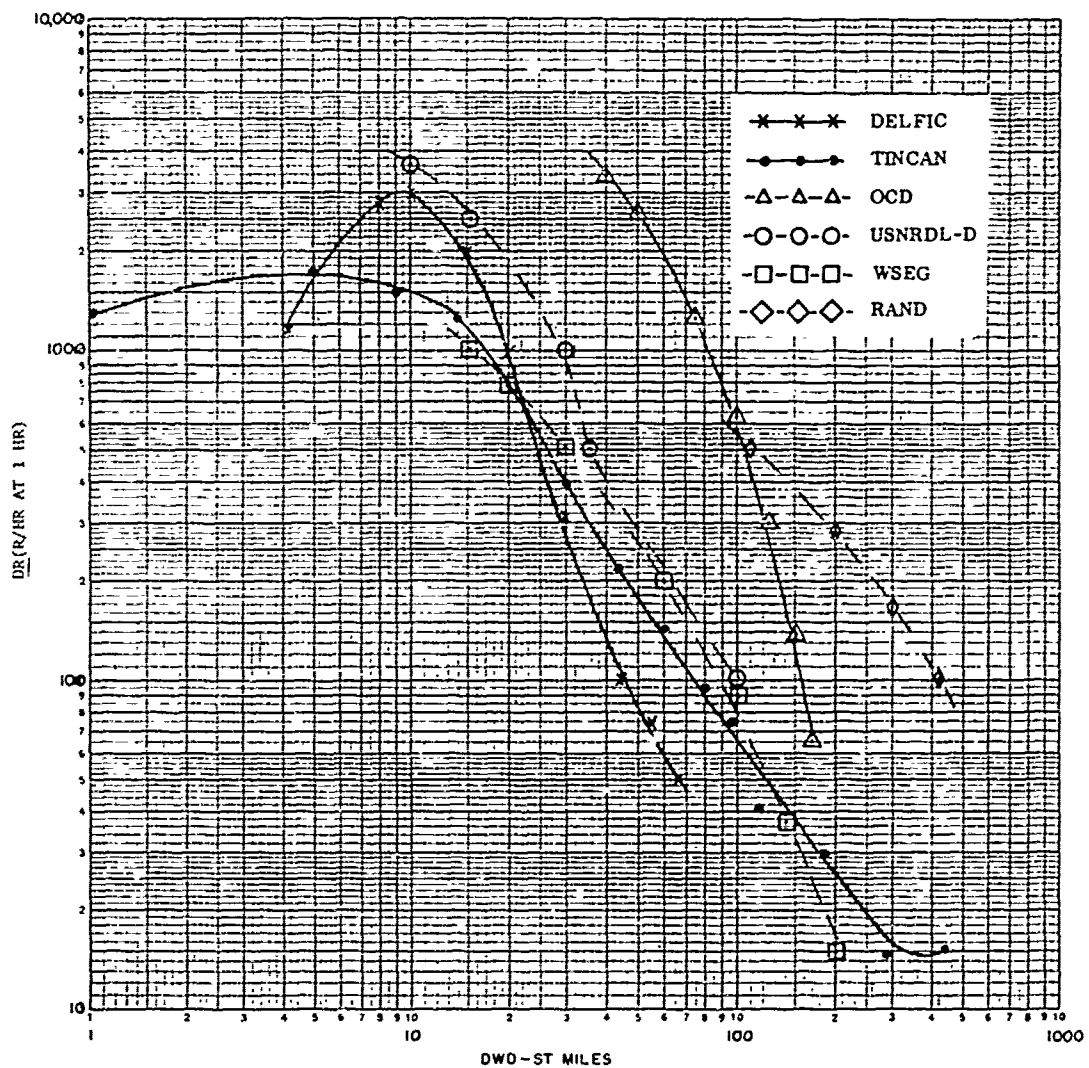
Figure 4-19. DR as a function of DWD, case V - 1 MT
(Reference 4-6).

55

Figure 4-20.   DR as a function of DWD, case XI - 10 MT
              (Reference 4-6).
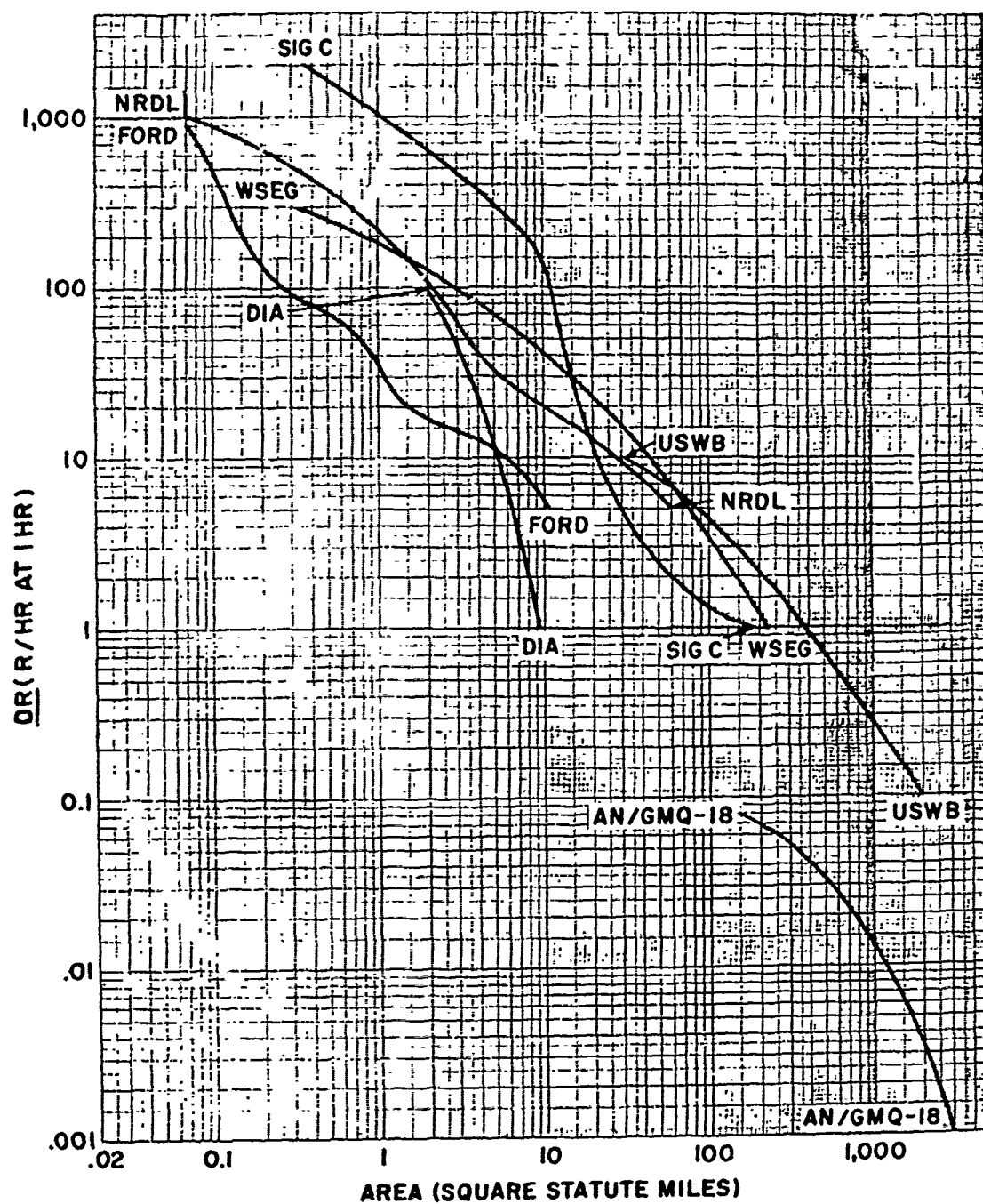
Figure 4-21. Area enclosed by exposure rate contours as a function of DR cases III and IV - 1.2 KT (Reference 4-4).
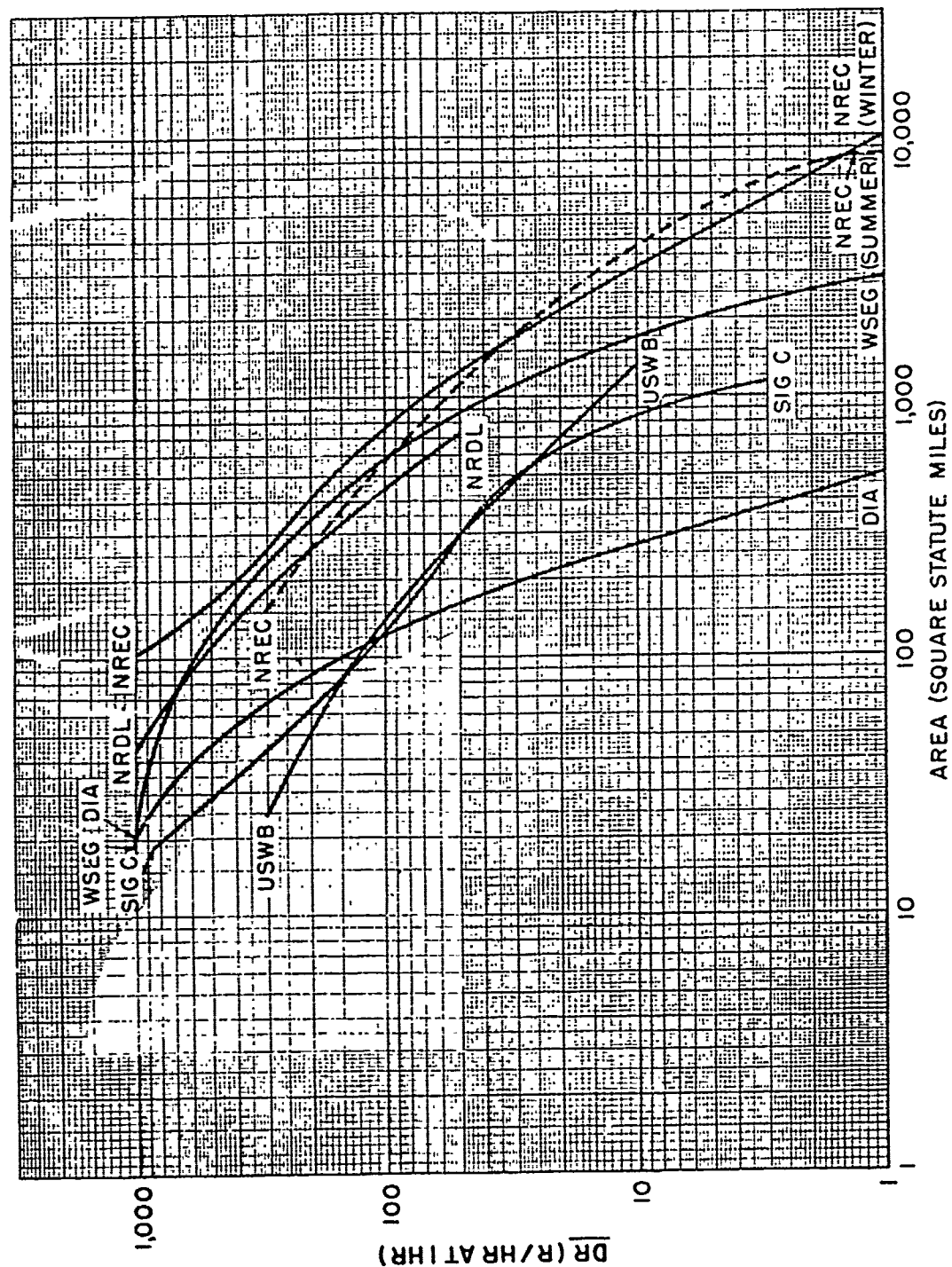
Figure 4-22. Area enclosed by exposure rate contours as a function of DR, case VIII - 100 KT (Reference 4-4).
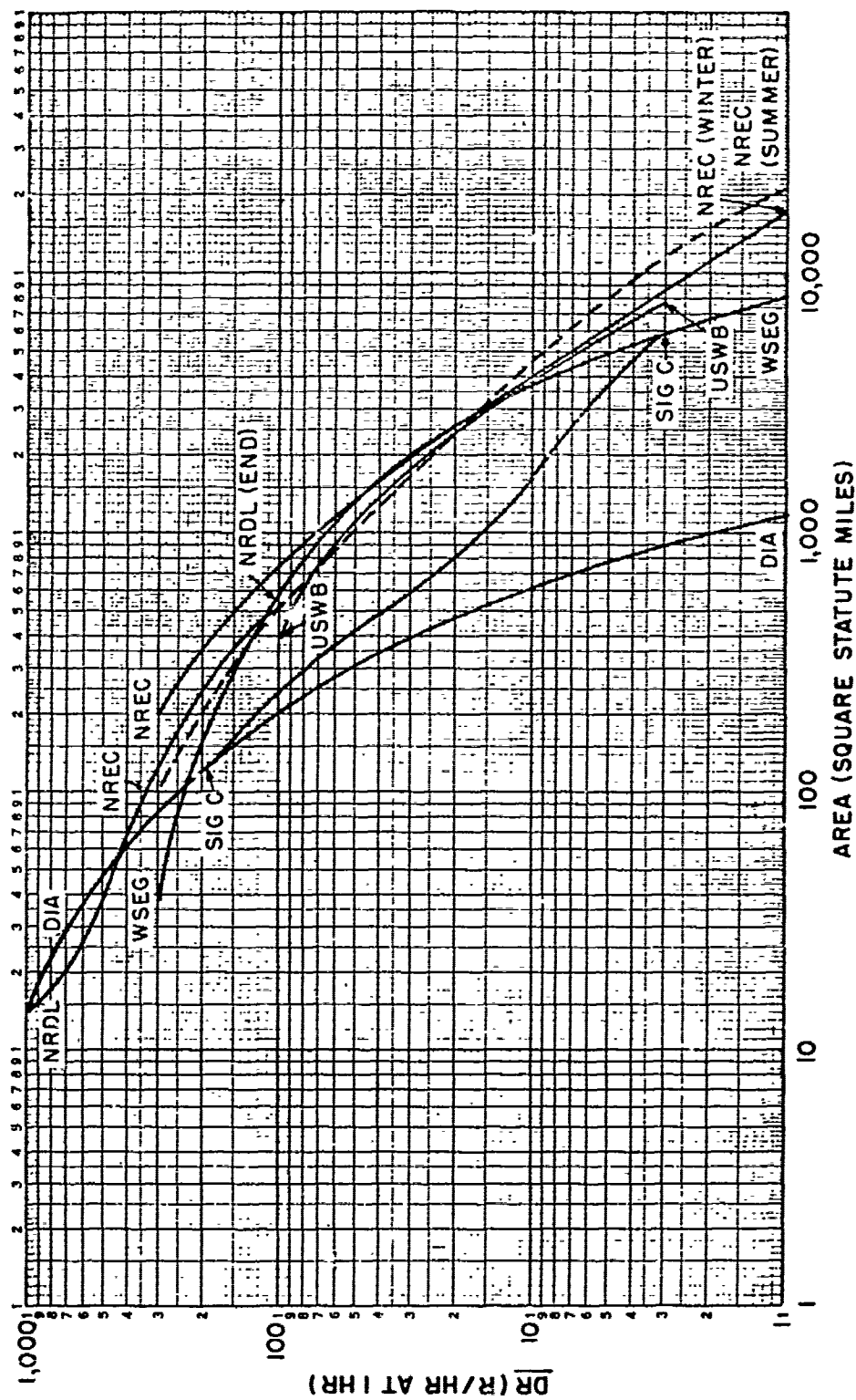
Figure 4-23. Area enclosed by exposure rate contours as a function of DR, case IX - 100 KT (Reference 4-4).
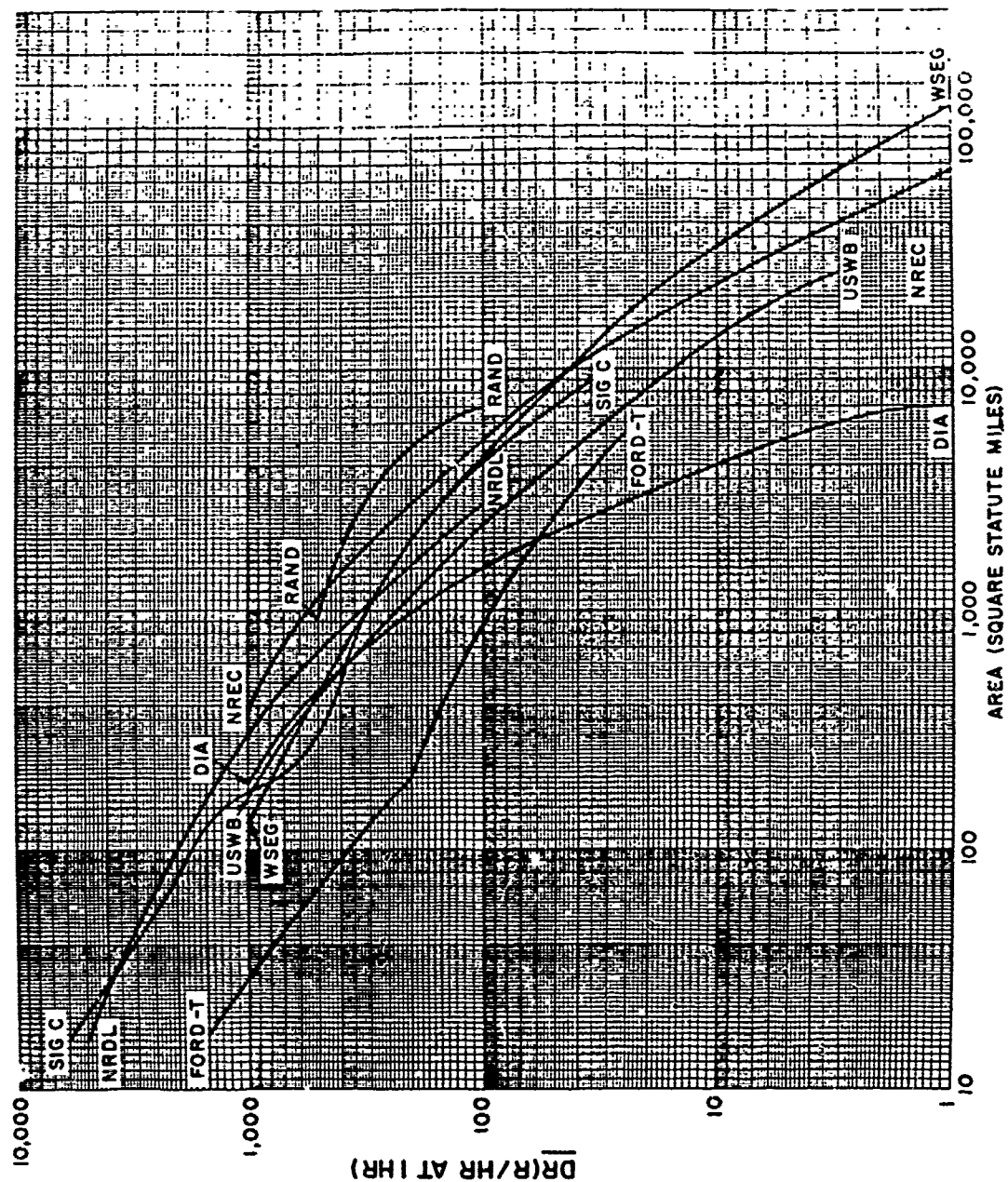
Figure 4-24. Area enclosed by exposure rate contours as a function of DR, case V - 1 MT (Reference 4-4).

60
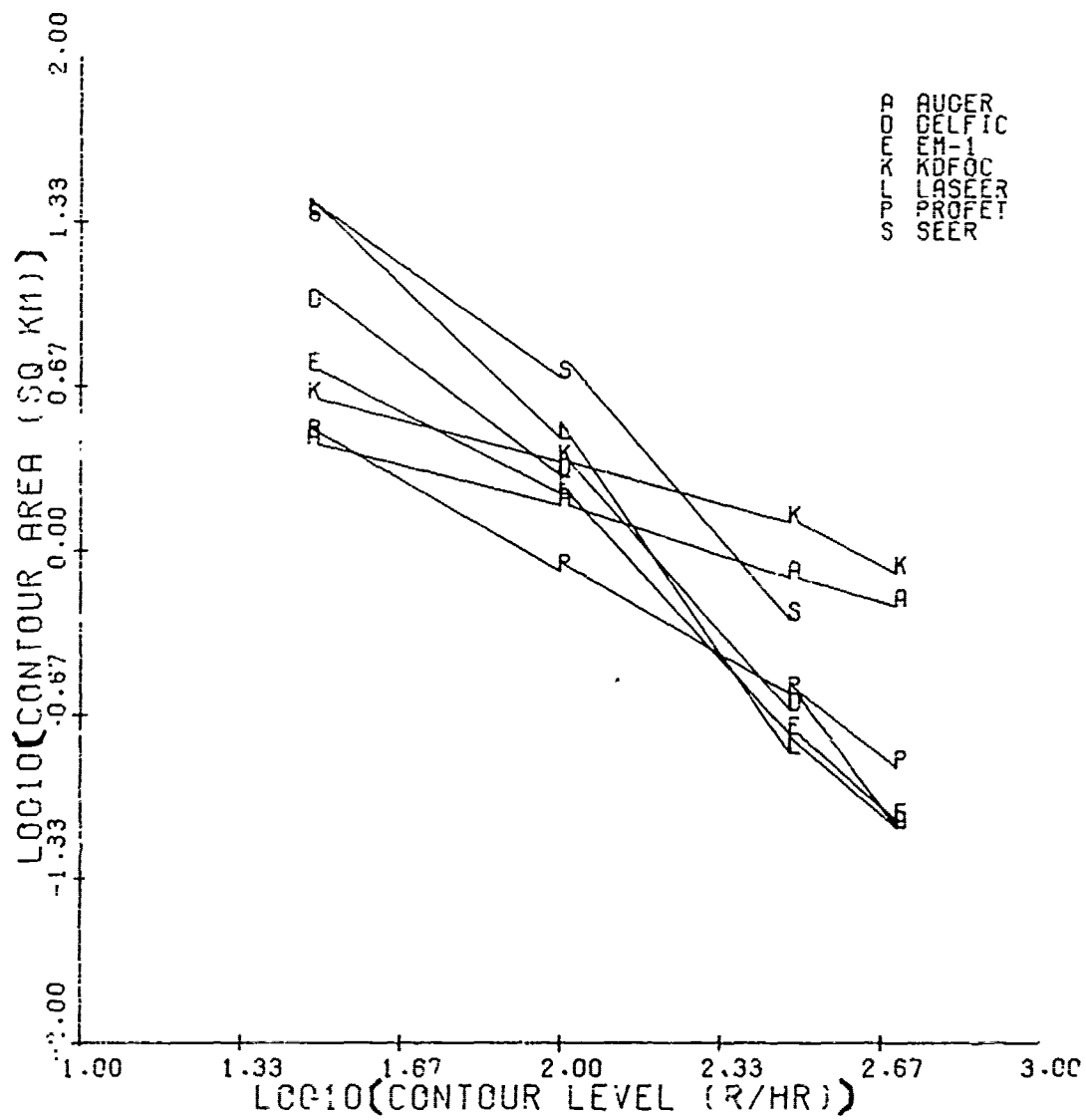
Figure 4-25. 1.0 KT surface shot, 100% fission (contours are 30, 100, 300, 500 R/hr) (Reference 4-3).
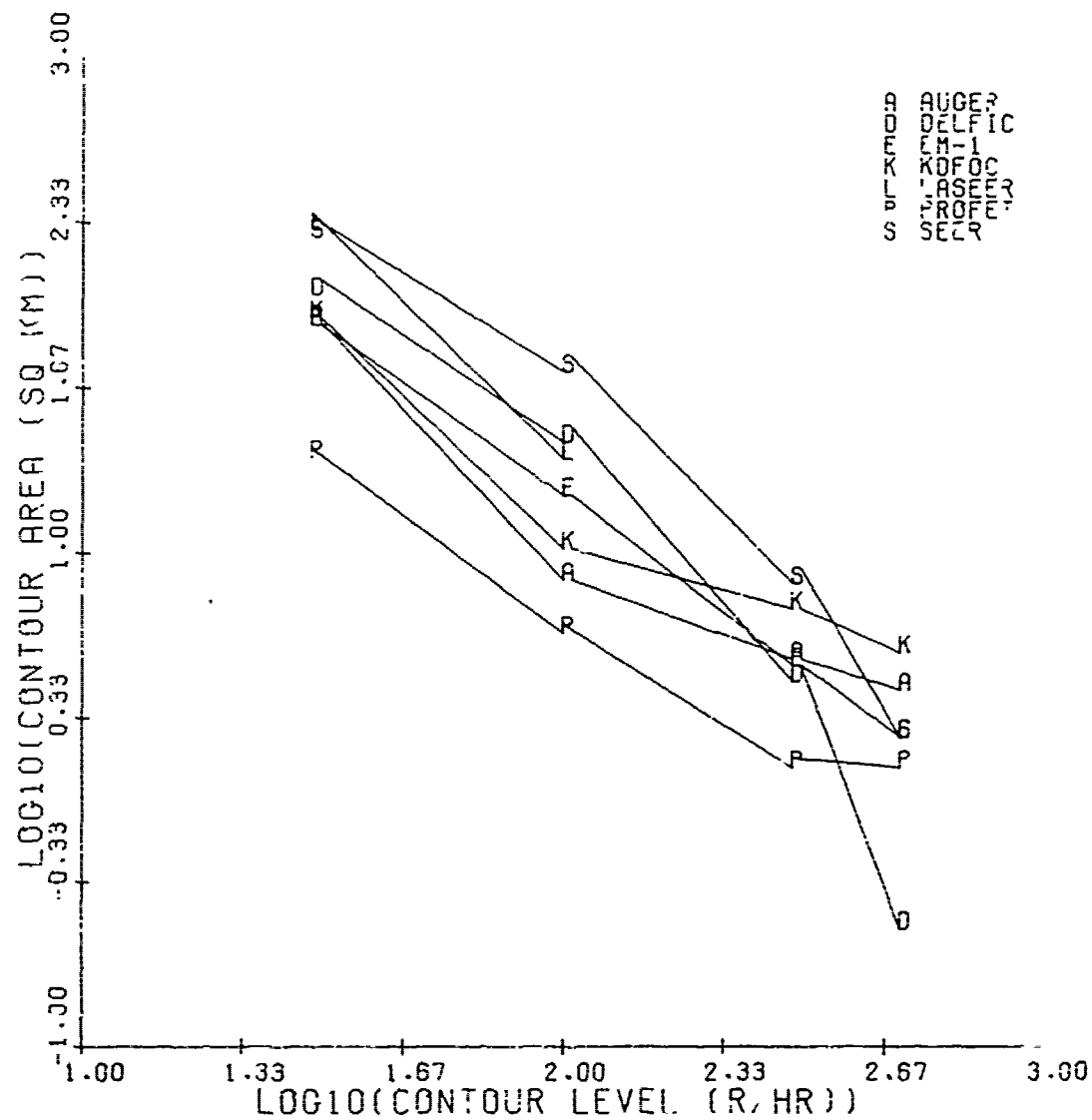
Figure 4-26. 10.0 KT surface shot, 100% fission (contours are 30, 100, 300, 500 R/hr) (Reference 4-3).
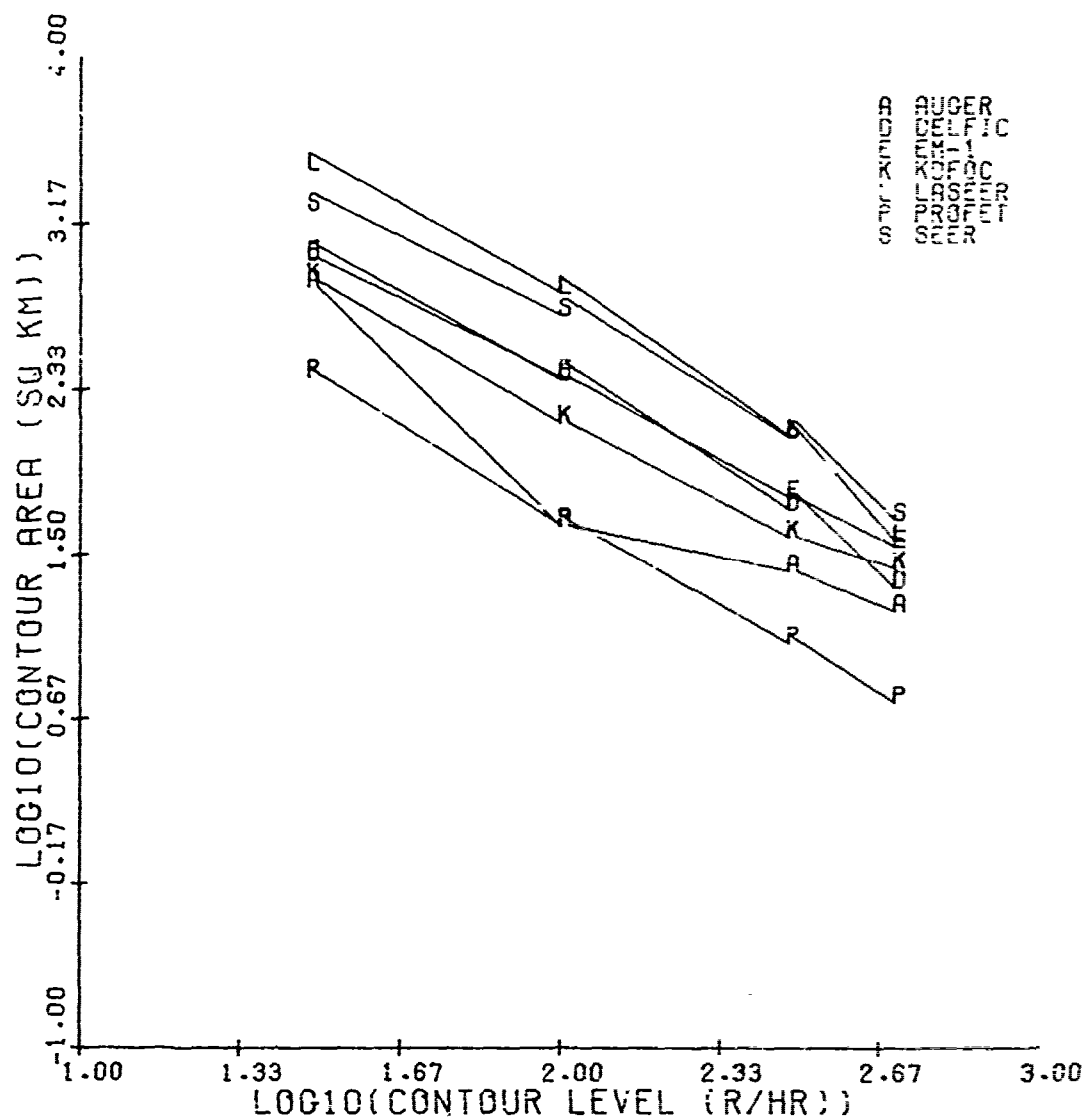
Figure 4-27. 100.0 KT surface shot, 100% fission (contours are
30, 100, 300, 500 R/hr) (Reference 4-3).
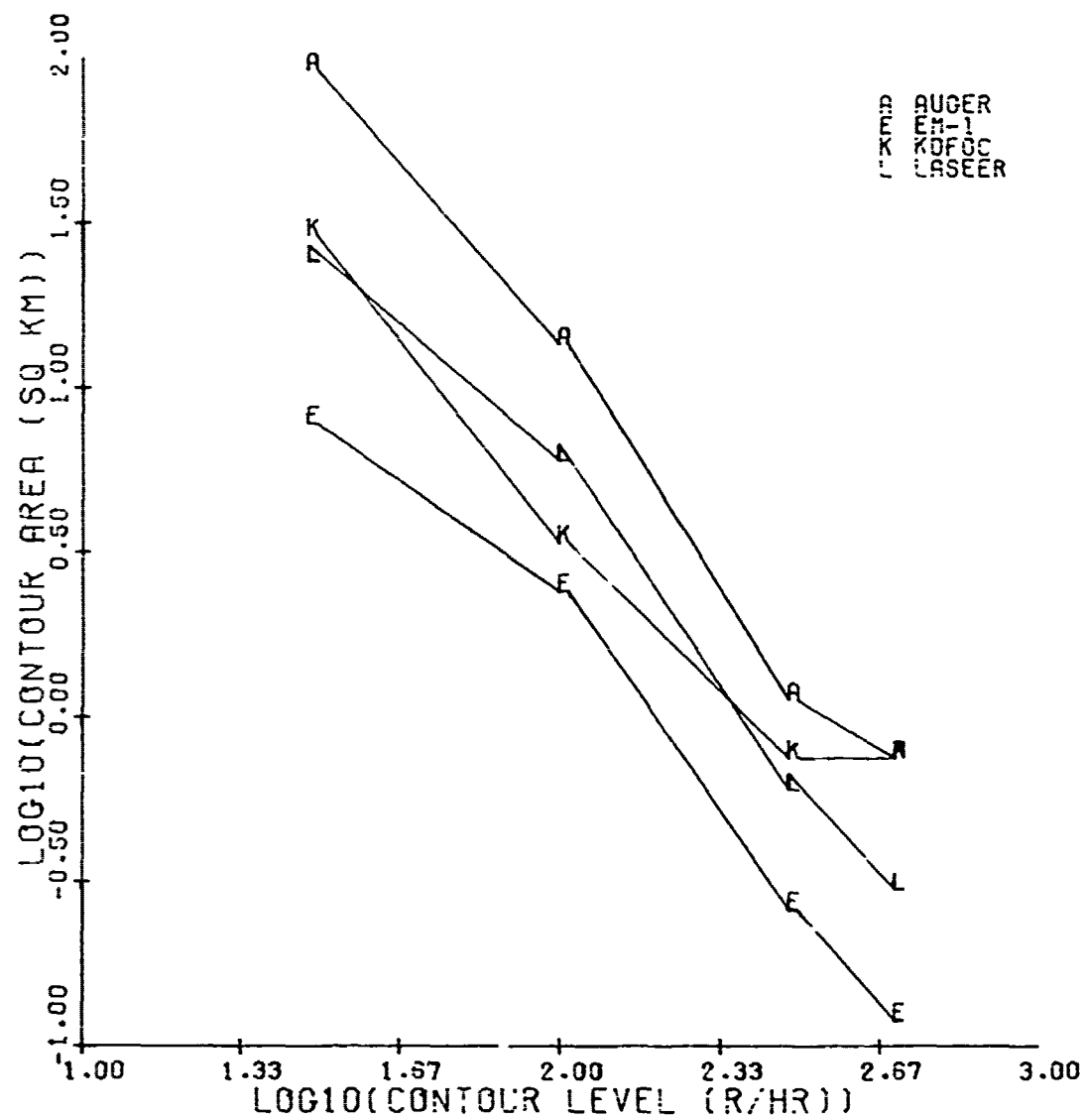
Figure 4-28. 1.0 KT shot at SDOB 5.0, 100% fission (contours are 30, 100, 300, 500 R/hr) (Reference 4-3).
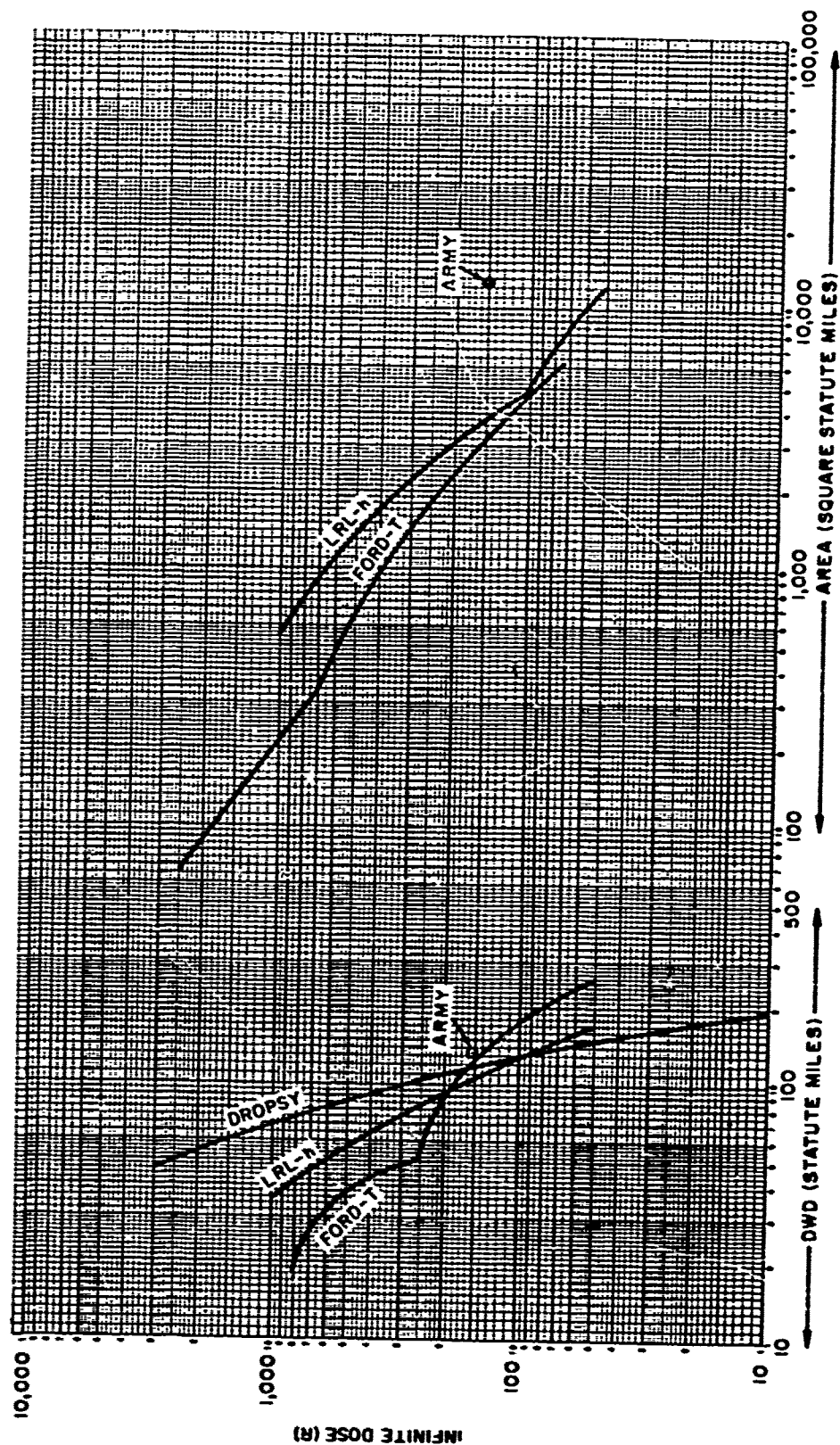
Figure 4-29. Infinite time exposure as a function of DWD and area, case V - 1 MT (Reference 4-4).

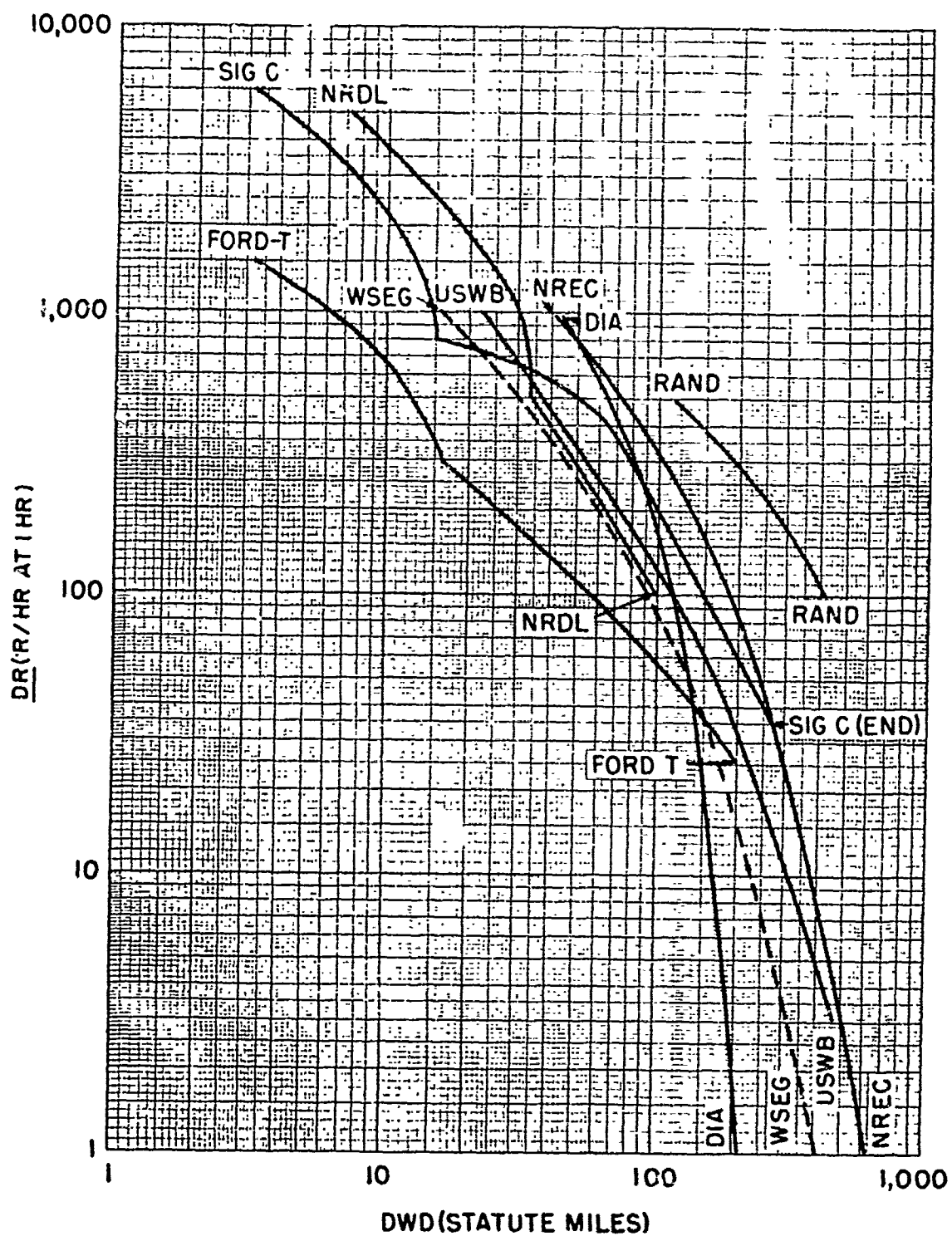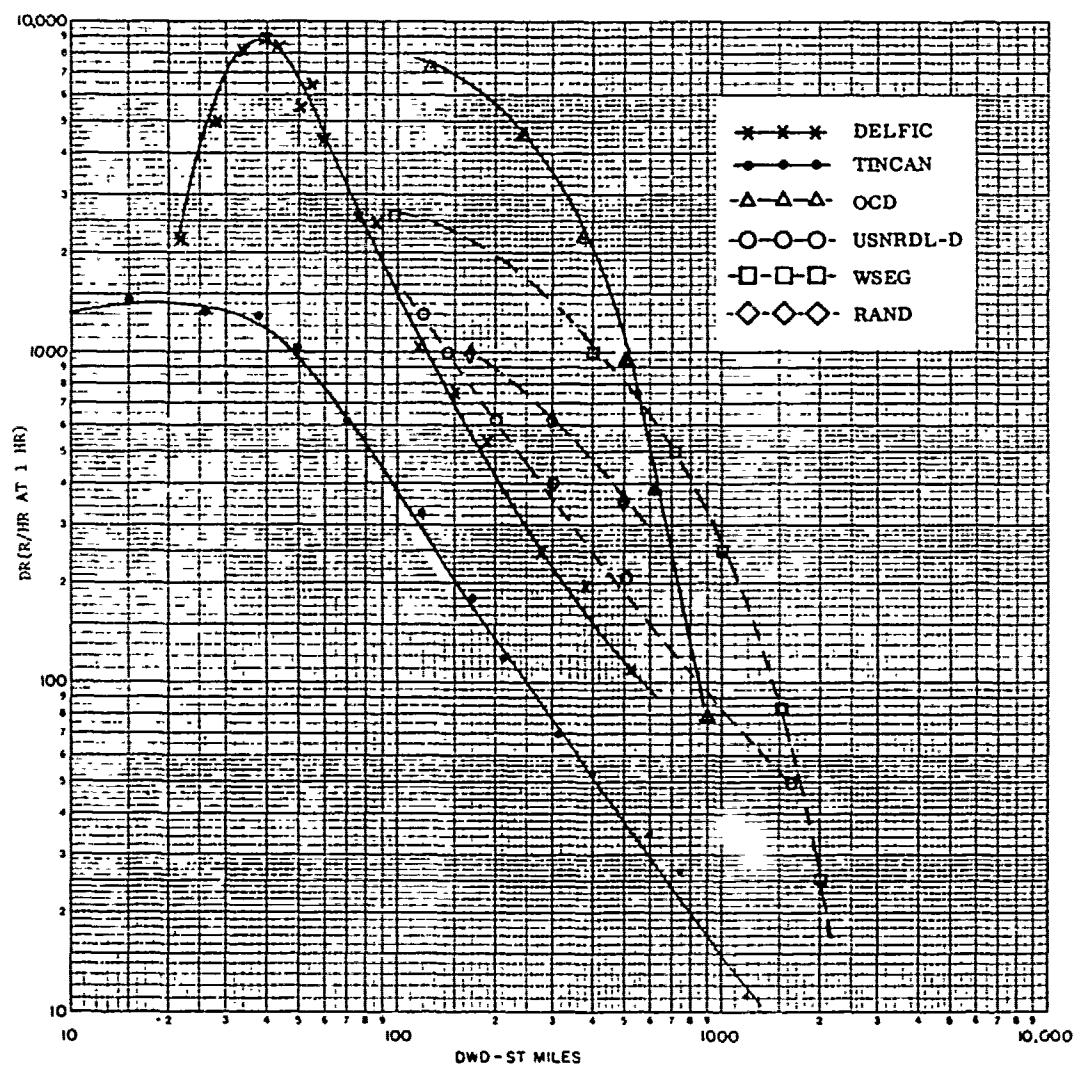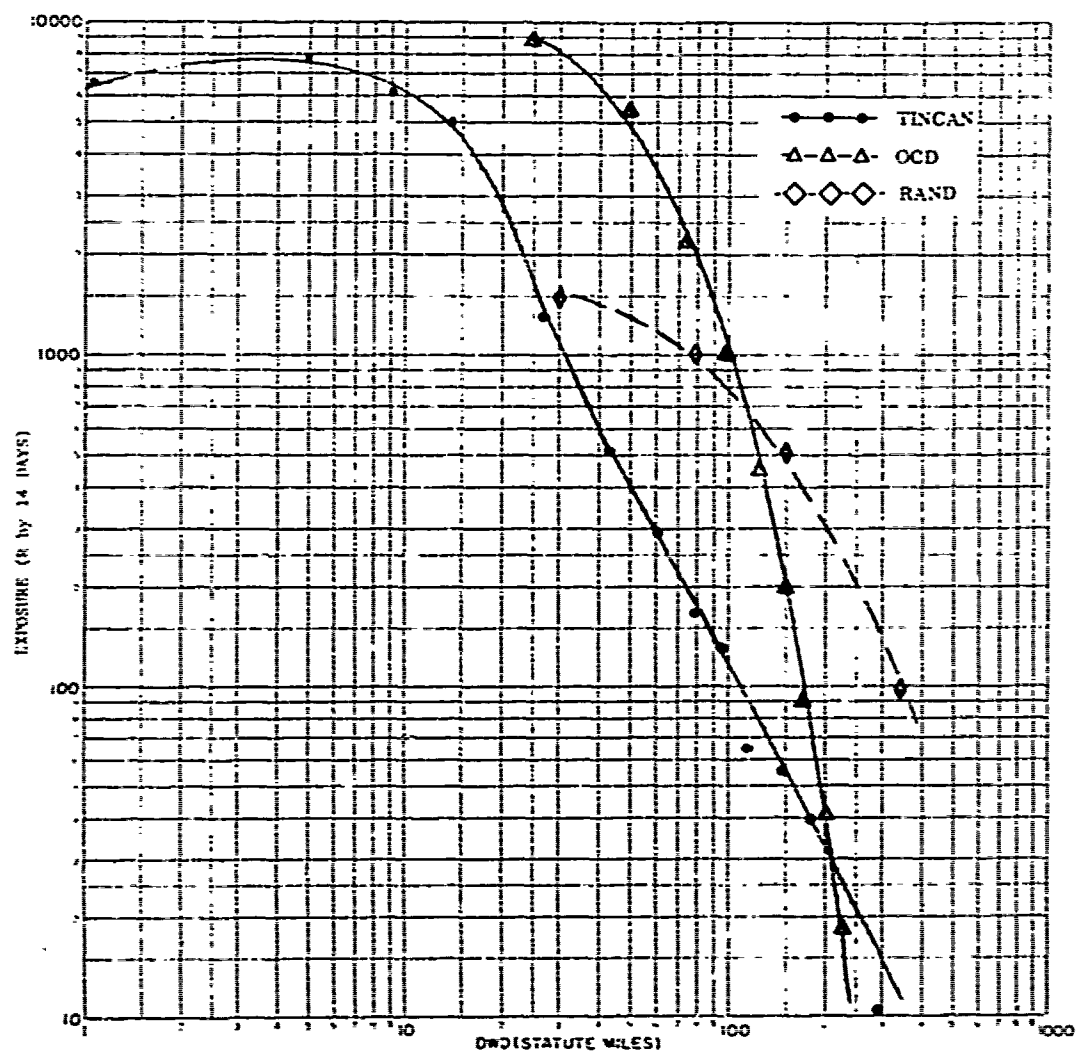Figure 4-30. Exposure as a function of DWD, case V -
1 MT (Reference 4-6).

SECTION 5

COMPARISON OF EXPERIMENTAL DATA WITH PREDICTED POINTS

The DELFIC model has received more attention than others and examples of
its predictions are compared herein to field observations made during weapons
testing. Because device yield is a required input to fallout models and digi-
tizing of the initial conditions at the device is not a prediction process,
illustration of both these operations should be sought elsewhere. However,
cloud altitude at stabilization is a prediction by DELFIC models. Norment and
Woolf (Reference 5-1) made direct comparisons between field data taken from
each of 56 nuclear detonation clouds and DELFIC simulations of their cloud rise.
In the comparison and evaluations, Norment made an assessment of the adequacy
of the cloud predictions for three parameters. The DELFIC parameters of cloud
top height, cloud bottom, and cloud center altitude were compared on a shot-
by-shot basis with the observed cloud top, cloud bottom, and cloud center
altitudes. Comparisons of the respective predicted cloud parameters and the
observed cloud data points are reproduced in Figures 5-1, 5-2, and 5-3. Sub-
sequently, the DELFIC Cloud Rise Module (CRM) was updated twice (References
5-2, 5-3).

Height of the stabilized cloud is crucial to fallout pattern location and
radiation intensity, and the precision with which it is located will be pursued.
The validation and update of DELFIC (Reference 5-3) had least squares fits to
the field data and some figures are shown from that study. Weapon yield for
53 shots is correlated with height of the stabilized cloud top in Figure 5-4
on a log-log fit. Most of the collected observed data are clumped between
1 and 100 KT. In Figure 5-5, DELFIC-predicted cloud top heights are directly
compared to the field observations in the log-log domain with some non-lineari-
ties. Turi , from en mass predictions, single-shot data and DELFIC predic-
tions for 1 45, 15,000 KT are reproduced in Figures 5-6, 5-7, and 5-8, res-
pectively. The predicted dimensions of cloud top and base heights and
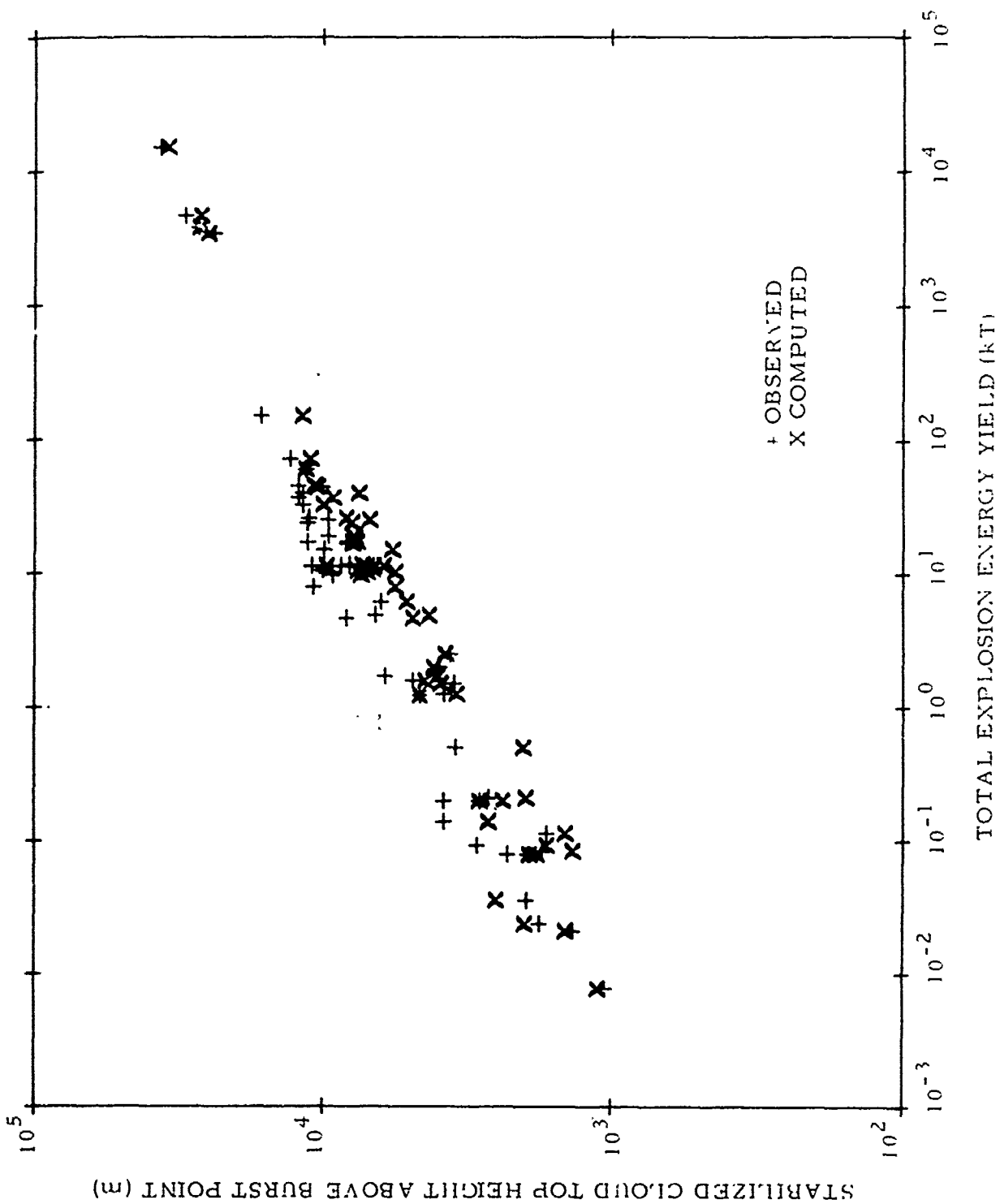
Figure 5-1. Simulated and observed stabilized cloud top heights versus yield (Reference 5-1).
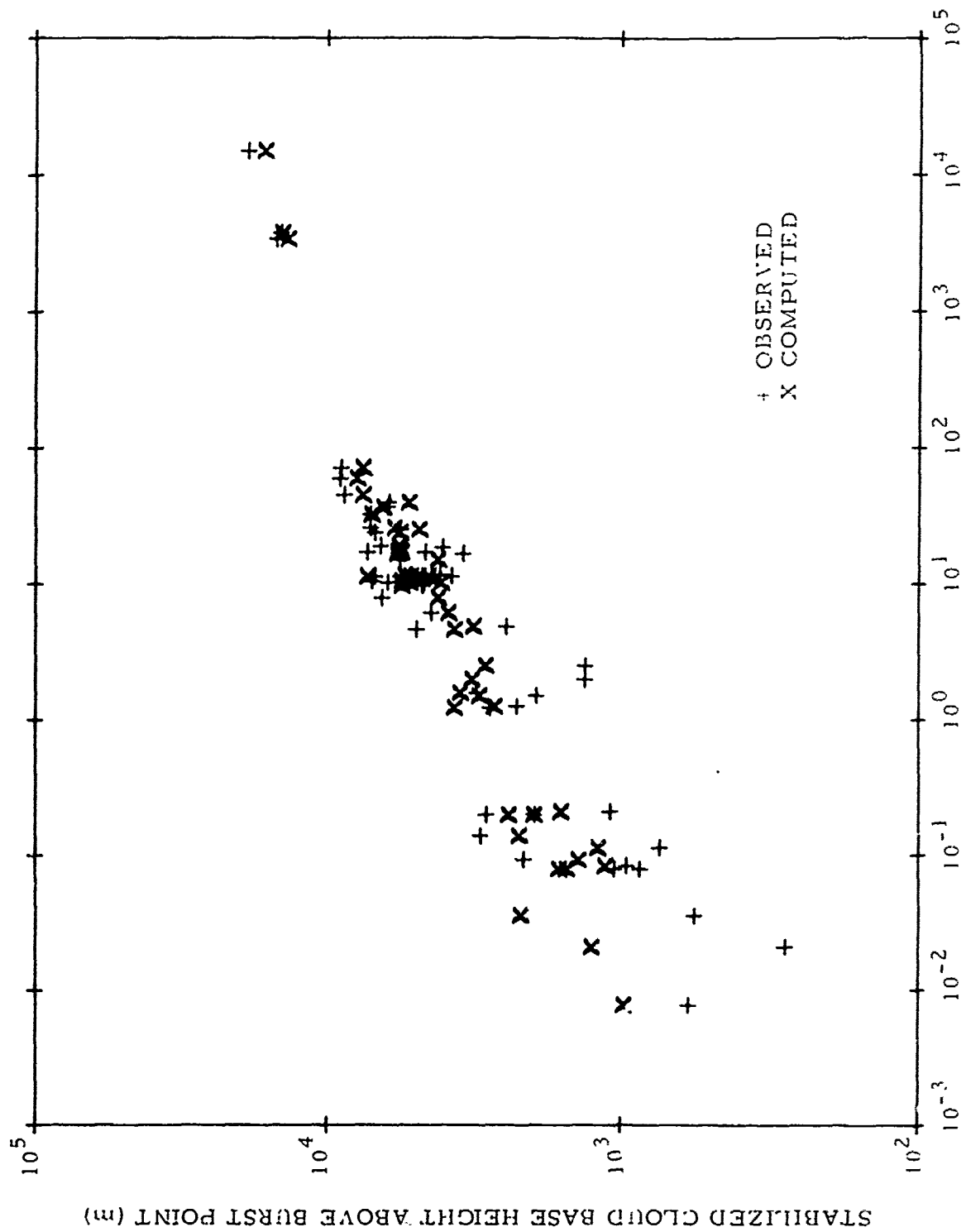
Figure 5-2. Simulated and observed stabilized cloud base heights versus yield (Reference 5-1).
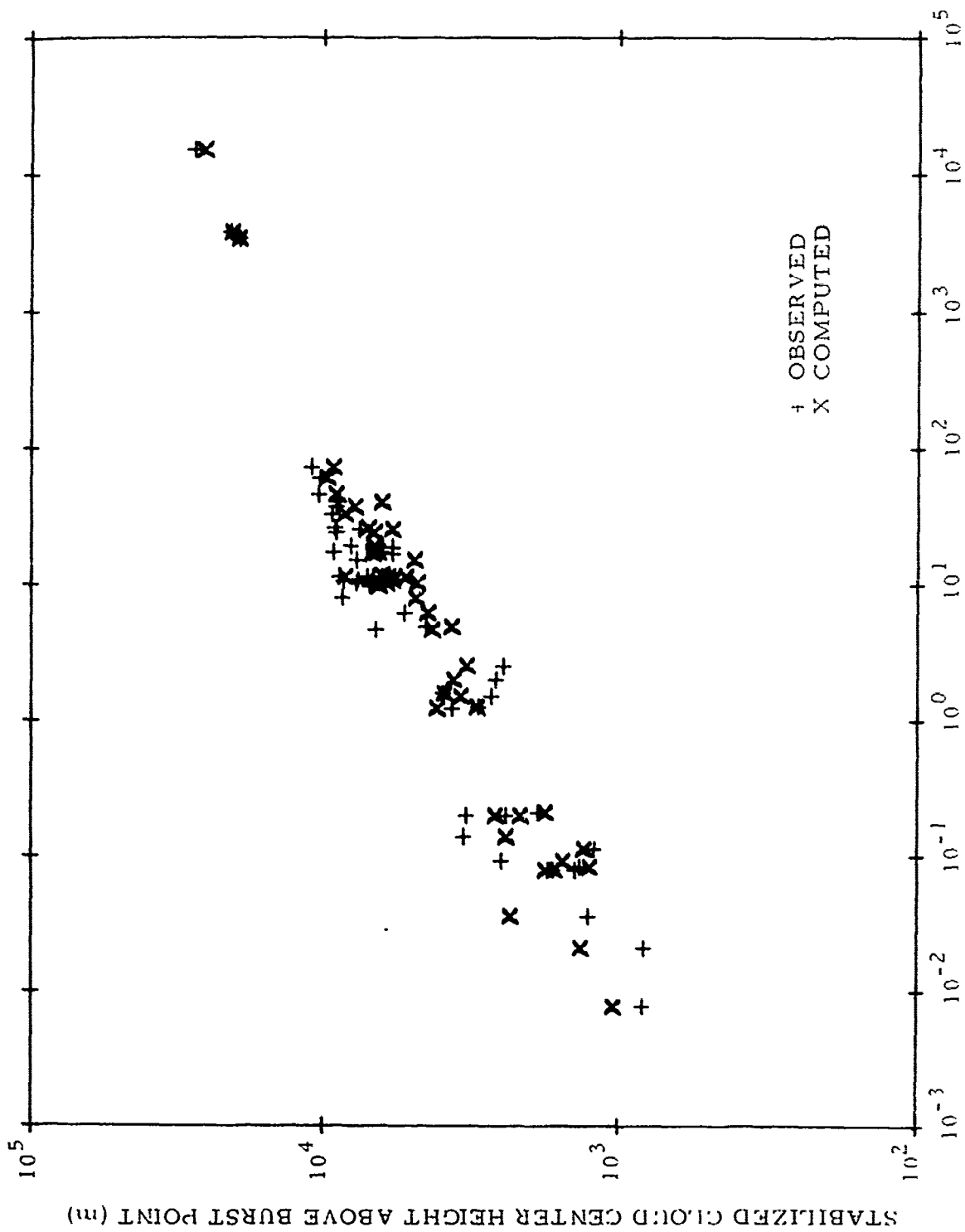
Figure 5-3. Simulated and observed cloud center heights versus yield (Reference 5-1).
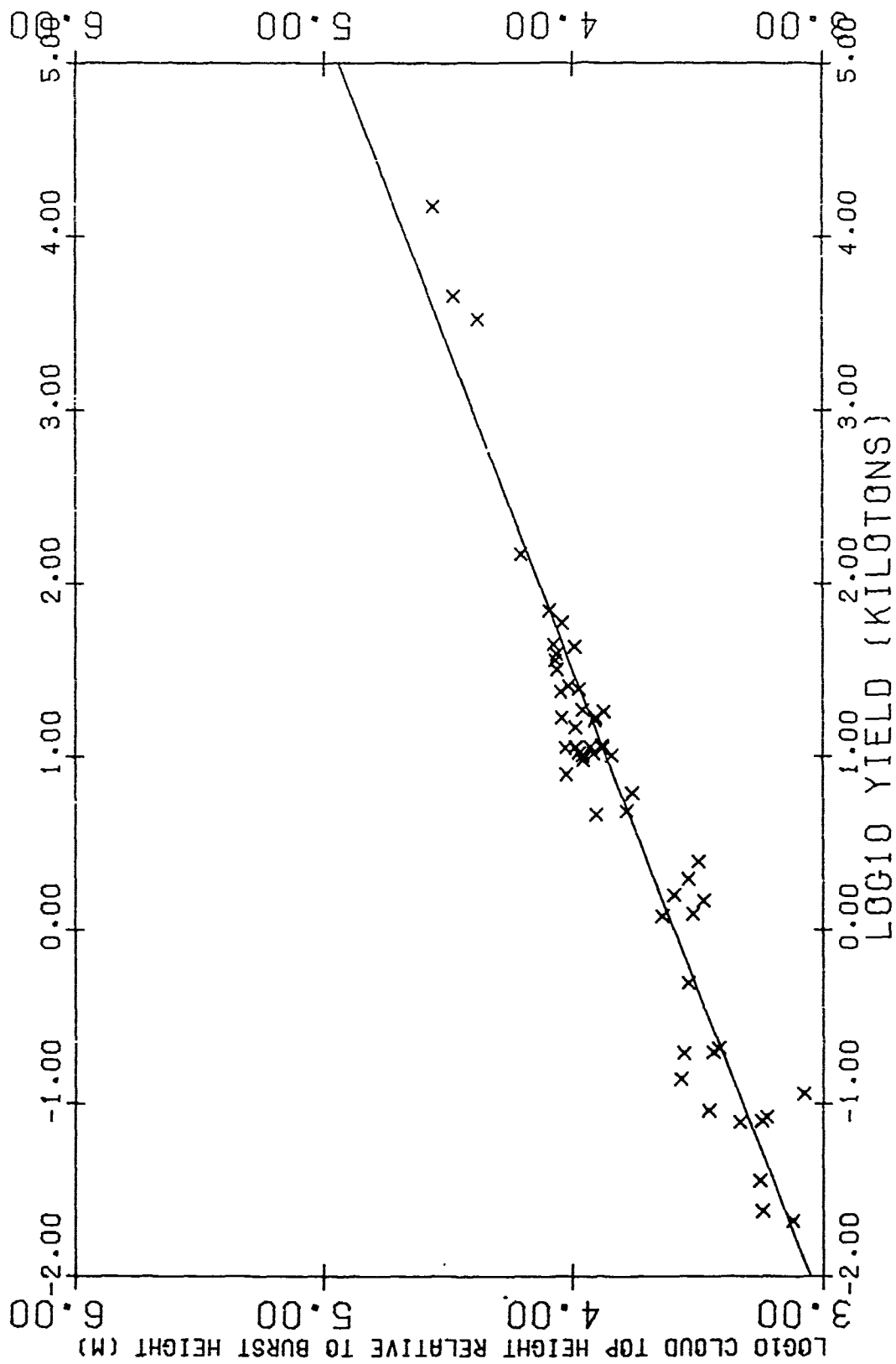
Figure 5-4. Observed stabilized cloud top heights versus yield for 53 shots in the yield range 0.021 to 15,000 KT. (The straight line is a least-squares fit to the data) (Reference 5-3).

71
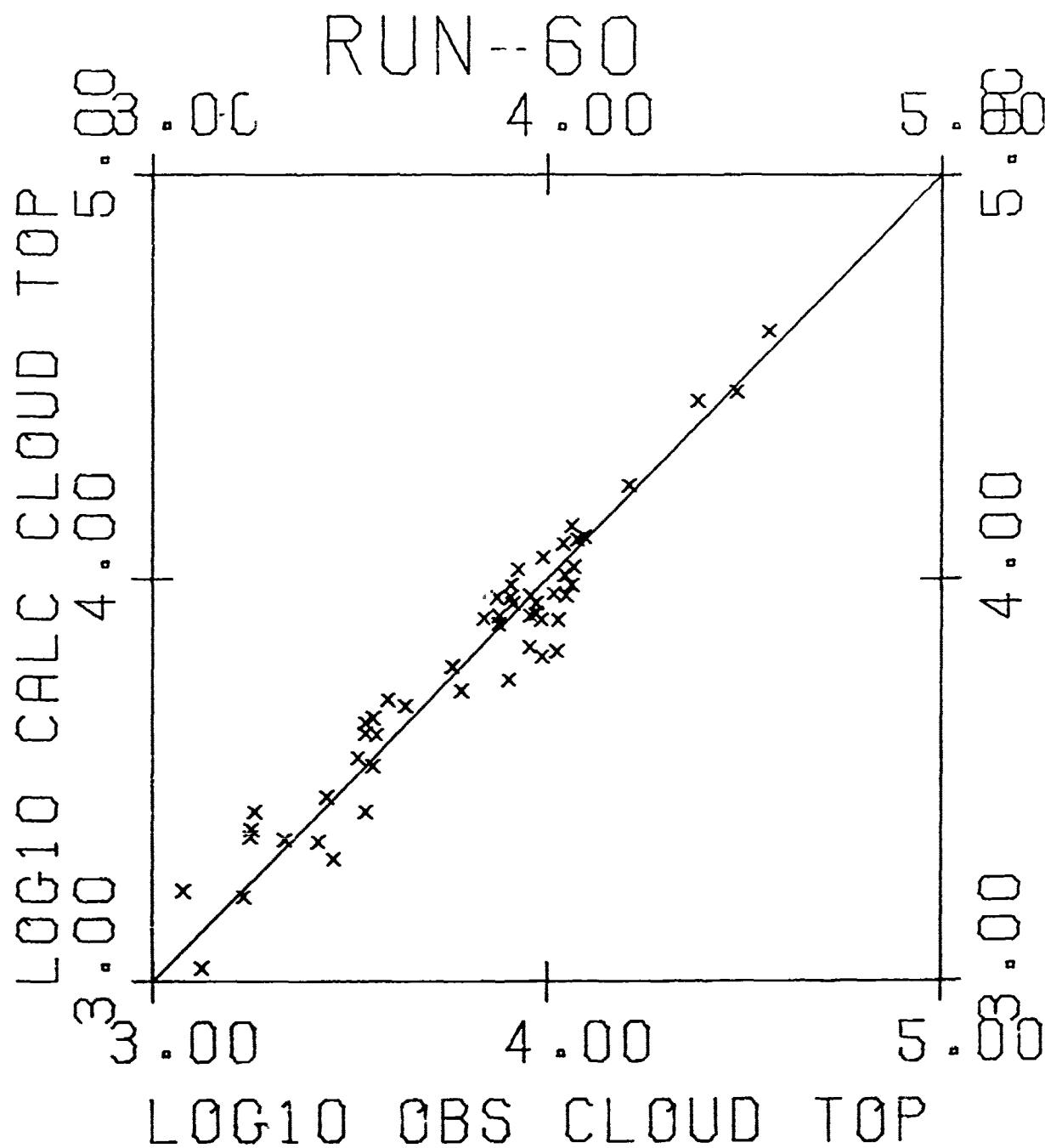
Figure 5-5. Calculated versus observed stabilized cloud top heights (meters relative to burst height) for 53 shots in the yield range 0.021 to 15,000 KT for the refined CRM (Reference 5-3).
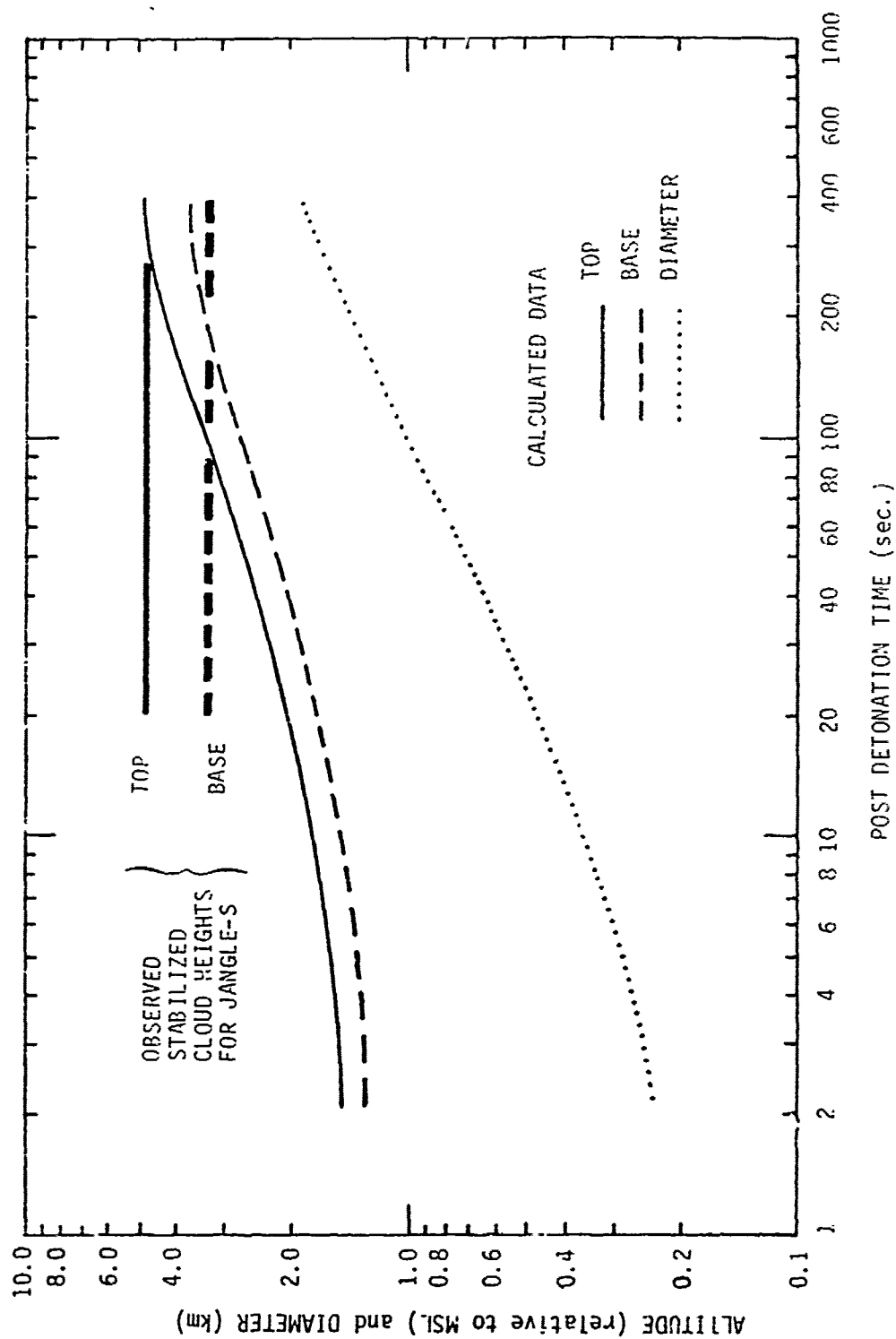
Figure 5-6. Calculated cloud development for a 1.2-KT surface burst at a ground zero altitude of 1,284 meters. (The 30°N January standard atmosphere was used in the simulation. Observed stabilized cloud heights for shot Buster-Jangle Sugar are shown.) (Reference 5-3)
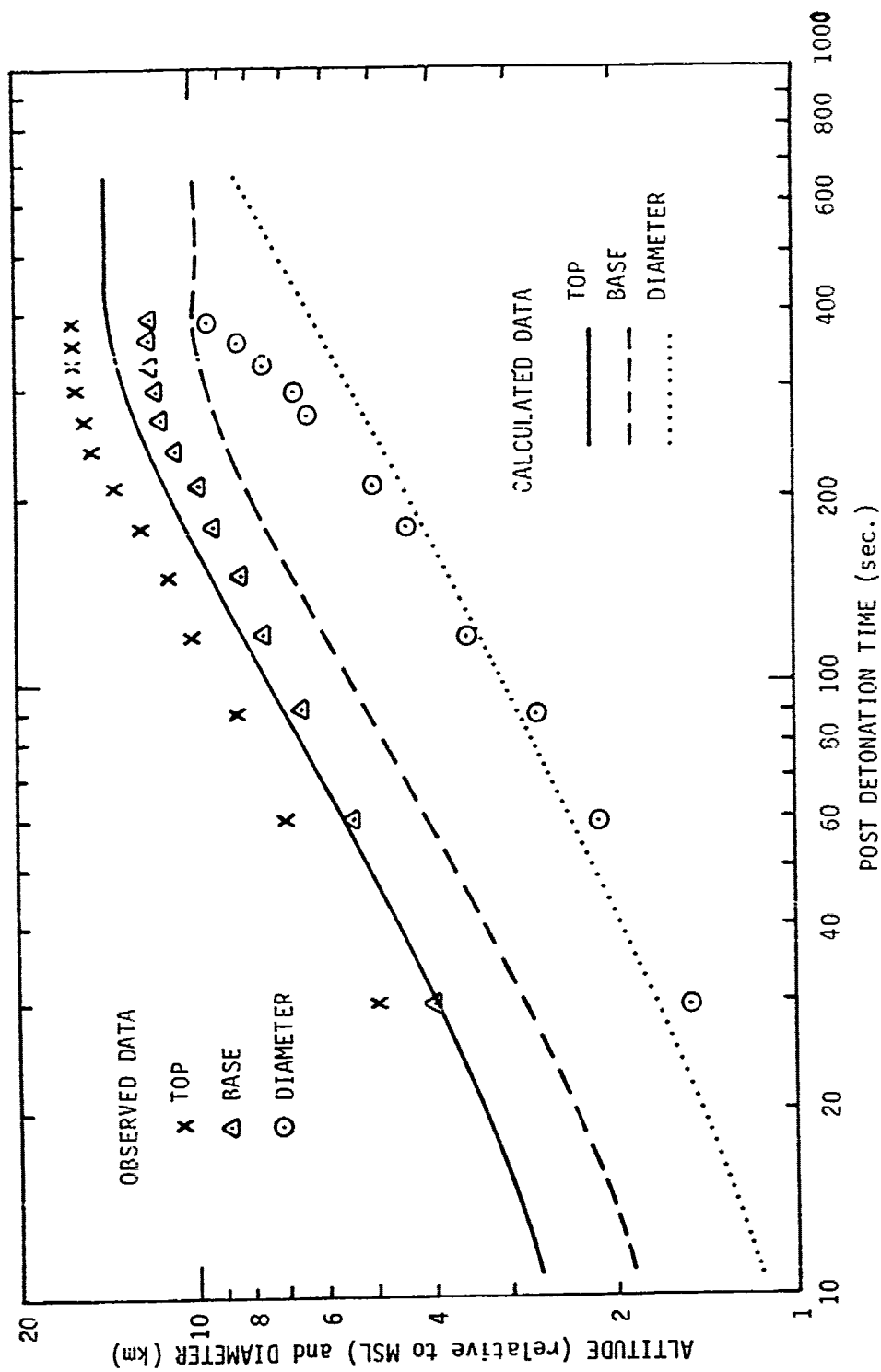
Figure 5-7. Observed and calculated development of the Upshot-Knothole Simon cloud. (Simon was a 45-KT tower shot at the Nevada Test Site. Atmospheric data observed on-site at shot time were used in the simulation.) (Reference 5-3)

74

diameters leave some questions open about model competence. A more thorough analysis of the adequacy of DELFIC predictions over a weapon yield range is demonstrated in Table 5-1, between 1×10^{-2} to 1×10^5 KT. The predicting CRM is based on: (1) a 1970 revision of DELFIC (Reference 5-1), (2) the least-squares power functions, designated Equation 13 and Equation 14, and these are fitted to the widely used DASA 1251-V observed data summary (Reference 5-4) as illustrated in Figure 5-4. The DASA 1251 results are computed from equations in the original report (Reference 5-4). Above approximately 100-KT yield, the power function over-predicts compared to the original DASA 1251 equations. Below 100 KT, the DELFIC CRM cloud base agrees better with the observed cloud heights. Forecasts of cloud top and cloud base heights by SEER, EM-1 and WSEG-10 models, with increasing yield, are demonstrated against the observed data from DASA 1251-V.

The proof of modelling competence lies in having agreement between the predicted fallout parameters and the fallout pattern on the ground. DR contour configurations predicted from standardized input by a variety of models are shown in Section 4, with model outputs pitted against one another. The difficult prediction is that of the area enclosed by radiation isodose contours from subsurface shots, where contour width is combined with a contour length. In the following tables, recent predictions (Reference 5-5) from seven models repeatedly are compared to data from a specific shot. The detonations are from devices in the low-KT range, where the best predictions are made (Reference 5-6), beginning above ground and reaching increasingly deeper burial depths. The tested models were DELFIC, EM-1, PROFET, SEER, LASEER, KDFOC, and AUGER. The shot data reproduced is taken from JANGLE-S, JOHNIE BOY, JANGLE-U, ESS, SCHOONER, CABRIOLET, and DANNY BOY. Their primary characteristics are given in Table 5-2. Abstracts from the shot maps for the comparisons between fallout patterns predicted by models are shown in Tables 5-3 through 5-9. Each subsequent pattern is from a more deeply buried scaled depth. The "hot line" in the abstracts from fallout maps is defined (in Reference 5-5) as reaching from GZ "to the furthest extent of a contour," and the azimuth is measured clockwise in degrees from North to the hot line.
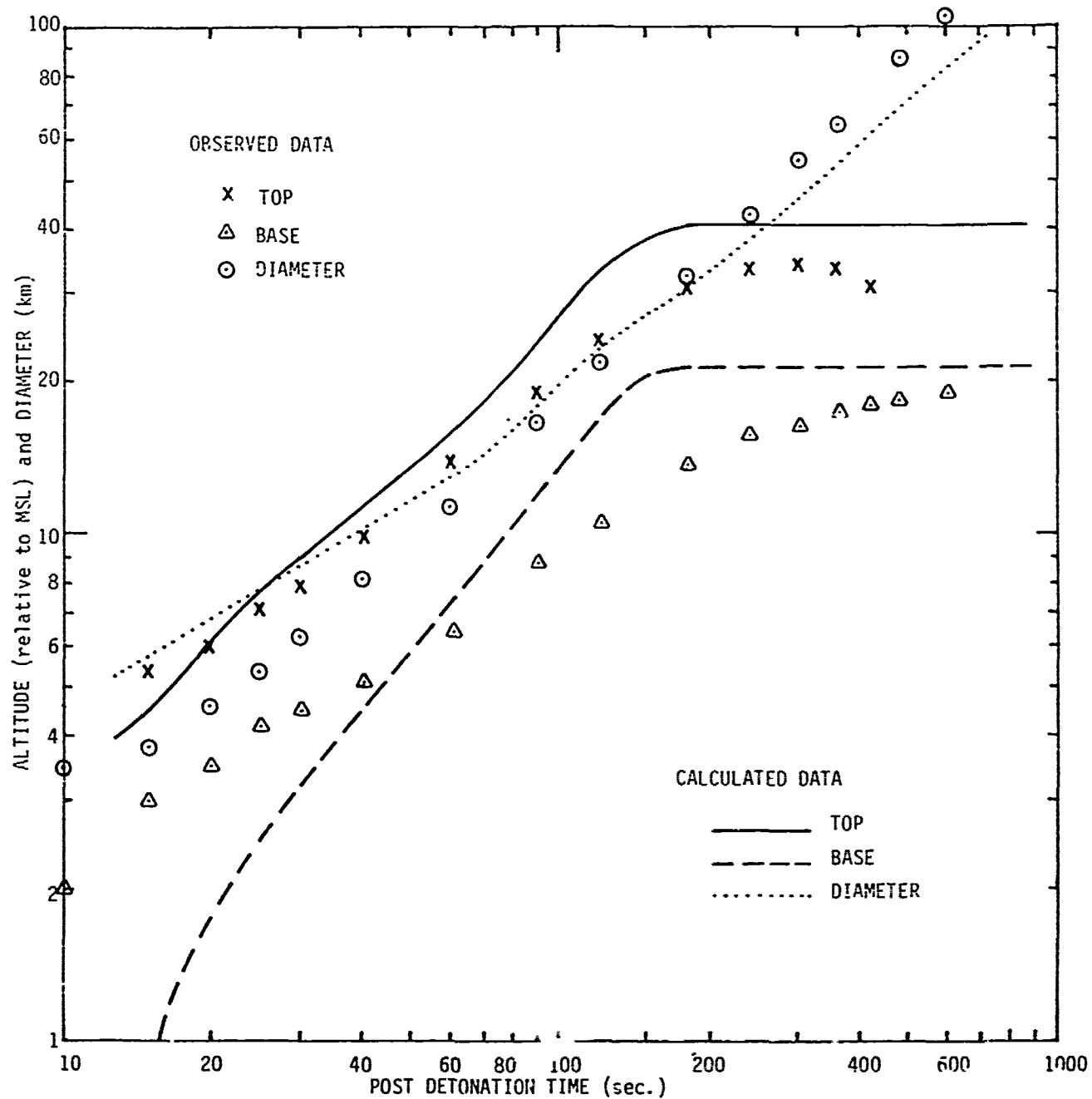
Figure 5-8.   Observed and calculated development of the Castle Bravo cloud.   (Bravo was a 15-MT surface burst on Bᵢkini Island in the Marshalls group.   Atmospheric data observed on-site at shot time were used in the simulation.) (Reference 5-3)

Table 5-1. Comparison of DELFIC CRM results with DASA 1251 equations.

Yield (KT)	Source*	Stabilized Cloud Dimensions (meters)		
		Top Height	Base Height	Radius
10^{-2}	CRM	1010	677	265
	Eqs. (13)&(14)	1130	479	
	DASA-1251	1301	722	122
10^{-1}	CRM	1805	1203	460
	Eqs. (13)&(14)	2103	972	
	DASA-1251	2204	1198	327
10^{0}	CRM	3210	2121	844
	Eqs. (13)&(14)	3914	1971	
	DASA-1251	3734	1987	873
10^{1}	CRM	6811	4676	1747
	Eqs. (13)&(14)	7283	3998	
	DASA-1251	6326	3290	2334
10^{2}	CRM	12194	7911	4851
	Eqs. (13)&(14)	13551	8107	
	DASA-1251	14393	9168	6239
10^{3}	CRM	18252	10748	14403
	Eqs. (13)&(14)	25217	16440	
	DASA-1251	21634	13277	15677
10^{4}	CRM	32516	16733	39478
	Eqs. (13)&(14)	46923	33339	
	DASA-1251	32519	19152	44577
10^{5}	CRM	59958	17712	178110
	Eqs. (13)&(14)	87315	67608	
	DASA-1251	48881	27499	119153

* CRM results are for sea-level surface bursts using the U.S. Standard
Atmosphere, Mid-Latitude, Spring/Fall. DASA-1251 height results are
computed from Equations (2.1)-(2.6) of Reference 5-4, and the radii
are computed from Equation (2.13) of Reference 5-4 for a stabilization
time of 10 minutes.

Table 5-2. Characteristics of test shots in parameter comparisons.

Shot	Yield (KT)	SDOB[a] (m)
JANGLE-S	1.2	-1.0
JOHNIE BOY	0.5	-0.74
JANGLE-U	1.2	4.9
ESS	1.3	19
SCHOONER	31	34
CABRIOLET	2.3	39
DANNY BOY	0.42	45

[a]Scaled depth of burial at detonation.

In the evaluation of prediction capability, each model had three isodose contours to predict for each of seven shots for a maximum score of 21. The accumulated numbers of predicted areas, within the enclosed isodose criteria of ± 30 percent, are shown in Table 5-10. The most capable predictors for these two surface and five buried shots were PROFET, EM-1, and KDFOC. PROFET has an 83 percent success rate where it produced isodose contours, and refused to predict contours for all of the underground shots. However, its overall success rate was 24 percent. SEER failed the criteria in all predictions, and had the highest refusal rate of 17 out of 21. In general, the models made a poor showing at predicting the contaminated areas in the yield range where they are most adept at predicting, the low KT range. Among the shots, JANGLE-U isodose enclosed areas were modeled best at 7 successes in 15 predictions and JOHNIE BOY was next at 6 successes in 21 predictions. The models were least able to predict the areas enclosed by isodose contours on ESS and CABRIOLET.

Table 5-3. Comparative pattern statistics from JANGLE-S and fallout models.*

Statistics

	Gamma Isodose Contour (R/hr)			
	35	100	300	500
JANGLE-S				
Hotline Length (m)	5066	3737	1498	693
Hotline Azimuth (deg)	5	1	346	342
Area (km²)	3.17	1.44	0.38	0.12
AUGER				
Hotline Length (m)	7320	4834	3496	2829
Hotline Azimuth (deg)	8	18	18	18
Area (km²)	7.04	2.59	1.33	0.85
DELFIC				
Hotline Length (m)	14843	5750	1420	1250
Hotline Azimuth (deg)	1	0	0	359
Area (km²)	12.35	2.61	0.61	0.23
EM-1				
Hotline Length (m)	16000	8100	3700	2600
Hotline Azimuth (deg)	8	8	8	8
Area (km²)	6.20	1.30	0.23	0.10
KDFOC				
Hotline Length (m)	6523	4343	3009	2343
Hotline Azimuth (deg)	8	18	18	19
Area (km²)	6.66	3.04	1.41	0.87
LASEER				
Hotline Length (m)	12881	6320	1501	500
Hotline Azimuth (deg)	8	8	358	357
Area (km²)	24.51	4.70	0.40	0.22
PROFET				
Hotline Length (m)	8274	3517	293	287
Hotline Azimuth (deg)	4	354	270	270
Area (km²)	3.60	0.56	0.14	0.14
SEER				
Hotline Length (m)	11426	5587		
Hotline Azimuth (deg)	10	10		
Area (km²)	18.34	4.02		

* Adapted from Reference 5-5

Table 5-4. Comparative pattern statistics from
JOHNIE BOY and fallout models.*

Statistics	Gamma Isodose Contour (R/hr)		
	10	50	100
JOHNIE BOY			
Hotline Length (m)	10623	4102	2733
Hotline Azimuth (deg)	345	343	345
Area (km²)	10.68	1.27	0.54
AUGER			
Hotline Length (m)	9431	3295	2035
Hotline Azimuth (deg)	347	352	348
Area (km²)	13.06	3.33	0.90
DELFIC			
Hotline Length (m)	9673	5399	3319
Hotline Azimuth (deg)	349	346	348
Area (km²)	7.66	2.24	1.10
EM-1			
Hotline Length (m)	10000	6500	4000
Hotline Azimuth (deg)	359	359	359
Area (km²)	5.80	1.90	0.58
KDFOC			
Hotline Length (m)	15300	3003	1367
Hotline Azimuth (deg)	355	350	23
Area (km²)	26.86	3.32	1.23
LASEER			
Hotline Length (m)	13042	5717	3195
Hotline Azimuth (deg)	345	344	345
Area (km²)	27.85	5.77	2.18
PROFET			
Hotline Length (m)	10495	4857	3067
Hotline Azimuth (deg)	348	348	346
Area (km²)	7.58	1.63	0.55
SEER			
Hotline Length (m)	13180	364	3622
Hotline Azimuth (deg)	348	346	345
Area (km²)	25.55	6.44	3.09

* Adapted from Reference 5-5

80

Table 5-5. Comparative pattern statistics from
JANGLE-U and fallout models.*

Statistics	Gamma Isodose Contour (R/hr)		
	100	200	500
JANGLE-U			
Hotline Length (m)	5231	2985	1380
Hotline Azimuth (deg)	25	18	348
Area (km²)	5.86	2.24	0.58
AUCER			
Hotline Length (m)	9457	5322	1543
Hotline Azimuth (deg)	36	24	48
Area (km²)	18.57	4.71	0.98
DELFIC			
Hotline Length (m)	2727	6533	2676
Hotline Azimuth (deg)	29	28	21
Area (km²)	6.60	3.30	0.92
EM-1			
Hotline Length (m)	9100	5300	2500
Hotline Azimuth (deg)	36	36	36
Area (km²)	2.50	0.55	0.099
KDFOC			
Hotline Length (m)	3694	2280	1499
Hotline Azimuth (deg)	25	27	50
Area (km²)	4.52	2.42	0.70
LASEER			
Hotline Length (m)	4140	2306	1173
Hotline Azimuth (deg)	46	23	20
Area (km²)	6.74	2.45	0.56

* Adapted from Reference 5-5

Table 5-6. Comparative pattern statistics from ESS and fallout models.*

Statistics	Gamma Isodose Contour (R/hr)			
	10	50	100	500
ESS				
Hotline Length (m)	7275	4186	2238	1192
Hotline Azimuth (deg)	134	136	127	124
Area (km²)	14.32	6.26	3.55	1.37
AUGER				
Hotline Length (m)	34570	13379	5129	1615
Hotline Azimuth (deg)	154	142	133	87
Area (km²)	203.9	36.08	5.66	2.05
EM-1				
Hotline Length (m)	26000-34000	13000-16000	8500-11000	2400-3100
Hotline Azimuth (deg)	149	149	149	149
Area (km²)	35.0-61.0	4.9-8.1	1.7-2.8	0.12-0.20
KDFOC				
Hotline Length (m)	33265	13458	3300	1509
Hotline Azimuth (deg)	152	140	128	81
Area (km²)	198.7	30.66	4.79	2.05
LASEER				
Hotline Length (m)	19307	8489	6100	964
Hotline Azimuth (deg)	136	140	138	142
Area (km²)	69.92	17.15	8.71	0.39

* Adapted from Reference 5-5

Table 5-7. Comparative pattern statistics from
SCHOONER and fallout models.*

Statistics	Gamma Isodose Contour (R/hr)			
	1	10	20	100
SCHOONER				
Hotline Length (m)	27517	9319	8232	830
Hotline Azimuth (deg)	50	1	1	142
Area (km²)	209.7	36.75	18.79	1.67
AUGER				
Hotline Length (m)	15155	2820	1990	919
Hotline Azimuth (deg)	23	56	40	37
Area (km²)	121.3	11.75	6.73	0.44
EM-1				
Hotline Length (m)	6300-24000	-	-	-
Hotline Azimuth (deg)	67	67	67	67
Area (km²)	0.96-14.0	-	-	-
KDFOC				
Hotline Length (m)	31178	3438	3151	1879
Hotline Azimuth (deg)	51	34	38	66
Area (km²)	230.9	12.75	7.23	1.422
LASEER				
Hotline Length (m)	21795	3979		
Hotline Azimuth (deg)	60	56		
Area (km²)	85.93	3.12		

*Adapted from Reference 5-5

Table 5-8. Comparative pattern statistics from
CABRIOLET and fallout models.*

Statistics	Gamma Isodose Contour (R/hr)		
	1	10	100
CABRIOLET			
Hotline Length (m)	2674	634	337
Hotline Azimuth (deg)	340	264	177
Area (km^2)	3.18	0.73	0.17
AUGER			
Hotline Length (m)	21407	3659	1959
Hotline Azimuth (deg)	43	351	15
Area (km^2)	193.4	4.55	2.04
EM-1			
Hotline Length (m)	4700-13000	1400-5600	240-960
Hotline Azimuth	47	47	47
Area (km^2)	0.98-14.0	0.048-0.72	0.0066-0.10
KDFOC			
Hotline Length (m)	21932	5410	2030
Hotline Azimuth (deg)	26	2	6
Area (km^2)	175.0	9.24	2.07
LASEER			
Hotline Length (m)	17387	5066	786
Hotline Azimuth (deg)	38	38	17
Area (km^2)	86.75	7.79	0.43

* Adapted from Reference 5-5

84

Table 5-9. Comparative pattern statistics from
DANNY BOY and fallout models.*

Statistics	Gamma Isodose Contour (R/hr)			
	5	10	50	100
DANNY BOY				
Hotline Length (m)	1778	1464	638	451
Hotline Azimuth (deg)	355	357	5	11
Area (km^2)	1.27	0.80	0.33	0.24
AUGER				
Hotline Length (m)	10368	7400	2752	1227
Hotline Azimuth (deg)	3.1	357	353	328
Area (km^2)	21.70	12.77	2.53	1.13
EM-1				
Hotline Length (m)	3400-6500	270-5000	130-2400	82-1600
Hotline Azimuth (deg)	11	11	11	11
Area (km^2)	0.073-2.7	0.0034-1.2	0.00036-0.13	0.00011-0.043
KDFOC				
Hotline Length (m)	16942	13753	6349	2157
Hotline Azimuth (deg)	357	2	3	13
Area (km^2)	36.68	26.25	6.60	2.38
LASEER				
Hotline Length (m)	15856	11916	5519	4013
Hotline Azimuth (deg)	353	356	355	355
Area (km^2)	27.80	16.23	4.35	2.45

* Adapted from Reference 5-5

Table 5-10. Predicted areas $\pm$ 0.30 of measured area on three isodose levels.[a]

Isodose Contour Predictor Model	Source of Abstracted Fallout Data							Fraction of Contour Within Criteria
	JANGLE-S	JOHNIE BOY	JANGLi	ESS	SCHOONER	CABRIOLET	DANNY BOY	
AUGER	0/3	1/3	0/3	0/3	0/3	0/3[b]	0/3	1/21
DELFIC	0/3	1/3	1/3	c	c	c	c	2/9
EM-1	1/3	1/3	0/3	1/3	0/1, 2c	1/3	2/3	6/19
KDFOC	0/3	0/3	3/3	0/3	2/3	0/3	0/3	5/21
LASEER	1/3	0/3	3/3	0/3	0/2, 1c	0/3	0/3	4/20
PROFET	2/3	3/3	c	c	c	c	c	5/6
SEER	0/1, 2c	0/3	c	c	c	c	c	0/4

a Isodose criteria: Contours with the highest radiation, mid-range and lowest radiation with full enclosed contours.

b Predicted enclosed area more than 50 times observed area within criterion of isodose contour.

c Isodose contour prediction absent.

REFERENCES

5-1. Norment, H.G. and S. Woolf, "Department of Defense Land Fallout Predic-
      tion System," Volume III: Cloud Rise (Revised), DASA 1800-III (Revised),
      ARCON Corporation, Wakefield, Massachusetts, September 1970.

5-2. Huebsch, I.O., "Analysis and Revision of the Cloud Rise Module of the
      Department of Defense Land Fallout Prediction System (DELFIC)," BRL-
      CR-254, Euclid Research Group, Berkeley, California, August 1975.

5-3. Norment, H.G., "Validation and Refinement of the DELFIC Cloud Rise
      Module," DNA 4320F, Atmospheric Science Associates, Bedford, Massa-
      chusetts, January 1977.

5-4. La Riviera, S.L. Brown, J.D. Sartor, and C.F. Miller, "Local Fallout
      from Nuclear Test Detonations, Volume 5: Transport and Distribution
      of Local (Early) Fallout from Nuclear Weapons Tests," Stanford Research
      Institute, Menlo Park, California, Unpublished.

5-5. Norment, H.G., "Analysis and Comparison of Fallout Prediction Models,"
      Atmospheric Science Associates, Bedford, MA 01730. Unpublished.

5-6. Norment, H.G., "Evaluation of Three Fallout Prediction Models: DELFIC,
      SEER, and WSEG-10," DNA Draft, Atmospheric Science Associates, Bedford,
      MA, April 1978.

SECTION 6

ESTIMATES OF ERRORS

Observations of stabilized cloud altitude are inconsistent and therefore difficult to analyze for error (Reference 6-1). Cloud radii measurements are even less precise because horizontal expansion continues indefinitely from detonation. Error comparisons between observed values and calculated parameters, on a point-by-point basis, are generally indecipherable. Consequently, smoothed functions are fitted to groups of observations, then calculated points are matched to points extracted from the fitted function. In discussing comparison criteria for judging prediction parameters of stabilized clouds, Norment stated that the cloud top elevation is the most important variable for two overriding reasons. First, it "is by far the most accurately observed cloud property," and second, it "is the most critical cloud property in determining which winds are involved in the transport and deposition of fallout (Reference 6-2)."

QUANTITATIVE ASSESSMENTS

Cloud top height sets the maximum fall distance for radioactive particles, their final time of arrival at the ground surface, and the end of buildup of radiation fields. The shape of the rising cloud near stabilization has been defined for modelling purposes. DELFIC uses an ellipsoidal cloud of 0.75 eccentricity during cloud rise (Reference 6-2). The ellipsoidal eccentricity has an experimentally derived standard deviation of 0.08, based on 10 shots over the nuclear yield range from 3.5 KT to 15 MT. An empirical refit to observed data in DASA 1251 was also performed for DELFIC (Reference 6-2). Norment reported the least-squares fit to the height of the stabilized cloud top to be a power function, $Z_T = 3,914 \ W^{0.270}$, for 60 shots over the yield range 0.0005 to 15,000 KT. The variance calculated

for the least-squares fit of observations to the power function between yield and cloud top was compared to the variance of DELFIC calculations for cloud top heights. For the data set of 53 shots used (Figure 5-5), the respective variances were 0.0180 for the nuclear data observations and 0.00739 for DELFIC, a 59 percent reduction in variance by the model. The probability that the reduction was statistically significant was greater than chance in 98 out of 100 cases. In comments on the cloud rise module for DELFIC (Reference 6-2), Norment emphasized that predictions for yield range 20 MT to 100 MT are basically conjectures without physical verification. In addition, it should be noted that predictions from 100 KT to 15 MT are based on very sketchy data. The most substantial observation data base lies in the nuclear yield range from 0.01 to 75 KT (Figure 5-4).

In a less statistical, but an illuminating detailed assessment of model capabilities, Norment has made comparisons between fallout pattern isodose contours from six surface-shot nuclear tests and three models. The shots were JOHNIE BOY, JANGLE-S, SMALL BOY, KOON, ZUNI, and BRAVO, in the yield range from 0.5 KT to 15,000 KT. The models were DELFIC (ASA), SEER III, and WSEG-10. Site wind data and fallout patterns were taken from DASA 1251. The contour maps compared were the usual gamma radiation at 3 feet above the ground, in R/hr, at H+1 hour after detonation. Norment's table is reproduced here as Table 6-1; the comparative statistics are shown in summary format. DELFIC showed the better accuracy for the three isodose contour parameter forecasts of length, azimuth, and enclosed area. However, none of the statistics are of a quality that would warrant a troop commander to choose emplacements or base tactics soley on the distance away of the predicted fallout pattern location and radiation intensity.

The figure-of-merit analysis by Rowland and Thompson (Reference 6-3) is another way to compare predicted parameters with observed data from fallout patterns. This criterion was applied by Norment (Reference 6-4) to the six shots and three models discussed earlier (Table 6-2). A perfect fit between observed and predicted pattern would have a figure-of-merit of 1.0;

Table 6-1. Summary of test shot prediction statistics (Reference 6-4)

Number of cases fitting the criteria (via comparisons with the observed patterns) for:

Highest Level Contour
Midrange Level Contours
Lowest Level Contour

a. Contour Length*

Criteria[+]	DELFIC	SEER	WSEG-10
Prediction within 20% of observation	1 3 4 / 8	1 1 1 / 3	1 1 0 / 2
Prediction within 50% of observation	3 8 4 / 15	1 6 7 / 11	1 3 1 / 5
Overprediction by greater than 50%	0 1 1 / 2	1 2 1 / 4	1 3 3 / 7
Underprediction by greater than 50%	2 0 0 / 2	3 1 0 / 4	2 0 0 / 2

b. Contour Azimuth[#]

Criteria[+]	DELFIC	SEER	WSEG-10
Prediction within 2° of observation	1 4 2 / 7	0 2 0 / 2	0 1 1 / 2
Prediction within 5° of observation	1 5 3 / 9	0 3 3 / 6	0 1 2 / 3
Prediction between 5° and 10° of observation	1 1 0 / 2	1 3 1 / 5	1 2 1 / 4
Prediction greater than 10° from observation	3 3 2 / 8	1 2 1 / 4	1 3 1 / 5
Not predicted	0 0 0 / 0	3 1 0 / 4	2 0 0 / 2

c. Contour Area

Criteria[+]	DELFIC	SEER	WSEG-10
Prediction within 30% of observation	1 3 1 / 5	0 1 1 / 1	0 0 0 / 0
Prediction within factor range ¼ to 2 of observation	2 7 3 / 12	0 2 2 / 4	0 3 2 / 5
Overprediction between factor range 2 to 5	1 0 1 / 2	1 4 1 / 6	1 1 0 / 2
Underprediction between factor range 1/5 to 1/2	0 2 1 / 3	0 0 0 / 0	0 0 0 / 0
Overprediction by a factor greater than 5	0 0 0 / 0	1 2 2 / 5	1 1 2 / 4
Underprediction by a factor less than 1/5	2 0 0 / 2	3 1 0 / 4	2 1 0 / 3

*Contour length is the furthest distance from ground zero on the contour.

[#]Contour azimuth is the angle, measured clockwise from north, of the line that connects ground zero with the point of furthest distance from ground zero on the contour.

[+]For each part of the table there are 19 cases for DELFIC and SEER but only 14 for WSEG-10 because the WSEG-10 Small Boy prediction is not included. Also note that in each part the second criterion includes the first criterion cases.

Table 6-2. Figure-of-merit results (Reference 6-4)

a. Complete Listing

	DELFIC	SEER	WSEG-10
Johnie Boy	0.141	0.168	0.078
Jangle-S	0.423	0.118	0.072
Small Boy Reconstructed Winds DASA 1251 Winds	0.319 0.190	0.347 0.304	0.253 0.348
Koon	0.315	0.297	0.348
Zuni	0.104	0.156	0.180
Bravo-AFSWP D & O Winds DASA 1251 Winds	0.207 0.146	0.180	0.320 0.057
Bravo-RAND D & O Winds DASA 1251 Winds	0.103 0.078	0.152	0.362 0.098
Bravo-NRDL D & O Winds DASA 1251 Winds	0.060 0.044	0.068	0.141 0.177

b. Ranking of Results

Number of Predictions For Which the FM is Highest, Second Highest and Least

Rank	DELFIC	SEER	WSEG-10
Highest	1	2	2
Second Highest	3	2	-
Least	1	1	2

c. Results in Order of Value

Model	Shot	FM
DELFIC	Jangle-S	.423
WSEG-10	Koon	.348
SEER	Small Boy	.347
DELFIC	Small Boy	.319
DELFIC	Koon	.315
SEER	Koon	.297
WSEG-10	Zuni	.180
SEER	Johnie Boy	.168
SEER	Zuni	.156
DELFIC	Johnie Boy	.141
SEER	Jangle-S	.118
DELFIC	Zuni	.104
WSEG-10	Johnie Boy	078
WSEG-10	Jangle-S	.072

a total miss becomes 0.0 (the table is self explanatory). A more exten-
sive evaluation (Reference 6-5) was conducted with seven shots and 10 pre-
dictors and the results of those comparisons are reproduced in Table 6-3.
Among the two tables, only three of the composite isodose contour compari-
sons rated a figure-of-merit of 0.5, which is a low level of accuracy for
utilizing the predictions about the patterns in field decisions.

COMPARATIVE ASSESSMENTS

DELFIC is generally the most competent predictor among the models,
as illustrated by Figure 6-1. Closer inspection of the figure shows a pro-
nounced discontinuity in the DASA 1251 data curves for cloud top height and
for cloud base height around 10-KT yield.

In the initial collection and reporting of atmospheric observations
of cloud top altitudes and the altitudes of the bottoms of nuclear clouds,
the respective data were pooled. Data collected over the Nevada desert and
from above atolls in the Pacific Ocean were intermixed without regard for
the season of the year in which they were collected. An overlap occurred
in the range of yields for Pacific and Nevada shots; desert test yields
were 75 KT or less, and Pacific test yields went down to less than 1×10^{-2} KT
from 15,000 KT. When lines were fitted to graphs of yield versus stabilized
cloud top height, or cloud bottom elevation above the burst point, there was
a distinct break or discontinuity between Pacific cloud elevations and those
from the desert (Figure 6-1).

Plots computed by DELFIC show significant differences in predicted
cloud top height as latitude and season of the year changed (Reference 5-5).
The differences were greatest at ton yields and were almost gone in the low-
megaton range. The effects of season and latitude are demonstrated in
Figure 6-2. Wilsey and Crisco (Reference 6-6) divided the DASA 1251-V data
into groups according to geographic site and season of the year, and fitted
least-squares curves onto log-log plots of yield versus cloud elevation.

Table 6-3. Figure-of-merit results (Reference 6-5).

	CELFIC	PROFET	SEFR	KDFOC	ANGER	LASFER
Jangle-S	0.294	0.396	0.118*	0.115	0.127	0.137
Small Boy	0.160	0.406	0.316	0.482	0.491	0.237
Little Feller II	0.386	0.421	)**	0.088	0.369	0.044*
Johnnie Boy	0.531	0.450	0.246	0.289	0.425	0.294
Jangle-U	0.460			0.513	0.342	0.587
Ess				0.273	0.266	0.351
Schooner				0.372	0.352	0.139*
Cabriolet				0.014	0.013	0.074
Danny Boy				0.021	0.131	0.076
Palanquin				0.257	0.362	0.358

* Based on two predicted contours compared with four observed contours.

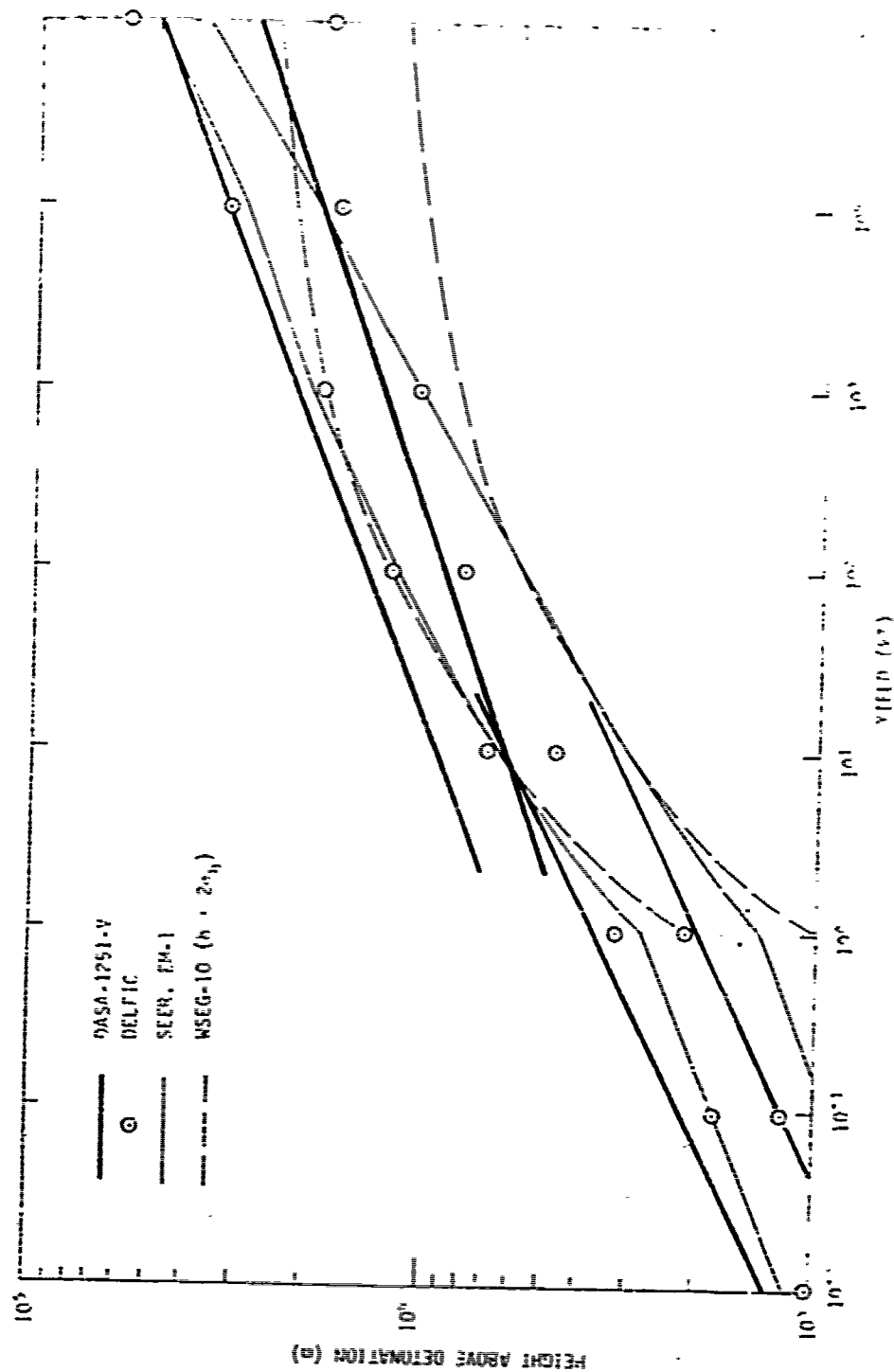** Based on one predicted contour compared with four observed contours.

Figure 6-1. Stabilized cloud top and base heights versus yield for surface bursts (Reference 6-5).
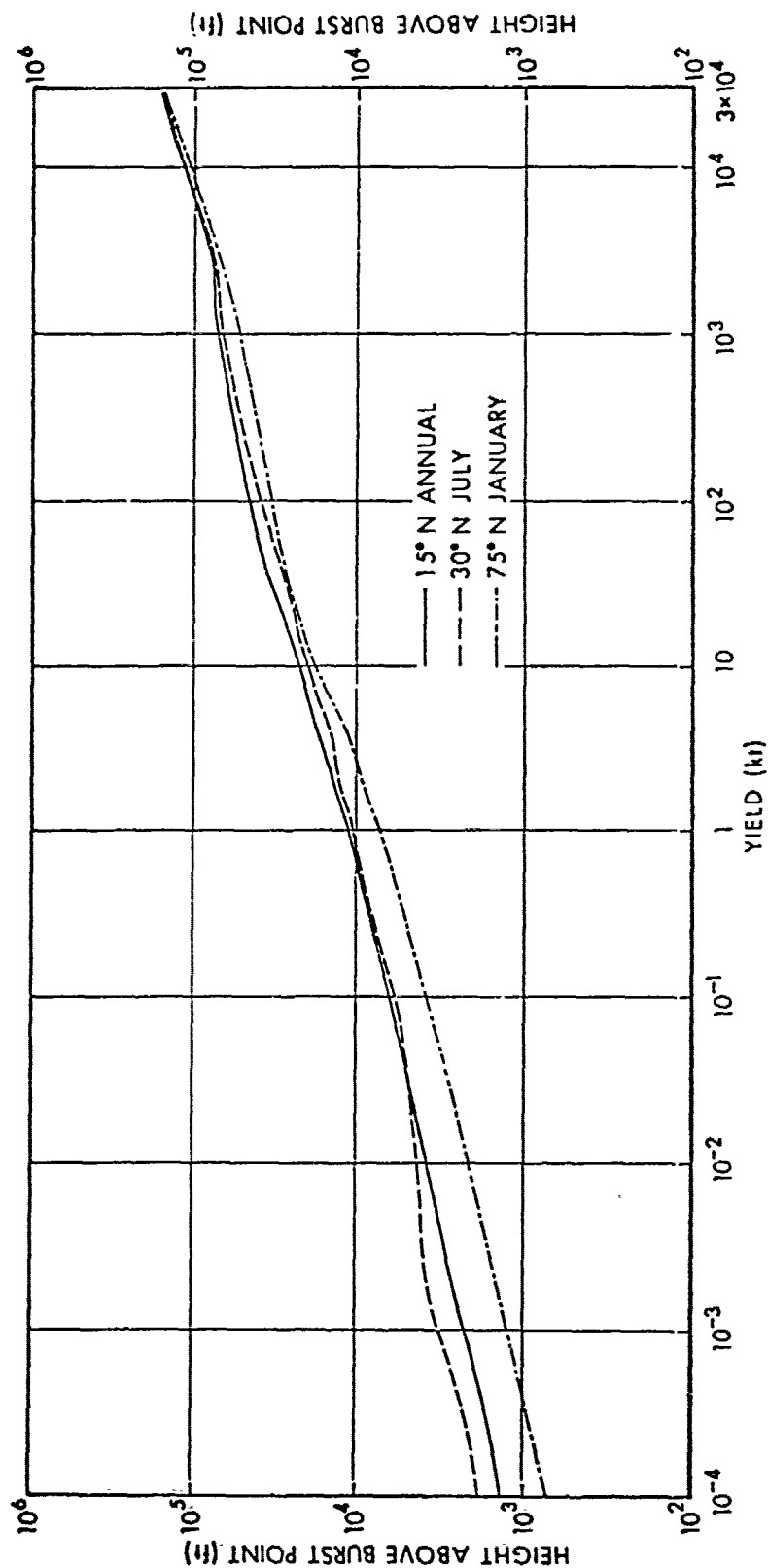
Figure 6-2. Cloud top heights computed by the DELFIC code, using three standard atmospheres (Reference 6-6).

Two Nevada data plots, shown in Figures 6-3 and 6-4, include the then "latest" DELFIC predictions (1977) using the site meteorology for the shots as model input. The collective readjusted plots, based on field data from Nevada and the Pacific, are shown in Figure 6-5 for cloud tops and Figure 6-6 for cloud bottom elevations above the heights of burst. The previous discontinuity is bridged best by the Nevada Spring and Fall data plots. This recent partitioning (1978) of the observed data indicates that better low-range yield predictions from the DELFIC code can be expected today.

Measurements taken at 3 feet above ground level show an apparent intensity of the gamma radiation at that site, unfortunately, they do not tell the amount of fallout gamma radiation at the site. The sensing device has an uneven response to different energy spectra that impact on it; it is only exposed to part of the gamma energy flux deposited in the field, and its sensor has significant directional characteristics (Reference 6-7). The differences in precision between instruments managed carefully during calibration and field use are a matter of a few percent (normally less than 5 percent) (Reference 6-8). The compensations invented to overcome electrical, environmental, and electromagnetic deficiencies and increase the accuracy of monitoring devices have been many and ingenious. The greatest uncertainty lies in the correction from field gamma measurements to an absorption-free plane lacking scattering and roughness effects. To reach this ideal flat-plane resting surface for radioactive particles, it was necessary to invent an effects summary, the normalization constant, commonly symbolized as "K" (measured at 3 feet above an ideal plane in $\dfrac{\text{R/hr at H+1 hour}}{\text{KT/mi}^2}$ by an errorless instrument).

Normalization factors have a lengthy history, which will be entered here via the 1962 USNRDL-DASA Fallout Symposium (Section 3). By 1962, the normalization factor had fallen from 3,700 R/hr per KT/mi^2 in 1950 (Reference 6-9) to those shown in Table 6-4. The 1962 range in values of normalization factors was fourfold. Current trends are towards higher factors as indicated for 1977 by Table 6-5, but the corrections make the range tenfold.
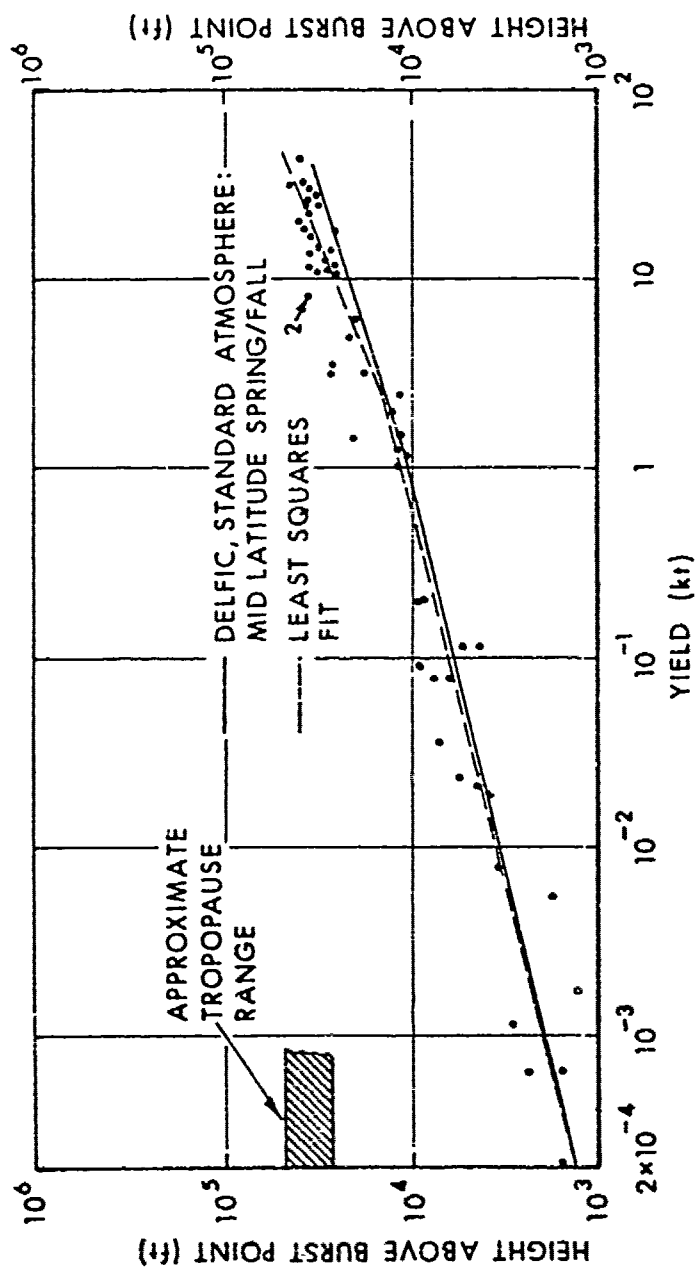
Figure 6-3. Cloud top heights versus yields, Nevada bursts, Spring and Fall (observed values and least-squares fit, and values computed by the DELFIC code using the standard atmosphere – midlatitude, Spring/Fall) (Reference 6-6).
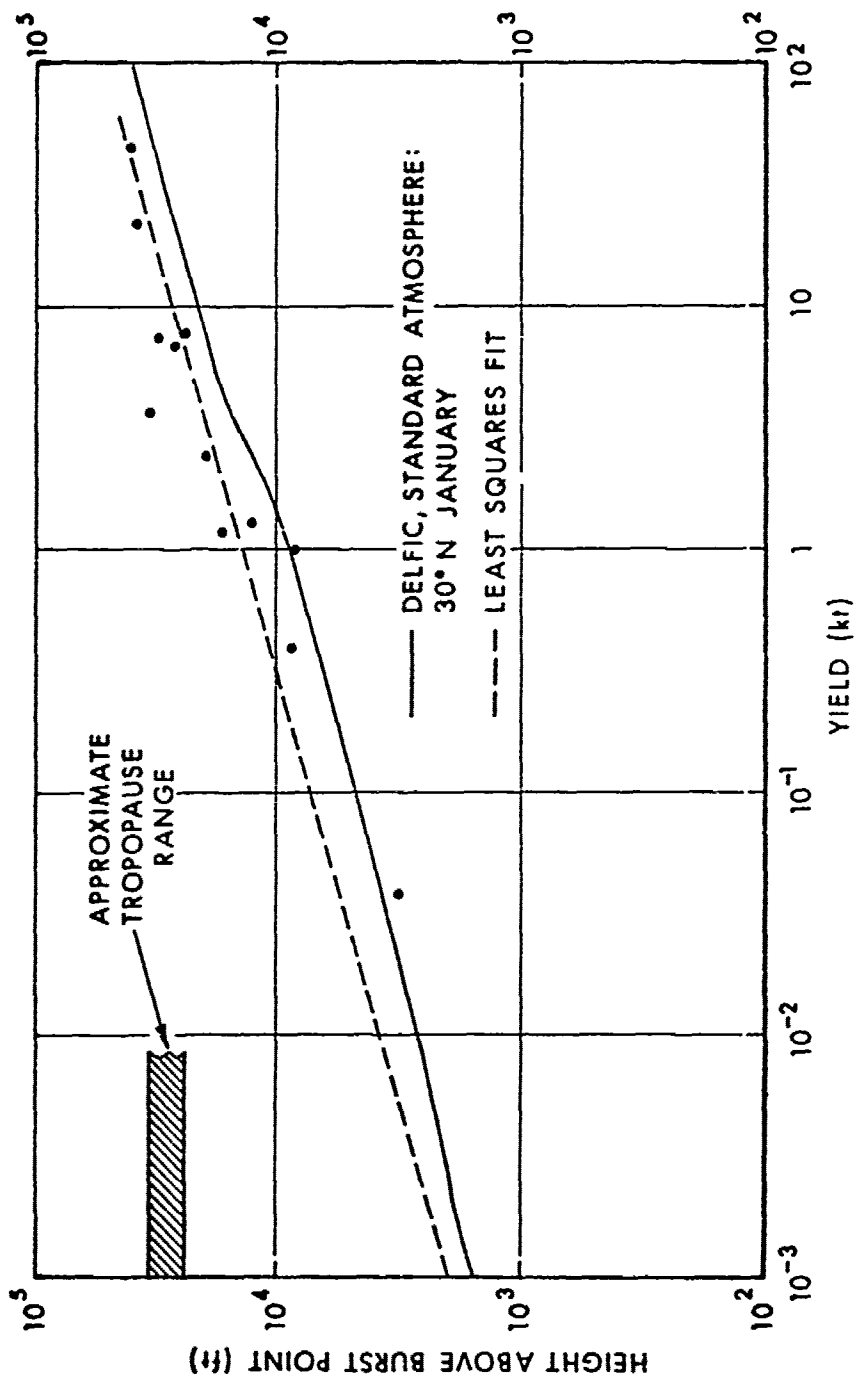
Figure 6-4. Cloud top heights versus yields, Nevada Winter season (observed values and least-squares fit, and values computed by the DELFIC code, using the standard atmosphere, 30 degrees North, January) (Reference 6-6).
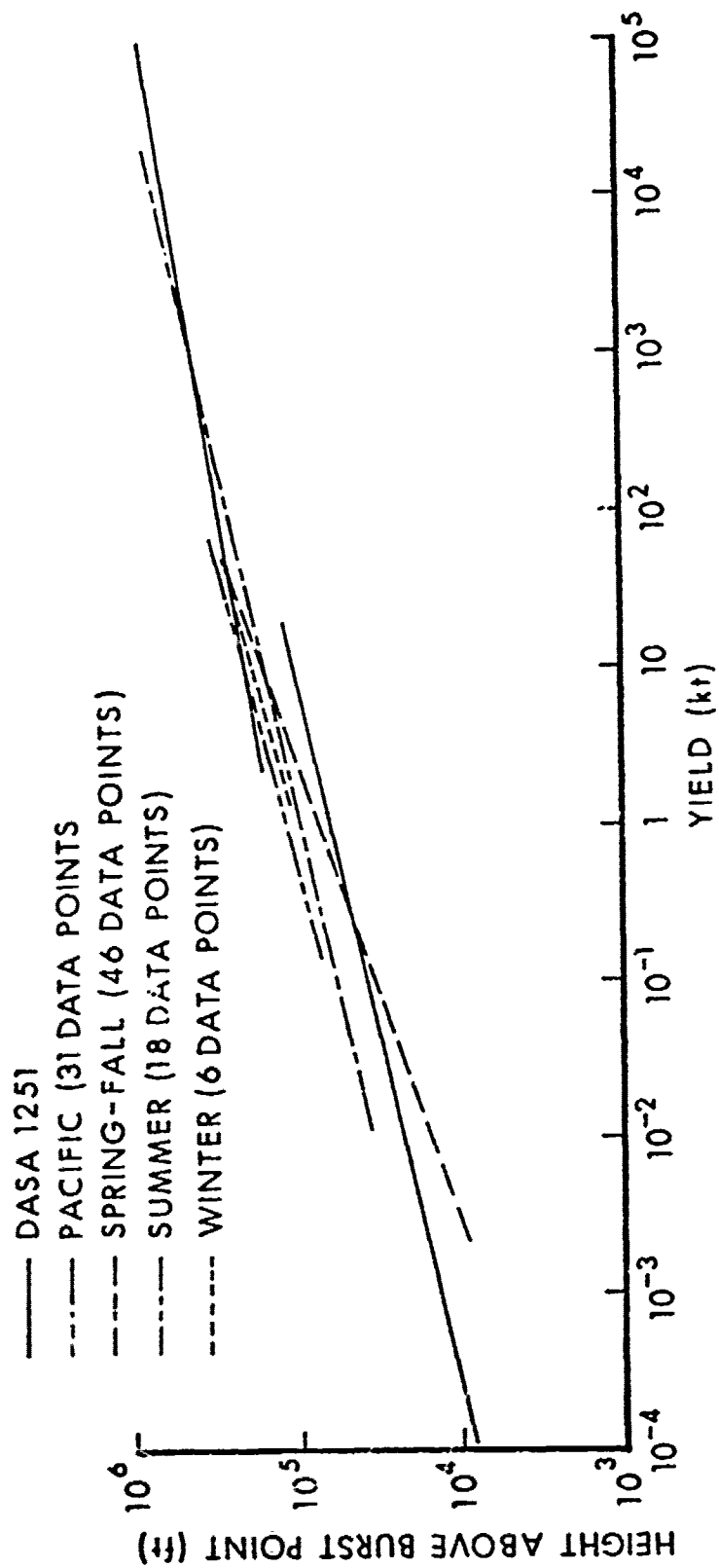
Figure 6-5. Summary of graphs based on observed cloud top heights versus yields (Reference 6-6).
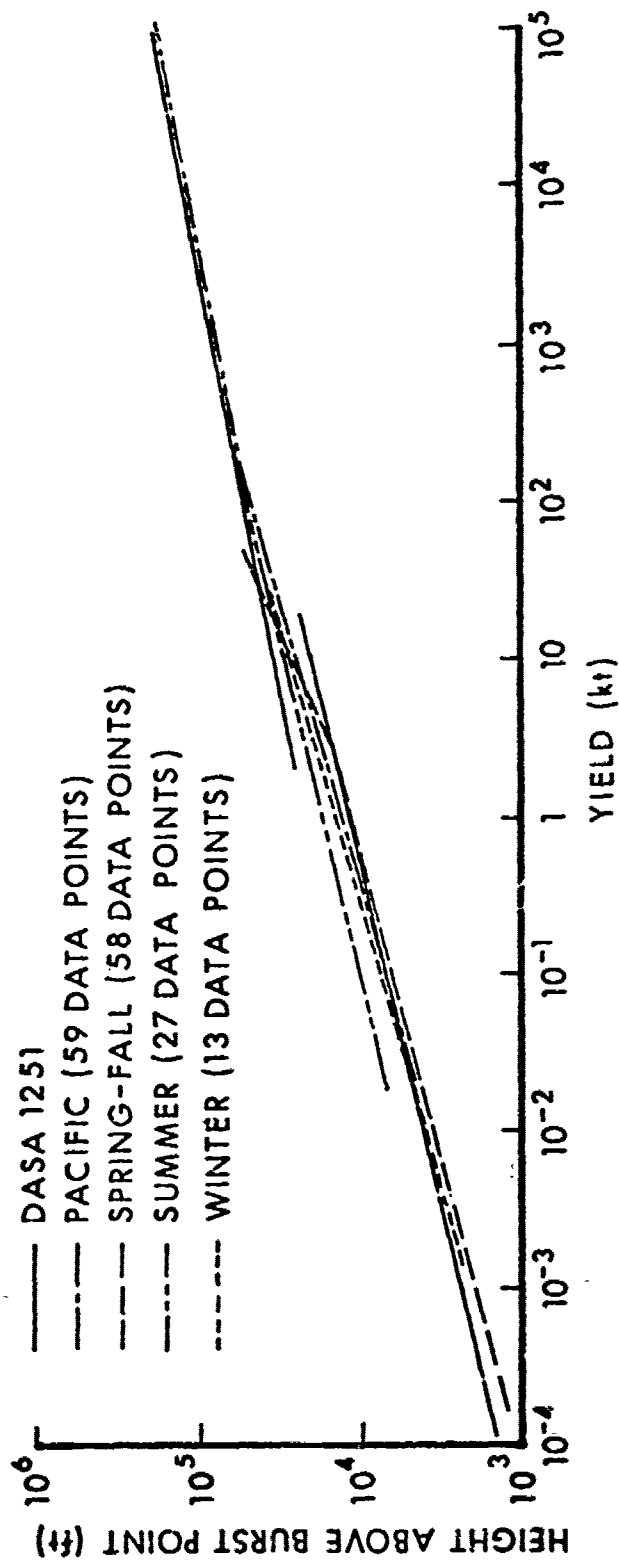
Figure 6-6. Summary of graphs based on observed cloud bottom heights versus yields (Reference 6-6).

Table 6-4. Normalization factors.

Model	NF (R/Hr per KT per Sq. Mile)
LRL-h	2700
Dropsy	2585
NREC	2500
WSEG	2400
RAND	1200
DIA	1100 (implicit) [a]
NRDL-D	1093
USWB	1025
Ford-T	900
TOR	870
Sig C	689
RADFO	not treated in this model
Army	not treated in this model
AN/GMQ-18	no information available

[a] Equivalent value[1]

Table 6-5. Surface burst K-factors.

Model	Nominal K-Factor $\left(\frac{r - mi^2}{hr - kT}\right)$	Fraction of Activity on Particles Larger than 50 μm	Correction[a] or Amplification[b] Factors	Effective K-Factor $\left(\frac{r - mi^2}{hr - kT}\right)$
DELFIC[c]	~2400	0.56	0.5	672
PROFET	~2700	0.47	0.5	634
SEER	2346	0.74	>2	>3472
KDFOC	2500	0.29	0.5	362
AUGER	2500	0.29	0.5	362
LASEER	2000	0.74	>1.4	>2072
WSEG-10	2500	0.79	-	2000

[a] DELFIC and PROFET apply a combined ground roughness and instrument response correction factor of 0.5. LASEER applies a ground roughness factor of 0.7. KDFOC and AUGER assume that only half the activity is in the cloud for a surface burst.

[b] SEER and LASEER arbitrarily multiply activity by a factor with a minimum value of 1.75, but which usually has a value of 2 or greater. (Though the users instructions do not call for it, we have applied a combined ground roughness-instrument response correction factor of 0.5.)

[c] The DELFIC nominal K-factor is a typical value computed from output of the DELFIC particle activity module. DELFIC does not use a preset or constant K-factor.

The note in Table 6-5 about DELFIC computing its correction factors instead of using a preset K-factor is a significant difference, since it allows DELFIC to compensate for the time at which measurements were taken by calculating the decay rate for each of the fission product isotopes individually and integrating them.

In Norment's analysis of fallout predictor modelling (Reference 6-5), he showed a number of fallout maps which should be seen for evaluating outputs in more detail. Some of the intermediate calculations in computing the isodose contours for the maps are shown in Table 6-6. Underground shots at SDOBs of 19, 34, and 45 meters were selected for reproduction here. Base surge dimensions have a high degree of unanimity, as does the radioactivity for ESS. The deviations in base surge radioactivity and main cloud radioactivity become divergent as the shots are placed deeper. The range in main cloud radioactivity proportion is a factor of two, as in Table 5-10; the output from AUGER is most different.

The phenomenon known as fractionation has had an inconclusive definition although studied intensively (References 6-11 and 6-12), but its effects on normalization factors can change them by a factor of five. It's effect on radioactive decay rates are less startling, but contribute to the deviations from the standard $t^{-1.2}$ function seen in field measurements. The field measured rate of radioactive decay can readily differ from $t^{-1.2}$ by a factor of two. Taken together, assuming fractionation is entirely responsible, a factor of 10 difference may occur between field measured and predicted gamma radiation intensities. This is entirely separate from variations between the normalization factors different modellers' prefer to use.

In this review, we have concentrated on the inconsistencies between dimensions at the level of the stabilized cloud and those variations in ground-level radiation. The objective has been to create an awareness of the need to assess fallout prediction code outputs, rather than to assume they are reliable at all times. Experimentalists have yet to fully account for the radiation produced by any of the numerous nuclear tests that created

Table 6-6. Comparative parameters from KDFOC, AUGER and LASEER in fallout prediction.

Shot Modelled[a]	Model Name	Base Surge Height (m)	Base Surge Radius (m)	Main Cloud Height (m)	Main Cloud Radius (m)	Fraction of Nominal K-Factor in the Clouds	Proportion of Activity in Main Cloud
ESS	KDFOC	1260	2520	2540	660	0.48	78%
	AUGER	1260	2520	3110	980	0.72	74%
	LASEER	1260	1900	2480	590	1.05	80%
SCHOONER	KDFOC	1400	6650	4200	1120	0.45	73%
	AUGER	1400	6650	5530	3780	0.46	49%
	LASEER	~1400	~6650	4180	1190	0.92	80%
DANNY BOY	KDFOC	390	1200	960	260	0.36	59%
	AUGER	390	1200	1800	600	0.29	32%
	LASEER	490	1180	990	220	0.82	60%

a Nuclear characteristics are shown in Table 5-2.

b From Reference 6-5.

a stabilized cloud followed by fallout. All attempts to generate a material balance for radioactivity have failed on the downwind, small particle component. When the modeller uses the field data as his guide, the model then becomes susceptible to the same inconsistencies found in the field data.

REFERENCES

6-1. Hawthorne, H.A., J.V. Rosenfeld, and R.H. Rowland, "Nuclear Cloud Dimensional Data, Volume 1 — Underwater and Water Surface Bursts," GE—TEMPO/DASIAC, Santa Barbara, CA, Unpublished.

6-2. Norment, H.G., "Validation and Refinement of the DELFIC Cloud Rise Module," DNA 4320F, Atmospheric Sciences Associates, Bedford, MA, January 1977.

6-3. Rowland, R.H., and J.H. Thompson, "A Method for Comparing Fallout Patterns," DNA 2919F, GE—TEMPO/DASIAC, Santa Barbara, CA, April 1972.

6-4. Norment, H.G., "Evaluation of Three Fallout Prediction Models: DELFIC, SEER and WSEG," DNA-Draft, Atmospheric Sciences Associates, Bedford, MA, April 1978.

6-5. Norment, H.G., "Analysis and Comparison of Fallout Prediction Models," Atmospheric Sciences Associates, Bedford, MA, Unpublished.

6-6. Wilsey, E.F., and C. Crisco, Jr., "An Improved Method to Predict Nuclear Cloud Heights," Ballistic Research Laboratory, Aberdeen Proving Ground, MD, Unpublished.

6-7. Work, G.A., "Operation TEAPOT: Project 6.1.2, Accuracy of Military Radiacs," WT-1138, Armed Forces Special Weapons Project, Albuquerque, NM, November 1957.

6-8   Rowland, R.H., "A Field Comparison of Radiation Survey Meters,"
        DASIAC TN 79-1 (Draft), GE—TEMPO/DASIAC, Santa Barbara, CA.

6-9   Glasstone, S. (Editor), "The Effects of Nuclear Weapons," Los Alamos
        Scientific Laboratory, Los Alamos, NM, 1950.

6-10   Seery, C.J., and M. Poian, "An Analysis of the Fallout Prediction
        Models; Volume II— Analysis, Comparison and Evaluation of Model
        Predictions," NRDL TRC-68-69, Ford Instrument Division, Sperry Rand,
        Long Island City, NY, September 1962. Presented at the USNRDL-DASA
        Fallout Symposium, August 1968.

6-11   Crocker, G.R., "The Effect of Radionuclide Fractionation on the
        Normalization Factor for Fallout Fields," USNRDL-TR-892, US Naval
        Radiological Defense Laboratory, San Francisco, CA, August 1965.

6-12   Thompkins, R.C., "Radiochemical Interpretations of SMALL BOY
        Fallout," BRL-1625, US Army Ballistic Research Laboratory, Aberdeen
        Proving Ground, MD, November 1972.

DISTRIBUTION LIST

DEPARTMENT OF DEFENSE

Command & Control Technical Center
ATTN: C-312, R. Mason

Defense Advanced Rsch. Proj. Agency
ATTN: TIO
ATTN: ITO

Defense Intelligence Agency
ATTN: DB-4C, P. Johnson
ATTN: DIO-GPF, W. Magathan
ATTN: RDS-3C
ATTN: DB-1, F. Walker
ATTN: DN
ATTN: DIR 4

Defense Nuclear Agency
ATTN: SPTD
ATTN: RAAE
ATTN: RATN
ATTN: STVL
ATTN: STSP
ATTN: VLWS
4 cy ATTN: TITL

Defense Technical Information Center
12 cy ATTN: DD

Field Command
Defense Nuclear Agency
ATTN: FCP
2 cy ATTN: FCPR

Field Command
Defense Nuclear Agency
Livermore Division
ATTN: FCPRL
ATTN: FCPRL, L-395

Field Command
Defense Nuclear Agency
Los Alamos Branch
ATTN: FCPRA

Interservice Nuclear Weapons School
ATTN: TTV

Joint Chiefs of Staff
ATTN: SAGA/SFD
ATTN: J-3
ATTN: SAGA/SSD
ATTN: J-5

Joint Strat. Tgt. Planning Staff
ATTN: JPS
ATTN: JLTW
ATTN: JP
ATTN: JL

Undersecretary of Defense for Rsch. & Engrg.
ATTN: Strategic & Space Systems (OS)

DEPARTMENT OF THE ARMY

Harry Diamond Laboratories
Department of the Army
ATTN: DELHD-I-TL

DEPARTMENT OF THE ARMY (Continued)

U.S. Army Ballistic Research Labs.
ATTN: DPDAR-BLV
ATTN: DRDAR-TSB-S
ATTN: DRDAR-VL

U.S. Army Nuclear & Chemical Agency
ATTN: MONA-ZB, D. Panzer
ATTN: Library

DEPARTMENT OF THE NAVY

Center for Naval Analysis
ATTN: NAVWAG

Naval Academy
ATTN: Nimitz Library/Technical Rpts. Branch

Naval Ocean Surveillance Info. Ctr.
ATTN: P. Maier

Naval Ocean Systems Center
ATTN: R. Hammond
ATTN: J. Hooper
ATTN: G. Myer

Naval Postgraduate School
ATTN: Code 1424, Library
ATTN: Code 56PR

Naval Research Laboratory
ATTN: Code 2627
ATTN: Code 8440, F. Rosenthal

Naval Surface Weapons Center
ATTN: Code U41
ATTN: Code F31
ATTN: Code R14
ATTN: Code U12
ATTN: Code F30

Naval War College
ATTN: Code E-11

Naval Weapons Evaluation Facility
ATTN: Technical Director
ATTN: G. Binns

Newport Laboratory
Naval Underwater Systems Center
ATTN: K. Walsh

Office of Naval Research
ATTN: Code 431
ATTN: Code 200

DEPARTMENT OF THE AIR FORCE

Air Force School of Aerospace Medicine
ATTN: Radiobiology Division

Air Force Weapons Laboratory
Air Force Systems Command
ATTN: SUL
ATTN: NSSB

DEPARTMENT OF THE AIR FORCE (Continued)

Assistant Chief of Staff
Studies & Analyses
Department of the Air Force
    ATTN: AF/SAMI
    ATTN: AF/SAGF

Deputy Chief of Staff
Research, Development, & Acq.
Department of the Air Force
    ATTN: AFRDQR
    ATTN: AFRDQSM

DEPARTMENT OF ENERGY CONTRACTORS

Lawrence Livermore Laboratory
    ATTN: L-24, G. Staehle
    ATTN: L-9, R. Barker
    ATTN: L-8, F. Barrish
    ATTN: L-21, M. Gustavson

Los Alamos Scientific Laboratory
    ATTN: E. Chapin
    ATTN: R. Stolpe
    ATTN: R. Sandoval
    ATTN: W. Lyons
    ATTN: M/S632, T. Dowler

Sandia Laboratories
    ATTN: J. Kaizur
    ATTN: 3141

Sandia Laboratories
Livermore Laboratory
    ATTN: T. Gold

OTHER GOVERNMENT AGENCIES

Central Intelligence Agency
    ATTN: OSR/SE/F, A. Rehm
    ATTN: OSI/NED
    ATTN: OSR/SEC

Federal Emergency Management Agency
    ATTN: D. Benson
    ATTN: Asst. Dir. for Rsch., J. Buchanon
    ATTN: C. McLain
    ATTN: L. Elderkin

U.S. Arms Control & Disarmament Agcy.
    ATTN: A. Lieberman

DEPARTMENT OF DEFENSE CONTRACTORS

Academy for Interscience Methodology
    ATTN: N. Pointer

BDM Corp.
    ATTN: J. Morgan

Boeing Co.
    ATTN: L. Harding

66th MI Group
    ATTN: RDA, T. Greene

DEPARTMENT OF DEFENSE CONTRACTORS (Continued)

Decision-Science Applications, Inc.
    ATTN: Dr. Galiano

General Electric Company-TEMPO
    ATTN: DASIAC

General Electric Company-TEMPO
    ATTN: DASIAC

Kaman Sciences Corp.
    ATTN: F. Shelton
    ATTN: V. Cox

Kaman Sciences Corp.
    ATTN: T. Long

Martin Marietta Corp.
    ATTN: M. Yeager
    ATTN: F. Marion

Mathematical Applications Group, Inc.
    ATTN: M. Cohen
    ATTN: M. Beer

McDonnell Douglas Corp.
    ATTN: Technical Library Services

McLean Research Center, Inc.
    ATTN: W. Schilling

Mission Research Corp.
    ATTN: D. Sowle

Pacific-Sierra Research Corp.
    ATTN: G. Lang

Pacific-Sierra Research Corp.
    ATTN: G. Moe

R & D Associates
    ATTN: C. MacDonald
    ATTN: R. Montgomery
    ATTN: J. Marcum

Rand Corp.
    ATTN: Library
    ATTN: J. Digby
    ATTN: T. Parker

Science Applications, Inc.
    ATTN: M. Drake
    ATTN: J. Martin

Science Applications, Inc.
    ATTN: J. Goldstein
    ATTN: J. McGahan
    ATTN: W. Layson

Science Applications, Inc.
    ATTN: D. Kaul

Systems, Science & Software, Inc.
    ATTN: J. Cane